A desire accomplished is sweet to the soul...

Proverbs 13:19

University of Alberta

Dissolution Kinetics of Liquid-Liquid Dispersions using Local Rates of Turbulent Dissipation

by

Solomon C. Ibemere 

A thesis submitted to the Faculty of Graduate Studies and Research in partial fulfillment of the requirements for the degree of Master of Science
in
Chemical Engineering

Department of Chemical and Materials Engineering

Edmonton, Alberta
Spring 2006

Your file Votre référence
ISBN: 0-494-13826-2
Our file Notre référence
ISBN: 0-494-13826-2

Abstract

A simplified mechanistic model which captures the inhomogeneity in a pitched blade turbine (PBT) stirred tank using 5-mixing zones with local dissipation energy rates estimated from experimental data; tracks the transient drop size distribution in the stirred tank using population balances and published correlations for drop break-up and mass transfer while simultaneously predicting the solute concentration in the bulk of the stirred tank has been developed. Simulation studies done using the model show that the dissolution time increases with increased agitation and lower continuous phase viscosity. The effect of interfacial tension (studied independent of the solubility of the dispersed phase) on the dissolution time was insignificant while the dominant controlling mechanism for the mass transfer rate was the approach to the solubility limit. For most common liquid-liquid systems, 200 blend times would suffice for complete dissolution.

Acknowledgements

The completion of this work would not have been possible without the support of several people who helped in guiding me through the difficult concepts of modeling fluid systems; computer programming; and gave encouragements when everything just seemed chaotic.

I would like to thank, in particular, my Supervisor Dr. Suzanne Kresta, who painstakingly taught me the concepts in fluid mixing and modeling and gave me all the support I needed to succeed. I remain grateful.

I would also like to recognize the invaluable contributions made by Gary Anthieren and Joseph Mmbaga in guiding me through the complexities of programming. My appreciation goes to my colleagues in the Mixing group; Sujit, Shad, Oscar, Vasselina, Alena, and Ahmed – who designed the experiment procedure used in my model validation.

Finally, to my fiancée Mariam Onipe, I say thank you for all the love, support and encouragement. My appreciation also goes to my Parents and siblings for being there, always.

Table of Contents

List of Tables

List of Figures

List of Symbols

The symbols listed below are intended for general references. Multiple definitions for a symbol may exist within the body of this thesis due to the need to ensure consistency with the nomenclature used in mixing correlations and calculations. Where a symbol is used for more than one purpose, the proper definition will be given where used.

A	surface area of a drop, m^2
A	constant
a	constant
a	mean, m
B	total change due to birth processes, s^{-1}
b	standard deviation, m
C	concentration, mol L^{-1} *or* kg m^{-3}
C	off-bottom impeller clearance, m
C	Courant number
C_S	solute concentration at equilibrium, mol L^{-1} *or* kg m^{-3}
C_{ic}	interface concentration at continuous phase side, mol L^{-1} *or* kg m^{-3}
C_{id}	interface concentration at dispersed phase side, mol L^{-1} *or* kg m^{-3}
C_d	dispersed phase concentration, mol L^{-1} *or* kg m^{-3}
C_{bulk}	bulk concentration in stirred tank, mol L^{-1} *or* kg m^{-3}
ΔC	concentration driving force, mol L^{-1} *or* kg m^{-3}
c	advection speed or velocity, m s^{-1}
c	constant
D	impeller diameter, m
D	total change due to death processes, s^{-1}
d_p	drop diameter, m

D_{AB}	Molecular diffusion coefficient, $m^2\ s^{-1}$
D_{eff}	effective diffusivity, $m^2\ s^{-1}$
d	constant
G	dissolution rate, $m\ s^{-1}$
g	acceleration due to gravity, $m\ s^{-2}$
H	initial fluid height, m
i	interval index
i	iterative index
k	turbulent kinetic energy, $J\ kg^{-1}$
k_L	mass transfer coefficient, $m\ s^{-1}$
L	drop characteristic length, m
L	characteristic length, m
ℓ	characteristic length, m
ℓ	upper or lower limit of drop size interval, m
ΔL_i	spacing of *ith* size interval, m
m	mass of dispersed drops, kg
m	moment parameter
m	number of daughter drops formed
m	constant
M	mass of drops, kg
n	number density per size interval, m^{-1}
n	constant
$\overline{N}$	rate of mass transfer, $mol\ s^{-1}$
N	number of drops per size
N	impeller rotational speed, rps *or* rpm
N_A	Molar flux of dissolving component, $mol\ m^{-2}\ s^{-1}$
N_P	impeller power number
N_Q	impeller flow number

N_T	total number of drops
P	impeller power requirement, W
P	total number of drop size classes
p	statistical distribution function
Q	impeller pumping capacity, $m^3\ s^{-1}$
Q	volumetric flow rate, $m^3\ s^{-1}$
Q'_b	drop breakup rate, s^{-1}
Q'_c	coalescence rate, s^{-1}
q	constant
r	common geometric factor
r	radial distance, m
Re	Reynolds number
Sc	Schmidt number
Sh	Sherwood number
t	time, s
Δt	time step, s
T	tank diameter, m
u	characteristic velocity, $m\ s^{-1}$
u'	fluctuating velocity, $m\ s^{-1}$
u_l	streamwise component of velocity, $m\ s^{-1}$
$\overline{U}$	average local velocity, $m\ s^{-1}$
U	velocity, $m\ s^{-1}$
V	volume, m^{-3}
V	volume of mixing zone, m^{-3}
V_T	total volume of stirred tank, m^{-3}
w	baffle width, m
W	impeller blade width, m
x	spatial direction, m

x	constant
Δx	bin size, m
y	constant
z	axial distance, m
∇_z	velocity gradient in the axial direction, m s^{-2}

Greek

ε	rate of kinetic energy dissipation, W kg^{-1}
ν	Kinematic viscosity, m^2 s^{-1}
θ_{95}	tank blend time, s
ρ	density, kg m^{-3}
ρ_c	continuous phase density, kg m^{-3}
ρ_d	dispersed phase density, kg m^{-3}
$\Delta\rho$	density difference between phases, kg m^{-3}
σ	interfacial tension, N m^{-1}
δ	scale parameter
δ	Boundary layer, m
δ_d	Boundary layer on dispersed phase side, m
δ_c	Boundary layer on continuous phase side, m
μ	location parameter
μ	dynamic viscosity, Pa. s
φ	phase fraction
ξ	drop-eddy ratio
η	Kolmogorov length scale, m
α	constant
β	constant

Chapter 1

Introduction

1.1 Introduction

Mass transfer in liquid-liquid systems can either be pure dissolving in a two-component miscible system or solute transfer between immiscible components in dispersion. Immiscible liquid-liquid systems are commonly encountered in extraction and separation processes. Critical to achieving separation or extraction is the transfer of a solute between two immiscible liquids. Immiscible systems form stable dispersions while the dispersed drops in pure dissolving systems shrink in size and disappear due to dissolution. Although dispersions refer very generally to the distribution of one phase (dispersed phase) in another medium (continuous phase), it is usually associated with systems in which the dispersed drops attain an equilibrium size distribution after prolonged agitation.

Key mechanisms in liquid-liquid dispersions include: mass transfer between phases; interfacial forces; and mixing. A complete understanding of the liquid-liquid interfacial interactions and how they affect the dissolution process requires a treatise of science on the interfacial phenomena, the thermodynamics of the liquid-liquid interfaces, the degree of mixing or agitation imposed on the system and the mass transfer mechanism controlling solute transport between the phases. A brief summary of these four mechanisms is provided in this chapter.

In this thesis, a numerical model consisting of different mixing zones is used to represent hydrodynamic variations in the stirred tank. The drop population and mass transfer are tracked explicitly as the drops breakup and dissolve. Numerical models that can adequately reflect the dynamics of a physical system have the distinct advantage of providing further understanding on the driving mechanisms for drop dissolution. Issues such as cost, safety, repeatability or reproducibility of results and equipment reliability are not encountered and models give the flexibility to undertake sensitivity analysis on the system

variables to provide process understanding in the face of multiple interacting mechanisms.

This chapter begins with a discussion of the fundamentals of liquid-liquid interfacial interactions and the theory describing the spectrum of classification of liquid-liquid systems as miscible, immiscible and partially miscible systems. The effects of external forces; the hydrodynamics prevailing in the stirred tank and how it controls the liquid-liquid dispersion are discussed in this context.

1.2 Liquid-liquid Systems

Liquid-liquid dispersions in stirred tanks consist of polydispersed drops suspended in a continuous medium and subjected to varying turbulent characteristics. The dispersed drops experience different levels of turbulence, breakup rates and mass transfer rates as they circulate throughout the stirred tank. Modeling of the dispersed system requires the use of local approximations for the spatial variations in turbulent characteristics.

1.2.1 Miscibility

Liquids forming homogenous mixtures in which dissolution is complete at all concentrations are completely miscible while liquids with zero mutual solubility are considered immiscible. Between these two extremes, all other mixtures are partially miscible.

Mixing operations involving miscible liquids are identified as blending operations and the correlations for blend time are well documented (Grenville, 1992). However, some recent studies on miscible liquid-liquid systems (Hemsing, 2001; Kennedy, 2003) have shown longer dissolution times relative to the blend times predicted from documented correlations. Figure 1-1 shows the kinetic data obtained using polymer additives in a water treatment facility (Hemsing, 2001).

The ordinate (y-axis) in the figure represents the amount of dispersed particles in solution and shows that the blend time is only a few seconds while the dissolution time for the polymer additive is much longer and varies with the mixing intensity in the stirred tank. In this case, the polymer is completely soluble in water but there is a very significant resistance to dissolution.

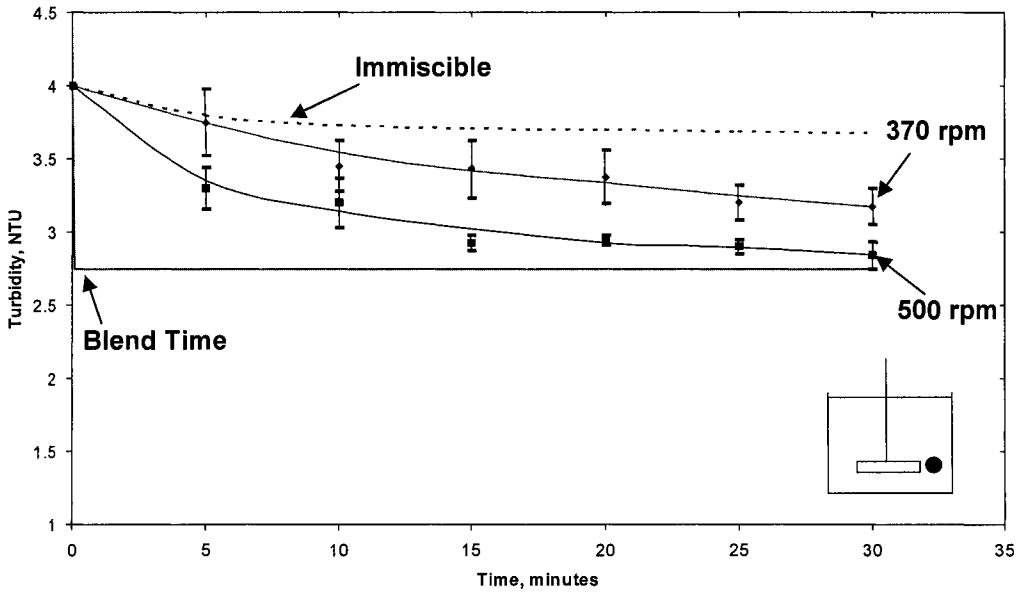

Figure 1-1: Dissolution of polymer additive at 370 and 500 rpm for Pol-E-Z-652 (0.02 mg/ml) using a 3 inch paddle impeller. Polymer was injected at the tip of the impeller blades (Hemsing, 2001).

Immiscible liquids do not dissolve appreciably (as seen in the upper limit of Figure 1-1); hence while many studies have been done on liquid-liquid extraction, little has been done on the dissolution rates of pure liquid dispersions. For the spectrum of partially miscible liquids, the rate of dissolution can vary greatly depending on the interfacial interactions on the molecular level. The inhomogeneity in partially miscible liquids exists as a result of the dissimilarity in the liquid interfacial properties. Several factors such as; chemical structure, polarity, molecular weight, temperature, pressure, cross-linking and long chains have been identified as having a significant influence on the level of miscibility

for mixed liquids (Senichev et al., 2001). Liquids with similar properties can coexist together forming homogenous solutions while those with dissimilar properties tend to form immiscible systems. This is reflective of the saying that "like dissolves like".

1.2.2 Dispersion, Dissolution and Blending

Drops are formed either by pumping liquid through a feed pipe or by breakup in a high shear field produced by an external source, e.g. a mechanical agitator in a baffled stirred tank. When a drop is formed at the exit of the feed pipe under very slow flow conditions, its size will be of the same size as the internal diameter of the feed pipe. As the fluid velocity through the feed pipe increases, the inertial forces overwhelm the pseudo static conditions and the dispersed phase flows out as a continuous stream. In a stirred tank, agitation is provided using a mechanical stirrer (impeller) and the regions closest to the agitator have high shear rates or high drop breakup rates, both of which diminish with distance from the agitator. The volume swept by the impeller (impeller region) and region adjacent to the impeller where the swept stream is discharged (impeller discharge region) have high shear rates thus the stream issuing out of the feed pipe is exposed to the prevailing high shear region and undergoes breakup and redispersion.

Depending on the degree of miscibility of the liquid-liquid system, either the term blending or dissolution can be appropriate. For completely miscible systems, the process objective is to achieve a predetermined degree of homogeneity and this is done by blending. The time required to attain the predetermined degree of homogeneity is the blend time. For immiscible and slightly miscible systems, agitation results in the formation of droplets which are redistributed throughout the entire stirred tank. While immiscible liquid-liquid dispersions evolve only by drop breakup and coalescence processes, slightly miscible systems dissolve slowly and eventually form a homogenous mixture.

The time taken to completely dissolve all the dispersed drops is the dissolution time.

Depending on the viscosity of the fluids or the nature of the fluids (Newtonian or non-Newtonian), there are a number of correlations available for equipment design in blending processes (Kramers et al., 1953; Norwood and Metzner, 1960; Hoogendoorn and den Hartog, 1967; Khang and Levenspiel, 1976; Grenville, 1992). This information provides a baseline for comparison in this investigation of the dissolution time.

Accurate prediction of dissolution time for slightly miscible systems is difficult (if not impossible) because of the multi-mechanism processes taking place simultaneously, coupled with the turbulence inhomogeneity in the stirred tank. Prediction of the dissolution time requires accurate description of the prevailing hydrodynamics of the stirred tank, accurate modeling of the drop breakup, coalescence and solute transfer processes occurring, and a robust and stable numerical scheme to resolve the systems of equations depicting each drop size class in the polydispersed system.

1.3 Hydrodynamics

The hydrodynamic behavior in a stirred tank is primarily affected by the power input. More power input by mechanical energy implies more flow and turbulence characteristics within the stirred tank. An understanding of the hydrodynamic properties in the stirred tank is critical for drop size distribution modeling; thus, they will be discussed in some detail below.

1.3.1 Flow Characteristics in a Stirred tank

Stirred tanks consist of the tank vessel, impeller(s), and usually baffles. The impeller is used to provide angular momentum and turbulence to the fluid.

When baffles are present, the angular momentum is converted into axial upward flow.

The flow regime (turbulent, transitional or laminar) within a stirred tank depends on the power draw and is usually described by the impeller Reynolds number Re, which is given by the expression

$$\mathrm{Re} = \frac{ul}{\nu} \qquad (1.1)$$

ν is the kinematic viscosity ($\frac{\mu}{\rho}$), u and l represent the characteristic velocity and length scales, which for an impeller driven stirred tank are the tip speed of the impeller ($\propto ND$) and the impeller diameter (D). N is defined as the impeller rotational speed. Thus, for a stirred tank, equation (1.1) becomes

$$\mathrm{Re} = \frac{ND^2}{\nu} \qquad (1.2)$$

The flow within the impeller region is considered fully turbulent when $\mathrm{Re} \geq 2x10^4$, laminar when $\mathrm{Re} < 10$, and transitional for all other values.

The pumping capacity (Q) of an impeller is another important hydrodynamic property of the stirred tank. The pumping capacity refers to the amount of fluid discharged from an impeller, and can be related to the impeller swept volume using dimensional analysis. The expression for pumping capacity is given by

$$Q = N_Q ND^3 \qquad (1.3)$$

N_Q is the pumping number and is dependent on the Reynolds number and the size of the impeller (for a pitched blade turbine (PBT) impeller) because of the strong interactions between the impeller and the tank walls (Hemrajani and Tatterson, 2004). N_Q is given as 0.79 for a $D = T/3$ PBT impeller (Hemrajani and Tatterson, 2004).

The power consumed (P) by an impeller can be related to the impeller diameter (D) and impeller speed (N) using dimensional analysis (Rushton et al., 1950) or by angular momentum balances (Chapple et al., 2002). The expression for the power draw is given by

$$P = N_P \rho N^3 D^5 \qquad (1.4)$$

N_P is the power number and is dependent on the impeller type and geometry. Under non-turbulent conditions N_P will vary with the Reynolds number but becomes constant for any particular impeller geometry under turbulent conditions (Hemrajani and Tatterson, 2004).

The flow field generated by a four-bladed, 45°, PBT down pumping impeller is significantly affected by the tank configuration (Ranade and Joshi, 1989; Jaworski et al., 1996; Kresta and Wood, 1993). The discharge stream from the impeller blades leaves at an angle of about 45° to the horizontal and moves downwards until it impinges on the bottom of the tank. The impinging stream spreads outwards on the tank bottom and is converted into axial upward flow along the walls of the tank by the baffles until it is sucked back into the impeller to complete the circulation loop (Figure 1-2(a)). For high off bottom clearances, the discharge stream from the impeller will impinge on the tank wall instead of the bottom, causing the formation of secondary circulation loops at the bottom of the tank as seen in Figure 1-2(b) (Jaworski et al., 1996; Kresta and Wood, 1993).

The impeller off-bottom clearance must be strictly defined to avoid significant errors when the simulation work is done.

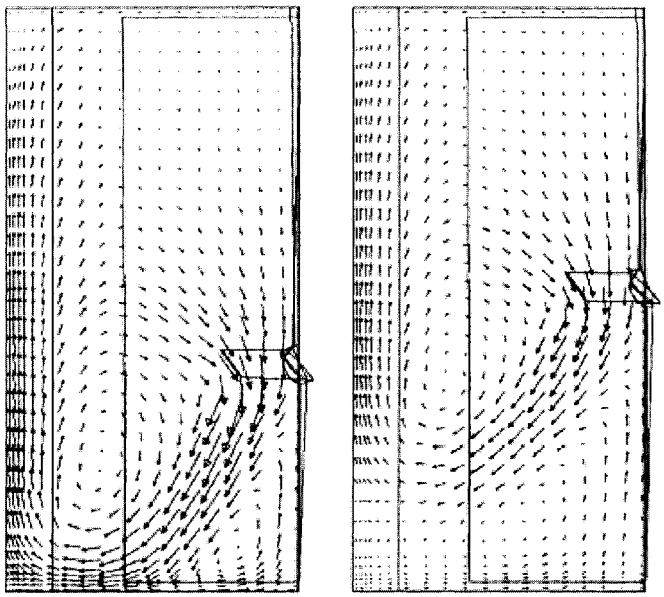

(a) C/D = 1.1 (D = T/3) (b) C/D = 1.5 (D = T/3)

Figure 1-2: Velocity vector fields showing the effect of off-bottom clearance (Battacharya and Kresta, 2002)

1.3.2 Turbulence and its approximation

Turbulence within stirred tanks arises when the impeller rotates rapidly generating sharp velocity fluctuations in the discharge streams from the impeller blades (Davies, 1972). These velocity fluctuations exhibit spatial and transient variations and thus are difficult to measure and characterize (Bradshaw, 1975; Hinze, 1955; Tennekes and Lumley, 1972). The turbulence condition in a stirred tank is represented using the rate of energy dissipation per unit mass (ε) which is exactly defined in terms of the spatial velocity gradients as

$$\varepsilon = -2\nu\left[\frac{1}{2}\left(\frac{\partial u'_i}{\partial x_j}+\frac{\partial u'_j}{\partial x_i}\right)\frac{\partial u'_j}{\partial x_i}\right] \qquad (1.5)$$

where ν is the kinematic viscosity and $\frac{\partial u'}{\partial x}$ is the fluctuating velocity gradient.

The simultaneous measurement of the spatial velocity gradients is extremely difficult, thus, indirect methods have been used in estimating ε (Kresta and Wood, 1993; Kresta, 1998). From an analysis of several length scales (L) and characteristic velocity scales (u), Kresta (1998) showed that the local maximum dissipation can be estimated using

$$\varepsilon = A\frac{u^3}{L} = \frac{u_1^{\,3}}{(D/10)} \qquad (1.6)$$

A is a constant, ε is the local energy dissipation rate, u_1 is the streamwise component of the fluctuating velocity and the length scale is one-tenth the impeller diameter.

In deriving equation (1.6), Kresta (1998) assumed that all three components of the velocity gradients were equal, implying local isotropy. Energy spectrum measurements using root mean square (RMS) velocities (Kresta, 1998) and a comparison of all three fluctuating velocity components (Kresta and Wood, 1991) show that the impeller region and the impeller discharge regions can be approximated using local isotropy. However, the assumption of local isotropy cannot be applied in the bulk of the stirred tank. Thus, the dissipation in the bulk is calculated by subtracting the energy dissipation in the impeller and impeller discharge regions from the total power-input per unit mass and averaging it over the remainder of the tank.

1.4 Liquid-liquid Dispersion Models

Dispersion models for liquid-liquid systems have focused on accurately predicting drop characteristics such as the drop size distribution, concentration

profile and rates of either drop breakup or coalescence. These characteristics depend on the interaction between the dispersed and continuous phases and previous models on liquid-liquid systems available in the literature have modeled these interactions using different descriptions for the two phases. The differences in the published models include: turbulence modeling in the continuous phase; drop size evolution mechanisms; and the modeling approach used in accounting for the drop population.

Previously, the turbulent conditions in the stirred tank have been treated as uniformly homogenous, that is, the whole stirred tank is treated as a field of homogenous isotropic turbulence (Park and Blair, 1975; Hsia and Tavlarides, 1980, 1983; Skelland and Kanel, 1992). However, numerous velocity measurements (Cutter, 1966; Kresta, 1998) now show that the turbulence intensity near the impeller is very high, whereas the remainder of the tank is relatively quiescent. Consequently, models composed of several compartments (zones) have evolved. Some authors have only modeled the impeller region and the rest of the tank using a two zone model (Coulaloglou and Tavlarides, 1977; Tsouris and Tavlarides, 1994; Maggioris et al., 2000 etc.) while others have used pre-selected volumes with dissipation energy and volumetric flow rates determined using computational fluid dynamics (CFD) analysis and/or experimental data (Baldyga et al., 1995; Alopaeus et al., 1999; Kresta et al., 2003). The dispersed drop population is commonly modeled using either population balance models or simulation techniques such as the Monte Carlo method (Spielman and Levenspiel, 1965), or the quiescence interval method (Shah et al., 1977). Due to the difficulty in accurately modeling the simultaneous drop-drop interactions (coalescence), drop-eddy interaction (breakup) and solute mass transfer, most models make assumptions to reduce the complexity by eliminating one of these mechanistic processes. Models that have been developed to predict the drop size distribution in liquid-liquid dispersion in the absence of mass transfer (Alopaeus et al., 1999, Valentas et al., 1966; Valentas and Amundson, 1966, Ramkrishna, 1974, Bajpai et al., 1976) assume that the system is chemically equilibrated. Other models

incorporating solute transfer (Curl, 1963; Bayens and Laurence, 1969; Jeon and Lee, 1986; Skelland and Kanel, 1992) focus on slightly dilute systems to eliminate the coalescence term.

1.4.1 Population Balance Modeling

The population balance equation (model) is used to account for the distribution of particles (or drops) in a dispersion system. It is a statement of continuity representing the net change in formation and disappearance in a particulate system. The pioneering work done on population balance modeling is ascribed to Hulburt and Katz (1964), and it has received wide application (Valentas and Amundson, 1966; Coulaloglou and Tavlarides, 1977; Sastry and Gaschignard, 1981; Hounslow et al., 1988; Marchal et al., 1988; Tsouris and Tavlarides, 1994; Zimmermann et al., 1995; Kumar and Ramkrishna, 1996; Kostoglou et al., 1997; Chen et al., 1998; Lee et al., 2001; Mahoney and Ramkrishna, 2002; Goodson and Kraft, 2004 etc.). The population balance equation is written as

$$\frac{\partial n}{\partial t} + \nabla_z \cdot (Un) = -\frac{\partial}{\partial L}(Gn) + Q'_b + Q'_c \qquad (1.7)$$

Equation (1.7) is the mathematical description for a particulate system undergoing mass transfer $-\frac{\partial}{\partial L}(Gn)$, drop breakup Q'_b, drop coalescence Q'_c, and drop convection $\nabla_z \cdot (Un)$. Equation (1.7) can be summarized as

$$\frac{\partial n}{\partial t} = B - D \qquad (1.8)$$

Where B is the sum of all processes creating new particles and D is the sum of all processes destroying the particles.

The processes that create new particles are referred to as "birth" processes while those that destroy particles are "death" processes. Accurate modeling of the particle distribution depends on the accurate description of the phenomenological processes (drop breakup, drop coalescence and solute transfer) within the containing vessel.

Reviews of population balances can be found in Attarakih et al. (2004) and Ramkrishna (2000).

1.4.2 Drop Size Evolution Mechanism

The dispersion formed using the mechanical agitator in a turbulent stirred tank is continuously influenced by hydrodynamic processes (drop breakage, coalescence and mass transfer) which determine the drop size distribution. These processes occur simultaneously and independently, and depend on the local turbulent conditions. These processes are described individually below.

Drop Breakup

In stirred tanks, the forces causing drop dispersion are extremely nonuniform. Velocity gradients are highest near the impeller and diminish rapidly with distance from the impeller (Leng and Calabrese, 2004). Due to the difficulty in resolving the instantaneous velocity gradients, the forces are often characterized in terms of the energy dissipation rate (which is a product of the stress and the velocity gradient tensors) per unit mass (Cutter 1966; Calabrese, Chang & Dang 1986). Turbulent energy dissipation rates in the impeller region are often ~40 times greater than the average power draw per unit mass in the whole tank (Leng and Calabrese, 2004). Thus, a drop experiences varying shear and deformation rates as it circulates through the stirred tank.

Drop breakup in high shear field was first studied by Kolmogorov (1949) and it has since received tremendous consideration in the chemical engineering

literature. Significant work has been done in developing correlations to predict the equilibrium drop size distribution in immiscible dispersions (Shinnar 1961; Arai et al. 1977; Konno, Arai & Saito 1977; Wang & Calabrese 1986; Berkman & Calabrese 1988). Also, models for drop breakup frequency and daughter drop distribution have been developed for model prediction of drop size distribution in predetermined turbulent flow conditions (Coulaloglou & Tavlarides 1977; Konno et al. 1980; Prince & Blanch 1990; Tsouris & Tavlarides 1994; Luo & Svendsen 1996). A comprehensive review of these models can be found in the paper by Lasheras et al (2002).

To completely define the drop breakup properties of a dispersion system, the drop breakup frequency and daughter drop distribution models are required, and will now be described.

Breakup frequency

The probability of turbulent breakup for a drop subjected to external deforming forces depends on the surface restoring forces. Drop breakup will occur only when the deforming forces exceed the surface restoring forces. The deforming forces can either be pressure fluctuations or viscous stress in the continuous phase while the restoring forces are interfacial tension forces or viscous stress on the drop. Thus, the breakup phenomenon is determined by the flow characteristics, the drop size and the physical properties of the interacting liquid-liquid systems.

Sarimeseli and Kelbaliyev (2004) identified three basic theoretical principles on which most models are derived from: turbulent kinetic energy (Coulaloglou and Tavlarides, 1977); Maxwell distribution function (Konno et al., 1980); and kinetic theory of gases (Prince and Blanch, 1990; Tsouris and Tavlarides, 1994; Luo and Svendsen, 1996; Martinez-Bazan et al., 1999). Irrespective of the theoretical support for the derivation of the breakup frequency

model, each model is a product of two parameters: drop-eddy collision frequency and the collision efficiencies. The definitions of each of the parameters differ depending on the model (Lasheras et al., 2002) but can be understood, qualitatively, as the fraction of drops that breakup within a given time frame.

With the exception of the model proposed by Luo and Svendsen (1996), all models have unknown parameter(s) that must be determined experimentally. This condition poses a limitation for modeling of drop breakup processes, hence, the Luo and Svendsen (1996) drop breakup frequency model is adopted for this model effort.

Daughter drop distribution

Lasheras et al (2002) classified models for daughter drop size distribution into three groups: statistical models (Valentas et al., 1966; Chatzi and Kiparissides (1992); Kostoglou & Karabelas, 1997; Diemer & Olson, 2002), phenomenological models (Prince & Blanch, 1990; Nambiar et al., 1992; Tsouris & Tavlarides, 1994; Luo & Svendsen, 1996; Sathyagal & Ramkrishna, 1996; Lehr & Mewes, 2001; Lehr et al., 2002) and hybrid models based on a combination of both (Konno et al. 1983; Cohen 1991). The basic difference between these groups is the theory on which they are formed. Statistical models use statistical functions such as truncated normal distribution curves to fit the daughter drop distribution resulting from a breakup event; phenomenological models are based on a balance of stresses existing at the drop surface and/or drop-eddy collisions probability; and the hybrid models use statistical approximations for the phenomenological models (Konno et al., 1980).

The number of droplets resulting from a single breakup event varies: it is either assumed a priori, or derived using empirical relations obtained from available experimental data. Binary breakage is most often assumed (Ruiz and Padilla, 2004). This assumption is not necessary restrictive since the breakage of a

parent drop in any number of daughter drops can be simulated efficiently by a rapid sequence of binary breakage events (Ruiz and Padilla, 2004).

The daughter size distribution of these models also varies. While some models predict minimum probability for equal size breakup (Tsouris and Tavlarides, 1994; Nambiar et al., 1992; Luo and Svendsen, 1996), others predict a maximum probability for equal breakup (Konno et al., 1980; Lee et al., 1987; Martinez-Bazan et al., 1999). Sathyagal and Ramkrishna (1996) and Kostoglou and Karabelas (1998) showed that the former model gives results that are radically different from experimentally observed distributions while the latter model is less intuitive because equal drop breakup requires more energy. These discrepancies are indicative of the variation in drop interactions, and the breakage mechanisms that exist for different liquid systems (Ruiz and Padilla, 2004).

Coalescence

Drop coalescence is a phenomenon that is commonly observed in drop dispersions suspended in fluid motion. It can be defined as a process resulting in the formation of larger drops from combining smaller drops. In simple terms, it can be understood as the reverse of the drop breakup process although the physics is quite different. Coalescence is determined by the collision between drops in motion, and since not all collisions result in coalescence, a measure of probability is used in defining the efficiency of the coalescence process. Therefore, two parameters are used in describing coalescence; collision rate and coalescence efficiency.

The collision rate is a measure of the frequency of collision experienced by the dispersed drops due to convection by eddies in the surrounding continuous fluid while the coalescence efficiency is the probability of coalescence per collision. The probability of coalescence in any drop collision event depends on the collision force, the cleanliness of the interface, and the contact time (Leng and

Calabrese, 2004). Leng and Calabrese (2004) also report that for two colliding drops, the continuous film between the drop surfaces must drain to a critical thickness before rupture and combination can occur, that is, the contact time for the collision event must exceed the time it takes for the film to drain to its critical thickness (the critical film drainage time).

However, drop coalescence is not a well understood field and research in this area is very limited. This is partly due to the difficulty of achieving an exclusive experimental study of drop coalescence without the interference of drop breakup events. It is more common, in practice, to eliminate the coalescence effect by using dispersions with very low dispersed phase fractions (typically $\varphi < 0.01$); where interactions between drops will be only drop breakup and coalescence is assumed negligible due to very few drop collision events (Ramkrishna, 1974; Lagisetty et al., 1986; Wang and Calabrese, 1986; Calabrese et al., 1986; Sathyagal and Ramkrishna, 1996). In this thesis, $\varphi \leq 0.01$ for all cases.

1.5 Dissolution

Mass transfer is typically observed in multi-component immiscible systems in which material transport is achieved over the contact surfaces. When material is transferred from one phase to another across the interface separating them, the resistance to mass transfer in each phase causes a concentration gradient. The concentrations of the diffusing material in the two phases immediately adjacent to the interface are unequal and can be related by the laws of thermodynamic equilibrium. It is assumed that thermodynamic equilibrium is reached at the interface almost immediately when the two phases are brought into contact (Knudsen et al., 1997). Figure 1-3 shows the concentration gradients near an interface. The direction of material transfer is from the dispersed phase to the continuous phase. From the figure, mass transfer can be represented as consisting of the following steps:

i. mass transfer from the bulk of the dispersed phase to the interface

ii. mass transfer across the interface

iii. mass transfer from the interface to the bulk of the continuous phase

The contribution of the resistance offered by the second step in the overall mass transfer process is usually considered negligible when compared to the resistance offered in transporting the solute to and away from the interface so the phase boundary is assumed to be in a state of thermodynamic equilibrium both with respect to composition and temperature (Sawistowski, 1983).

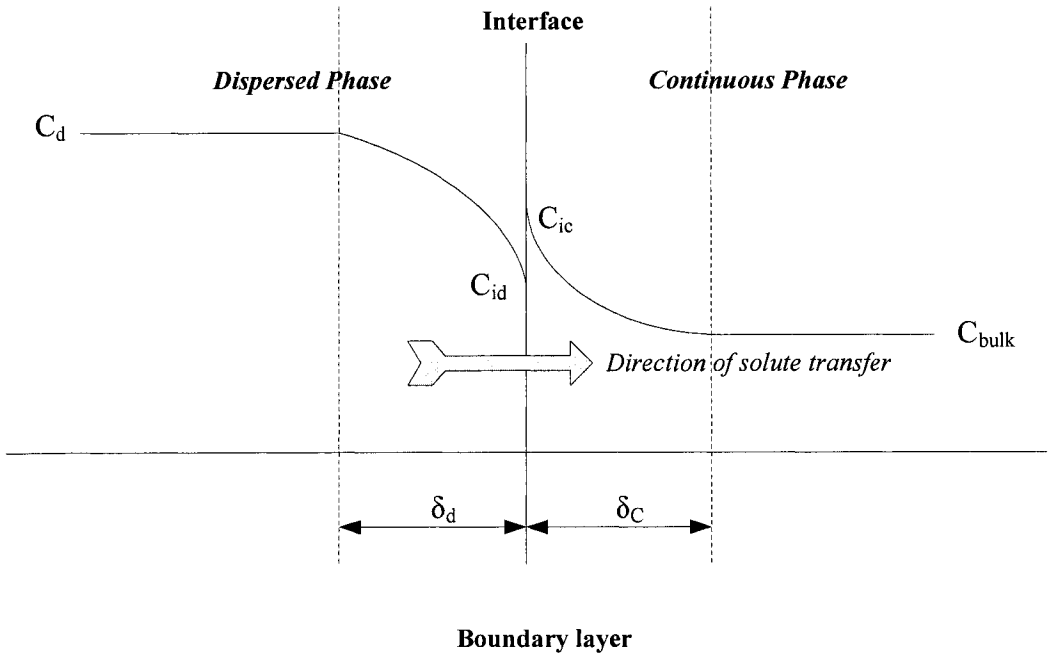

Figure 1-3: Concentration gradient near the interface of a 2-phase system

For solute transfer between immiscible liquids, there exists a concentration gradient within the dispersed drops due to the drop side resistance and the concentration profile is similar to Figure 1-3. Purely dissolving systems offer no drop side resistance and concentration gradient (Figure 1-4), thus the rate of mass

transfer is proportional to the difference between the bulk concentration, C_{bulk}, and the saturation concentration at the interface, C_S.

The mass transfer flux, N_A, for this case can then be written as

$$N_A \propto (C_S - C_{bulk}) \qquad (1.9)$$

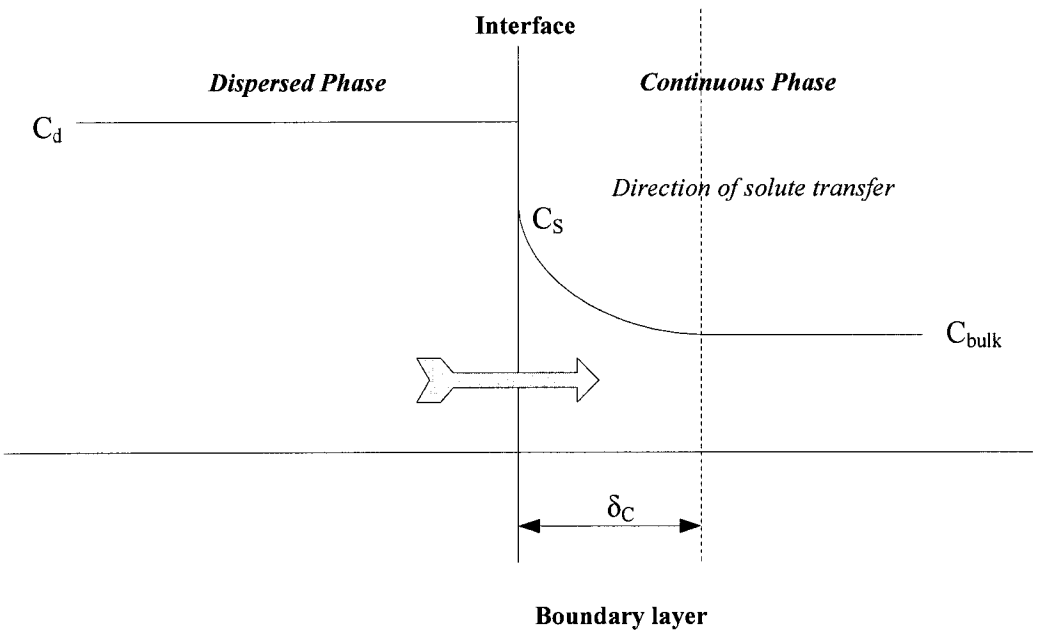

Figure 1-4: Concentration gradient near at the boundary layer

Equation (1.9) can be rewritten as an application of Fick's law to diffusion of the dispersed drop through the liquid film adhering closely to the dissolving drop.

$$N_A = \frac{D_{AB}}{\delta_C}(C_S - C_{bulk}) \qquad (1.10)$$

where D_{AB} is the molecular diffusivity through the boundary layer, δ_C is the thickness of the boundary layer, N_A, C_S, and C_{bulk} remains defined as above.

Equation (1.10) is qualitatively described as a ratio of the driving force, $(C_S - C_{bulk})$, to the resistance, $\frac{\delta_C}{D_{AB}}$, offered by the boundary layer at the interface. For turbulent systems, mass transfer is not only accomplished through molecular diffusion but can be enhanced by small eddies of the same scale as the particles (or drops in this case). The modified form of equation (1.10) is

$$N_A = \frac{D_{eff}}{\delta_C}(C_S - C_{bulk}) \qquad (1.11)$$

D_{eff} is the effective diffusivity comprising of molecular and eddy diffusion contributions.

Due to the difficulty inherent in the determination of the thickness of the boundary layer as an independent variable, it is included in the ratio $\frac{D_{eff}}{l}$, which is represented by the mass transfer coefficient, k_L. l is the characteristic length appropriate to the geometry of the system. The film thickness depends primarily on the hydrodynamics of the system (Wilhelm et al., 1941) and hence on the Reynolds number and the Schmidt number (Sawistowski, 1983). Thus, various correlations have been developed for different geometries in terms of the following dimensionless variables:

$$Sh = f(\mathrm{Re}\,Sc) \qquad (1.12)$$

$$Sh = A\,\mathrm{Re}^x\,Sc^y \qquad (1.13)$$

where Sh is the Sherwood number, Re is the Reynolds number, Sc is the Schmidt number, A is a constant and x and y are exponents that are determined empirically or by experiments.

Mass transfer coefficient

Correlations for mass transfer coefficients have an extensive bibliography. Numerous investigators have carried out studies to determine mass transfer coefficients both empirically and theoretically. Some of these studies are summarized in Perry's Handbook (Tables 5-21 to 5-28); Pangarkar et al (2002); Kumar and Hartland (1999).

The models, and hence the correlations, used in determining mass transfer coefficients depend on the type of phases involved, the specific geometry or type of stirred tank, the type of flow and the dispersed phase fraction. Some of the models available in the literature are based on the following theories:

- The film theory (Whitman, 1923) is based on the heat transfer analogy and assumes that mass transfer is achieved by diffusion through a stagnant film adjacent to the interface. Although this assumption is theoretically incorrect (Kumar and Hartland, 1999), it is an approximation that has been shown to give satisfactory results for low Schmidt numbers (Toor and Marchello, 1958).

- The penetration theory (Higbie, 1935) assumes that fluid elements are carried by turbulent eddies between the bulk of the fluid and the surface of the particle and that during the time the elements stay at the surface, transfer occurs through molecular diffusion. All elements are assumed to stay at the interface for the same time interval.

- The surface renewal theory (Danckwerts, 1951) is a modified form of the penetration theory. It is based on a random distribution of the residence

times of fluid elements at the interface with the probability of replacement of the fluid element assumed to be independent of its age.

Generally, mass transfer coefficients are represented by equation (1.13). Depending on the hydrodynamic conditions, the exponent n on the Schmidt number can vary between 1/3 and 0.5 such that in the relation $k_L \propto D_{AB}{}^q$, the variation of q is limited to a value between 0.5 and 0.67 (Sawistowski, 1983). The dependence of the mass transfer coefficient on particle size varies depending on the system considered and the tank and impeller geometries. Despite considerable literature on both theoretical and experimental studies of continuous phase mass transfer coefficient, there is no generally accepted correlation because of the peculiarities of different systems.

Only mass transfer correlations for pure dissolving solids or liquid-liquid extractions are available in the literature, and neither is perfectly suited to the study of pure dissolving drops. Solid dissolution correlations are usually expressed as a form of equation (1.14)

$$Sh = 2 + A\,\mathrm{Re}^m\, Sc^n \qquad (1.14)$$

Sawistowski (1983) observed that the use of equation (1.14) for drop dispersion systems is inaccurate. This is because the validity of equation (1.14) is restricted to solid spheres and the equation is a theoretical abstraction for a single particle in an infinite medium. Although both solid dissolution and drop dissolution result in the disappearance of the solute, they differ considerably on how the hydrodynamics within the stirred tank affects them. Drops are subjected to deformation, breakup, internal circulation and oscillation which result in higher mass transfer rates. Also, surface slip on the drops causes them to have higher slip velocities compared to the solid spheres.

However, compared to immiscible liquid-liquid systems, pure dissolving drops shrink until they disappear completely by dissolution while the former reaches equilibrium distribution after prolonged agitation. Also, pure dissolving drops have no mass transfer resistance on the drop side while immiscible liquid-liquid extraction systems present mass transfer resistances in both immiscible liquids.

The selection of an appropriate correlation for mass transfer coefficient is based on similarity of geometries, phases, and performance in the model. Table 1-1 shows a variation of -0.7 to 0.33 for the exponent on particle size for different solid-liquid and liquid-liquid extraction systems studied by several researchers. In view of the uncertainty on the exponent for drop size, several correlations will be compared to experimental data for this system.

Table 1-1: Particle size dependence for different mass transfer coefficient correlations

Researcher	System studied	Tank Configuration	Correlation for k_L	Exponent on d_p
Levins and Glastonbury (1972)	S-L[1]	Baffled tank with flat, curved, and pitched blade turbine impellers	if $\Delta\rho$ is not significant; $\left(2+0.44\left(\frac{d_p^{4/3}\varepsilon^{1/3}}{\nu}\right)^{0.62}\left(\frac{D}{T}\right)^{0.17}\left(\frac{\nu}{D_{AB}}\right)^{0.36}\right)\left(\frac{D_{AB}}{d_p}\right)$	-0.18
			if $\Delta\rho$ is significant; $\left(2+0.47\left(\frac{d_p u}{\nu}\right)^{0.5}\left(\frac{\nu}{D_{AB}}\right)^{0.38}\right)\left(\frac{D_{AB}}{d_p}\right)$	-0.5
Asai et al. (1988)	S-L	Baffled cylindrical flat bottomed stirred tank with turbine impeller	$\left(2^{5.8}+\left(0.61\left(\frac{\varepsilon^{1/3}d_p^{4/3}}{\nu}\right)^{0.58}\left(\frac{\nu}{D_{AB}}\right)^{0.33}\right)^{5.8}\right)^{1/5.8}\left(\frac{D_{AB}}{d_p}\right)$	-0.23
Miller (1971)	S-L	Baffled stirred tank with turbine impeller	$\left(2+0.222\left(\frac{\varepsilon^{1/3}d_p^{4/3}}{\nu}\right)^{4/3}\left(\frac{\nu}{D_{AB}}\right)^{0.33}\right)\left(\frac{D_{AB}}{d_p}\right)$	-0.7
Sano et al. (1974)	S-L	Baffled stirred tank with turbine impeller	$\left(2+0.4\left(\frac{d_p^{4/3}\varepsilon^{1/3}}{\nu}\right)^{0.62}\left(\frac{\nu}{D_{AB}}\right)^{0.33}\right)\phi\left(\frac{D_{AB}}{d_p}\right)$	-0.2

[1] S-L: Solid-Liquid dissolution

Kuboi (1974)	S-L	Baffled stirred tank with turbine impeller	$\left(2+0.49\left(\left(\frac{\varepsilon d_p^{\,4}}{\nu^3}\right)^{1/3}\left(\frac{\nu}{D_{AB}}\right)\right)^{0.5}\right)\left(\frac{D_{AB}}{d_p}\right)$	-0.33
Skelland and Moeti (1990)	L-L[2]	Six flat blade turbine in baffled stirred glass vessel	$\left(1.23x10^{-5}\left(\frac{D^2N}{\nu}\right)^{0.67}\left(\frac{D}{d_p}\right)^{2}\left(\frac{d_p}{T}\right)^{0.5}\left(\frac{DN^2}{g}\right)^{5/12}\left(\frac{\rho d_p^{\,2} g}{\sigma}\right)^{5/4}\left(\frac{\nu}{D_{AB}}\right)^{0.33}\phi^{-0.5}\right)\left(\frac{D_{AB}}{d_p}\right)$	0.0
Glen (1965)	L-L	Six blade disk turbine in baffled stirred tank	$\left(\frac{D^2N}{\nu}\right)\left(\frac{d_p}{D}\right)^{0.33}\left(\frac{\Delta\rho}{\rho_d}\right)^{5/4}\left(\frac{\nu}{D_{AB}}\right)^{0.33}\left(\frac{D_{AB}}{D}\right)$	0.33
Calderbank and Moo-young (1961)	G-L[3] studies compared with L-L data	Aerated mixing vessels and columns	$0.13\left(\frac{P}{V}\nu\right)^{0.25}\left(\frac{\nu}{D_{AB}}\right)^{-0.67}$ where $\frac{P}{V}=A\left(\frac{(g\Delta\rho)^{4/3}\mu^{1/3}}{\rho^{2/3}}\right)$	0.0
Boyadzhiev and Elenkov (1966)	L-L	Baffled stirred tank with turbine impeller	$0.65\left(\frac{D_{AB}u}{d_p}\right)^{0.5}\left(\frac{\nu}{D_{AB}}\right)^{-1/6}$	-0.5

[2] L-L: Liquid-liquid extraction

[3] G-L: Gas-Liquid

1.6 Conclusions

The fundamentals of liquid-liquid systems and the underlying theories describing the hydrodynamics and the nonhomogeneity in the stirred tank have been introduced. The spatial variations in turbulent conditions within the stirred tank affect the transient drop population behavior. Accurate modeling of the nonhomogeneity requires the utilization of local turbulent conditions in describing the mechanistic properties driving the drop size distribution. An experimental technique for measuring the drop population properties will be provided in Chapter 2 while the underlying assumptions and fundamentals for numerical modeling of liquid-liquid dispersion systems will be discussed in Chapter 3. Experimental validation of the numerical model will be given in Chapter 4, where the model is also used to provide a better understanding of the dissolution process.

1.7 References

Alopaeus V., Koskinen J., and Keskinen K. I., 1999, *Simulation of the Population Balances for Liquid-Liquid Systems in a Non-ideal Stirred Tank. Part 1: Description and Quantitative validation of the Model*, Chem. Eng. Sci., **54** (24), 5887 – 5899.

Arai K., Konno M., Matunaga Y., and Saito S., 1977, *Effect of Dispersed-phase Viscosity on Maximum Stable Drop Size for Breakup in Turbulent Flow,* J. Chem. Eng. Jpn., **10** (4), 325 – 330.

Attarakih M. M., Bart H. J., and Faqir N. M., 2004, *Numerical Solution of the Spatially Distributed Population Balance Equation Describing the Hydrodynamics of Interacting Liquid-liquid Dispersions,* Chem. Eng. Sci., **59** (12), 2567 – 2592.

Bajpai R. K., Ramkrishna D., and Prokop A., 1976, *Coalescence Redispersion Model for Drop Size Distributions in An Agitated Vessel,* Chem. Eng. Sci., **31** (10), 913 – 920.

Baldyga J., Podgorska W., and Pohorecki R., 1995, *Mixing-Precipitation Model with Application to Double Feed Semi Batch Precipitation,* Chem. Eng. Sci., **50** (8), 1281 – 1300.

Bhattacharya S., Kresta M. S., 2002, *CFD Simulations of Three-dimensional Wall Jets in a Stirred Tank,* Can. J. Chem. Eng., **80**, 1 - 15.

Bayens C. A., and Laurence R. L., 1969, *A Model for Mass Transfer in a Coalescing Dispersion,* Ind. & Eng. Chem. Fund., **8** (1), 71.

Berkman P. D., and Calabrese R. V., 1988, *Dispersion of Viscous-Liquids by Turbulent Flow in a Static Mixer,* AIChE J., **34** (4), 602 – 608.

Bradshaw P., 1975, *Complex Turbulent flows,* J. of Fluids Eng. – Trans. Of the ASME, **97** (2), 146 – 154.

Calabrese R. V., Chang T. P. K., Dang P. T., 1986, *Drop Breakup in Turbulent Stirred-Tank Contactors I: Effect of Dispersed-phase Viscosity,* AIChE J., **32** (4), 657 – 666.

Calabrese R. V., Wang C. Y., and Bryner N. P., 1986, *Drop Breakup in Turbulent Stirred-Tank Contactors III: Correlations for Mean Size and Drop Size Distribution,* AIChE J., **32** (4), 677 – 681.

Chapple D., Kresta S. M., Wall A, and Afacan A, 2002, *The Effect of Impeller and Tank Geometry on Power number for a Pitched Blade Turbine,* Chem. Eng. Res. & Des., **80** (A4), 364 – 372.

Chatzi E. G., and Kiparissides C., 1992, *Dynamic Simulation of Bimodal Drop Size Distributions in Low-Coalescence Batch Dispersion System,* Chem. Eng. Sci., **47** (2), 445 – 456.

Chen Z., Pruss J., and Warnecke H. J., 1998, *A Population Balance Model for Dispersed Systems: Drop Size Distribution in Emulsions,* Chem. Eng. Sci., **53** (5), 1059 – 1066.

Cohen R. D., 1991, *Shattering of a Liquid Drop due to Impact,* Proceedings of the Royal Society of London Series A – Mathematical, Physical and Engineering Sciences, **435** (1895), 483 – 503.

Coulaloglou C. A., and Tavlarides L. L., 1977, *Description of Interaction Processes in Agitated Liquid-liquid Dispersions,* Chem. Eng. Sci., **32** (11), 1289 – 1297.

Curl R. L., 1963, *Dispersed Phase Mixing I:Theory and Effects in Simple Reactors,* AIChE J., **9** (2), 175 – 181.

Cutter L. A., 1966, *Flow and Turbulence in a Stirred Tank,* AIChE J., **12** (1), 35.

Danckwerts P. V., 1951, *Absorption by Simultaneous Diffusion and Chemical Reaction into Particles of Various Shapes and into Falling Drops,* Transactions Of the Faraday Society, **47** (9), 1014 – 1023.

Davies J. T., 1972, Turbulence Phenomena: An Introduction to the Eddy Transfer of Momentum, Mass, and Heat, Particularly at Interfaces; Academic Press, London, Great Britain.

Diemer R. B., and Olson J. H., 2002, *A Moment Methodology for Coagulation and Breakage Problems: Part 3 – Generalized Daughter Distribution Functions,* Chem. Eng. Sci., **51** (19), 4187 – 4198.

Goodson M., and Kraft M., 2004, *Simulation of Coalescence and Breakage: An Assessment of Two Stochastic Methods Suitable for Simulating Liquid-liquid Extraction,* Chem. Eng. Sci., **59** (18), 3865 – 3881.

Grenville R. K., 1992, *Blending of viscous Newtonian and Pseudo-plastic Fluids,* Ph.D. Dissertation, Cranfield Institute of Technology, Cranfield Bedfordshire, England.

Hemrajani R. R., and Tatterson G. B., 2004, *Mechanical Stirred Vessels,* cited from: Handbook of Industrial Mixing: Science and Practice; Paul E. L., Atiemo-Obeng V. A., and Kresta S. M., Eds.; John Wiley & Sons, Inc: Hoboken, New Jersey; 345 - 390.

Hemsing J. L., 2001, *Kinetics of Blending for Soluble Polymer Additives*, M.Sc. Dissertation, Department of Chemical & Materials Engineering, University of Alberta, Canada.

Higbie R., 1935, *The Rate of Absorption of a Pure Gas into a still Liquid during Short Periods of Exposure,* Trans. Of the American Inst. Of Chem. Eng., **31**, 365 – 389.

Hinze J. O., 1955, *Fundamentals of the Hydrodynamics Mechanisms of Splitting in Dispersion Process*, AIChE J., **1** (3), 289 – 295.

Hoogendoorn C. J., and Den Hartog A. P., 1967, *Model Studies on Mixers in Viscous Flow Region,* Chem. Eng. Sci., **22** (12), 1689.

Hounslow M. J., Ryall R. L., and Marshall V. R., 1988, *A Discretized Population Balance for Nucleation, Growth and Aggregation*, AIChE J., **34** (11), 1821 – 1832.

Hsia M. A, and Tavlarides L. L., 1980, *A Simulation Model for Homogeneous Dispersions in Stirred Tanks,* Chem. Eng. J. & BioChem. Eng. J., **20** (3), 225 – 236.

Hsia M. A, and Tavlarides L. L., 1983, *Simulation Analysis of Drop Breakage, Coalescence and Micromixing in Liquid-liquid Stirred Tanks,* Chem. Eng. J. & BioChem. Eng. J., **26** (3), 189 – 199.

Hulburt H. M., and Katz S., 1964, *Some Problems in Particle Technology – A Statistical Mechanical Formulation,* Chem. Eng. Sci., **19** (8), 555 – 574.

Jaworski Z., and Fort I, 1991, Studies on Mixing .79.: *Energy Dissipation Rate in a Baffled Vessel with Pitched Blade Turbine Impeller*, Collection of Czechoslovak Chem. Comm., **56** (9), 1856 – 1867.

Jaworski Z., Nienow A. W., and Dyster K. N., 1996, *An LDA Study of the Turbulent Flow Field in a Baffled Vessel Agitated by An Axial, Down-pumping Hydrofoil Impeller*, Can. J. Chem. Eng. **74** (1), 3 – 15.

Jeon Y. M., and Lee W. K., 1986, *A Drop Population Balance Model for Mass Transfer in Liquid-liquid Dispersion I: Simulation and Its Results,* Ind. & Eng. Chem. Fund., **25** (2), 293 – 300.

Kennedy C., 2003, *Mixing, Precipitation and coagulation with Alum*, M.Sc. Dissertation, Department of Chemical & Materials Engineering, University of Alberta, Canada.

Khang S. J., and Levenspiel O., 1976, *Mixing-Rate Number for Agitator-Stirred Tanks,* Chem. Eng., **83** (21), 141 – 143.

Knudsen J. G., Hottel H. C., Sarofim A. F., Wankat P. C., and Knaebel K. S., 1997, *Heat and Mass Transfer,* cited from: Perry's Chemical Engineers' Handbook, 7th Ed., Perry R. H., and Green D. W., eds., McGraw-Hill.; Section 5.

Kolmogorov A. N., 1949, *On the Breakage of Drops in a Turbulent Flow*, Dokl. Akad. Navk. SSSR **66** (5), 825 – 828.

Konno M., Aoki M., and Saito S., 1983, *Scale Effect on Breakup Process in Liquid-liquid Agitated Tanks,* J. Chem. Eng. Jpn., **16** (4), 312 – 319.

Konno M., Arai K., and Saito S., 1977, *Effects of Viscous and Inertial Forces on Drop Breakup in An Agitated Tank,* J. Chem. Eng. Jpn., **10** (6), 474 – 477.
Konno M., Matsunaga Y., Arai K., and Saito S., 1980, *Simulation Model for Breakup Process in An Agitated Tanks*, J. Chem. Eng. Jpn., **13** (1), 67 – 73.

Kostoglou M., and Karabelas A. J., 1997, *An Explicit Relationship Between Steady State Size Distribution and Breakage Kernel for Limited Breakage Processes,* J. of Physics A – Math. & General, **30** (20), L685 – L691.

Kostoglou M., and Karabelas A. J., 1998, *Theoretical Analysis of the Steady State Particle Size Distribution in Limited Breakage Processes,* J. of Physics A – Math. & General, **31** (44), 8905 – 8921.

Kostoglou M., Dovas S., and Karabelas A. J., 1997, *On the Steady-State Size Distribution of Dispersions in Breakage Processes,* Chem. Eng. Sci., **52** (8), 1285 – 1299.

Kramers H., Baars G. M., and Knoll W. H., 1953, *A Comparative Study on the Rate of Mixing in Stirred Tanks,* Chem. Eng. Sci., **2** (1), 35 – 42.

Kresta S. M., 1998, *Turbulence in Stirred Tanks: Anisotropic, Approximate, and Applied*, Can. J. Chem. Eng. **76** (3), 563 – 576.

Kresta S. M., and Wood P. E., 1991, *Prediction of the 3-Dimensional Turbulent Flow in Stirred Tanks,* AIChE J., **37** (3), 448 – 460.

Kresta S. M., and Wood P. E., 1993, *The Mean Flow Field Produced by a 45° Pitched Blade Turbine – Change in the Circulation Pattern due to Off-Bottom Clearance*, Can. J. Chem. Eng. **71** (1), 42 – 53.

Kresta S., Anthieren G., and Parsiegla K., 2005, *Model reduction for Prediction of Silver Halide Precipitation*, Chem. Eng. Sci., **60** (8/9), 2135 – 2153.

Kumar A., and Hartland S., 1999, *Correlations for Prediction of Mass Transfer Coefficients in Single Drop Systems and Liquid-Liquid Extraction Columns*, Chem. Eng. Res. & Des., **77** (A5), 372 – 384.

Kumar S., and Ramkrishna D., 1996, *On the Solution of Population Balance Equations by Discretization I & II,* Chem. Eng. Sci., **51** (8), 1311 – 1342.

Lagisetty J. S., Das P. K., and Kumar R., 1986, *Breakage of Viscous and Non-Newtonian Drops in Stirred Dispersions,* Chem. Eng. Sci., **41** (1), 65 – 72.

Lasheras, J.C., Eastwood, C., Martinez-Bazan, C., Montanes, J.L., 2002, *A Review of Statistical Models for the Break-up of an Immiscible Fluid Immersed into a Fully Developed Turbulent Flow*, International Journal of Multiphase Flow, **28**, 247-278.

Lee C. H., Erickson L. E., and Glasgow L. A., 1987, *Dynamics of Bubble Size Distribution in Turbulent Gas-Liquid Dispersions*, Chem. Eng. Comm., **61** (1/6), 181 – 195.

Lee G., Yoon E. S., Lim Yi, Le Lann J. M., Meyer X. M., and Joulia X., 2001, *Adaptive Mesh Method for the Simulation of Crystallization Processes including Agglomeration and Breakage: Potassium Sulfate System,* Ind. & Eng. Chem. Res., **40** (26), 6228 – 6235.

Lehr F., and Mewes D., 2001, *A Transport Equation for the Interfacial Area Density Applied to Bubble Columns,* Chem. Eng. Sci., **56** (3), 1159 – 1166.

Lehr F., Milles M., and Mewes D., 2002, *Bubble-Size Distributions and Flow Fields in Bubble* AIChE J., **48** (11), 2426 – 2443.

Leng D. E., and Calabrese R. V., 2004, *Immiscible Liquid-liquid Systems,* cited from: Handbook of Industrial Mixing: Science and Practice; Paul E. L., Atiemo-Obeng V. A., and Kresta S. M., Eds.; John Wiley & Sons, Inc: Hoboken, New Jersey; 639 - 753.

Luo H., and Svendsen F., 1996, *Theoretical Model for Drop and Bubble Breakup in Turbulent Dispersions*, AIChE J., **42** (5), 1225 – 1233.

Maggioris D., Goulas A., Alexopoulos A. H., Chatzi E. G., and Kiparissides C., 2000, *Prediction of Particle Size Distribution in Suspension Polymerization Reactors: Effect of Turbulence Nonhomogeneity*, Chem. Eng. Sci., **55** (20), 4611 – 4627.

Mahoney A. W., and Ramkrishna D., 2002, *Efficient Solution of Population Balance Equations with Discontinuities by Finite Elements,* Chem. Eng. Sci., **57** (7), 1107 – 1119.

Marchal P., David R., Klein J. P., Villermaux J., 1988, *Crystallization and Precipitation Engineering 1: An Efficient Method for Solving Population Balance in Crystallization with Agglomeration*, Chem. Eng. Sci., **43** (1), 59 – 67.

Martinez-Bazan C., Montanes J. L., and Lasheras J. C., 1999, *On the Breakup of An Air Bubble Injected into a Fully Developed Turbulent Flow I & II,* J. Of Fluid Mech., **401**, 157 – 207.

Nambiar D. K. R., Kumar R., Das T. R., and Gandhi K. S., 1992, *A New Model for the Breakage Frequency of Drops in Turbulent Stirred Dispersions,* Chem. Eng. Sci., **47** (12), 2989 – 3002.

Norwood K. W., and Metzner A. B., 1960, *Flow Patterns and Mixing Rates in Agitated Vessels,* AIChE J., **6** (3), 432 – 437.

Pangarkar V. G., Yawalkar A. A., Sharma M. M., and A. A. C. M. Beenackers, 2002, *Particle-Liquid Mass Transfer Coefficient in Two-/Three-Phase Stirred tank Reactors*, Ind. Eng. Chem. Res., **41** (17), 4141 – 4167.

Park, J. Y., and Blair, L.M., 1975, *The Effect of Coalescence on Drop Size Distribution in an Agitated Liquid-Liquid Dispersion*, Chem. Eng. Sci., **30** (9), 1057 – 1064.

Perry's Chemical Engineers' Handbook, 1997, 7th Ed., Perry R. H., and Green D. W., eds., McGraw-Hill.

Prince M. J., and Blanch H. W., 1990, *Bubble Coalescence and Breakup in Air-Sparged Bubble Columns,* AIChE J., **36** (10), 1485 – 1499.

Ramkrishna D., 1974, *Drop-Breakage in Agitated Liquid-liquid Dispersions,* Chem. Eng. Sci., **29** (4), 987 – 992.

Ramkrishna D., 2000, Population Balances: Theory and Applications to Particulate Systems in Engineering; Academic Press, San Diego, USA.

Ranade V. V., and Joshi J. B., 1989, *Flow Generated by Pitched Blade Turbines I: Measurements Using Laser Doppler Anemometer,* Chem. Eng. Comm., **81**, 197 – 224.

Ruiz M. C., and Padilla R., 2004, *Analysis of Breakage Functions for Liquid-liquid Dispersions,* Hydrometallurgy, **72** (3-4), 245 – 258.

Rushton J. H., Costich E. W., and Everett H. J., 1950, *Power Characteristics of Mixing Impellers,* Chem. Eng. Prog., **46** (8), 395 – 404.

Sarimeseli A., and Kelbaliyev G., 2004, *Modeling of the Breakup of Deformable Particles in Developed Turbulent Flow,* Chem. Eng. Sci., **59** (6), 1233 – 1240.

Sastry K. V. S., and Gaschignard P., 1981, *Discretization Procedure for the Coalescence Equation of Particulate Processes,* Ind. & Eng. Chem. Fund., **20** (4), 355 – 361.

Sathyagal A. N., and Ramkrishna D., 1996, *Droplet Breakage in Stirred Dispersions: Breakage Functions from Experimental Drop Size Distribution,* Chem. Eng. Sci., **51** (9), 1377 – 1391.

Sawistowski H., 1983, *Physical Aspects of Liquid-liquid Extraction,* cited from: Mass Transfer with Chemical Reaction in Multiphase Systems, **I**: Two-Phase Systems; Alper Erdogan, Ed.; Martinus Nijhoff Publishers: The Hague; 613 – 635.

Senichev V. Y., Tereshatov V. V., 2001, *General Principles Governing Dissolution of Materials in Solvents,* cited from: Handbook of Solvents; Wypych G., Ed.; ChemTec Publishing; Section 4.

Shah B. H., Ramkrishna D., and Borwanker J. D., 1977, *Simulation of Particulate Systems Using Concepts of Interval of Quiescence,* AIChE J., **23** (6), 897 – 904.

Shinnar R., 1961, *On the Behaviour of Liquid Dispersions in Mixing Vessels,* J. of Fluid Mech., **10** (2), 259.

Skelland A. H. P., and Kanel J. S., 1992, *Simulation of Mass Transfer in a Batch Agitated Liquid-Liquid Dispersion,* Ind. Eng. Chem. Res., **31** (3), 908 – 920.

Spielman L. A., and Levenspiel O., 1965, *A Monte Carlo Treatment for Reacting and Coalescing Dispersed Phase Systems,* Chem. Eng. Sci., **20** (3), 247

Tennekes H., and Lumley J. L., 1972, A First Course in Turbulence, MIT Press, Cambridge, MA, USA.

Toor H. L., and Marchello J. M., 1958, *Film-Penetration Model for Mass and Heat Transfer,* AIChE J., **4** (1), 97 – 101.

Tsouris C., and Tavlarides L. L., 1994, *Breakage and Coalescence Models for Drops in Turbulent Dispersions*, AIChE J., **40** (3), 395 – 406.

Valentas S. K., and Amundson N. R., 1966, *Breakage and Coalescence in Dispersed Phase Systems,* Ind. & Eng. Chem. Fund., **5** (4), 533.

Valentas S. K., Bilous O., and Amundson N. R., 1966, *Analysis of Breakage in Dispersed Phase Systems,* Ind. & Eng. Chem. Fund., **5** (2), 271.

Wang C. Y., and Calabrese R. V., 1986, *Drop Breakup in Turbulent Stirred-Tank Contactors II: Relative Influence of Viscosity and Interfacial-Tension,* AIChE J., **32** (4), 667 – 676.

Whitman W. G., 1923, *The Two-Film Theory of Gas Absorption,* Chem. & Met. Eng., **29** (4), 146 – 148.

Wilhelm R. H., Conklin L. H., and Sauer T. C., 1941, *Rate of Solution of Crystals,* Ind. & Eng. Chem., **33**, 453 – 457.

Zimmermann A., Joulia X., Gourdon C., and Gorak A., 1995, *Maxwell-Stefan Approach in Extractor Design,* Chem. Eng. J. & BioChem. Eng. J., **57** (2), 229 – 236.

Chapter 2

Experimental

2.1 Introduction[§]

Unit operations such as extractions, multiphase reactions and suspension polymerizations which are commonly found in the process industry are designed on the principle of material exchange between contacting immiscible liquids. For phases that are not in equilibrium, the rate of mass transfer and/or chemical reaction is greatly influenced by the available interfacial area between the phases and the deviation from equilibrium (i.e. the chemical potential between the two phases). Investigations into the mass transfer kinetics in a system require simultaneous measurements of the concentration of the dissolving component, or solute, and the interfacial area. The drop size distribution defines the available interfacial area for mass transfer while the solute concentrations define the extent of deviation from equilibrium. Accurate measurement of these parameters is crucial to successful modeling of the dissolution process and determination of the overall mass transfer coefficient, k_L.

In the next chapter, a mathematical model predicting the transient drop size distribution and dispersed phase concentration in the continuous phase will be discussed. In this chapter, a description of the experimental methodology employed in the simultaneous measurements of the transient droplet size distribution of pure solute and concentration of the dissolving component in the

[§] The experimental design, procedure and results discussed in this chapter were done primarily by Ahmed Fall, a post doctoral fellow who started this investigation.

continuous phase is provided. A description of the experimental design and the apparatus used to achieve this are also provided. The theory of the Phase Doppler Particle Analyzer (PDPA) used for droplet size and velocity measurements, and the gas chromatograph (GC) used for concentration measurements will be discussed in turn.

2.2 Mixing Tank and Impeller Geometry

Figure 2-1 shows the geometry of the impeller and mixing tank used in this experimental investigation. A flat bottomed cylindrical glass tank is enclosed (centrally) in a flat bottomed, square, glass tank and the space between the tanks is filled with tap water to a height above the liquid height in the mixing tank. This is done to ensure that refractive effects at curved surfaces are reduced significantly. The mixing tank diameter and the liquid height in it are equal, i.e. $H = T = 145mm$. Four equally spaced baffles ($w = T/10$) are placed around the periphery of the mixing tank while agitation is provided by a four-bladed, down-pumping, stainless steel 45° Pitched Blade Turbine (PBT) impeller, with a diameter ($D = T/3$) placed at an off-bottom clearance equal to the impeller diameter $C/D (= 1.0)$. The impeller speeds used for this experimental work were $550rpm$, $650rpm$ and $750rpm$; all higher than the minimum impeller speed required for turbulent flow for this configuration ($510rpm$). The impeller shaft is placed on the axis of the mixing tank to ensure that well defined hydrodynamic

conditions prevail through out the mixing tank. A $3mm$ internal diameter feed tube, made of stainless steel, placed at an offset of $20mm$ from the impeller shaft and $40mm$ above the impeller blades is used to feed the dispersed phase.

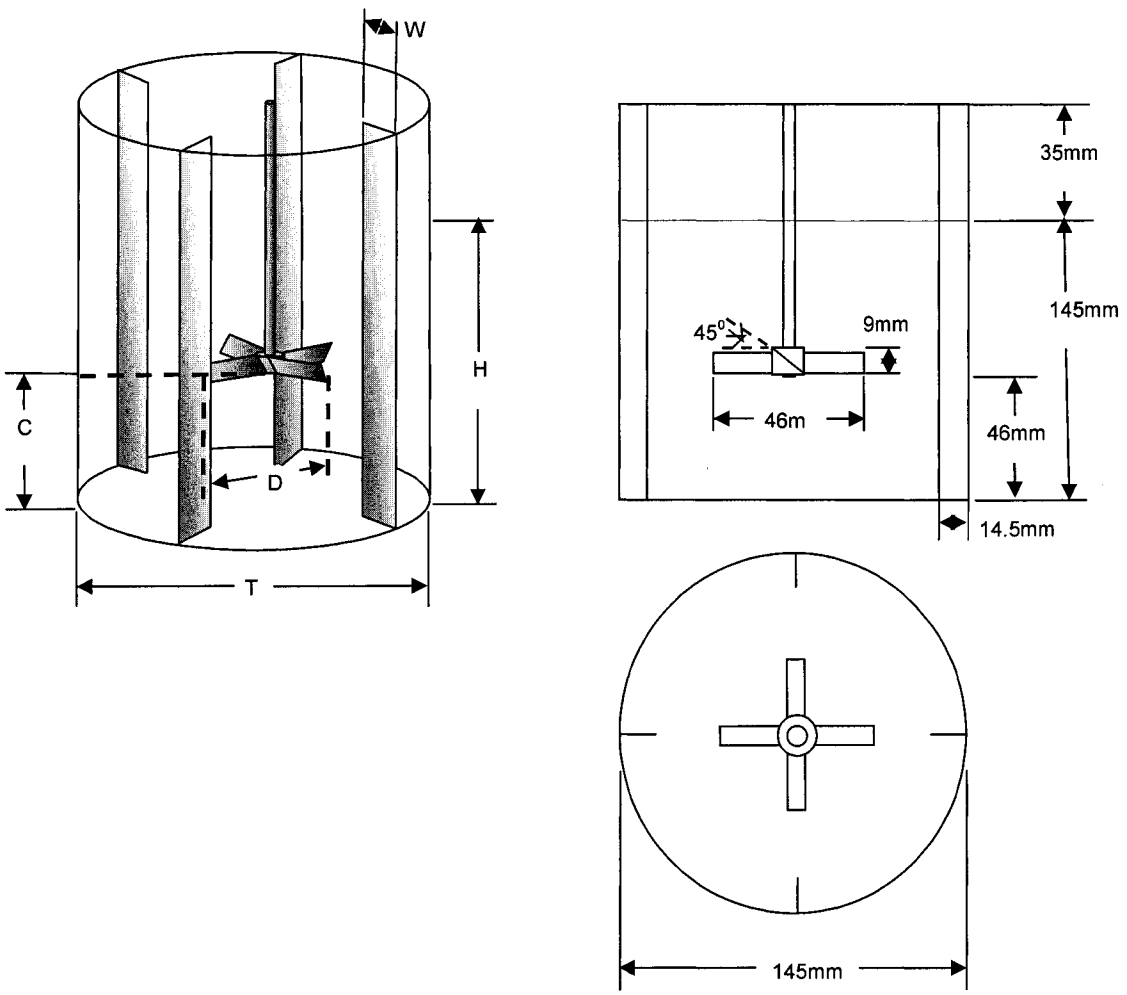

Figure 2-1: Tank and Impeller geometry

2.3 Gas Chromatograph

The Gas Chromatograph (GC) is widely used in industry to measure concentrations of volatile liquids and gaseous compounds. The components of a volatile or gaseous compound are separated based on their molecular weight and diffusivity to obtain the concentration in an unknown sample.

2.3.1 Overview

The GC operates on a chromatographic principle and is used in separation processes involving volatile organic compounds. The separation is based on the differences in partitioning behavior – distribution of the solute phase – between the flowing mobile gas phase and the stationary phase in the separation column. The low molecular weight components with high rates of molecular diffusivity travel faster than the high molecular weight components with lower molecular diffusivities. A simplified block diagram of the GC is shown in Figure 2-2. In its simplest form, the GC consists of a flowing mobile phase, an injection port, a separation column containing the stationary phase, a detector and a recorder or data system. An inert gas such as Argon or Helium is used as the carrier gas or mobile phase while a liquid on solid support is used as the stationary phase in most columns. The injection port consists of a rubber septum through which a syringe needle is inserted to inject the sample. The injection port is maintained at a higher temperature than the boiling point of the least volatile component in the sample mixture. The separation column is usually contained in a temperature-controlled oven because the partitioning behavior is temperature dependent. For component mixtures with a wide range of boiling points, separation is achieved by progressively increasing the oven temperature to elute the high-boiling point components. The vaporized sample is carried through the column to a detector which signals the chart recorder to report the response. Ideally, this chromatogram appears as Gaussian peaks.

The chromatogram from the GC is integrated to obtain the relative composition of the components in a sample mixture.

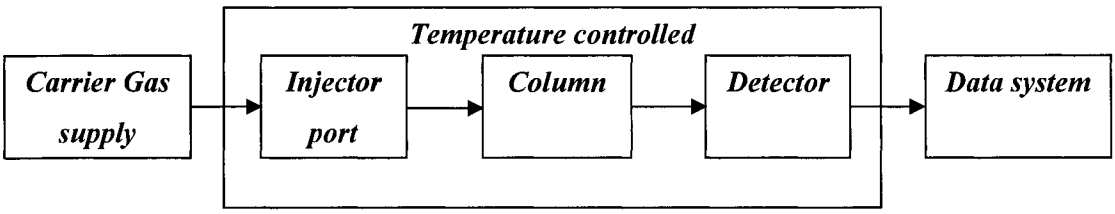

Figure 2-2: Simplified block diagram of the GC

2.3.2 Calibration

Calibration of the GC is performed to establish a correlation between the concentrations of diethyl malonate in Deionized Ultra Filtered (DIUF) water and the chromatograms obtained from the recorder. The use of an internal standard to compensate for the variable injection volumes inherent in the GC is a common practice, and for our case 2-Butanone is employed as the internal standard. Quantification of the relative amounts of each component in a sample is done by analyzing the peak area in the chromatogram. A larger peak area indicates a larger amount of the corresponding analyte.

The calibration curve is obtained using a constant concentration for 2-Butanone and varying the concentration of diethyl malonate over the range of concentration expected. A plot of the ratio of the area of the diethyl malonate to the area of 2-Butanone on the x-axis and the corresponding concentration of the diethyl malonate on the y-axis gives the calibration curve. This plot is presented in Figure 2-3 below. The calibration curve shows a linear relationship between the diethyl malonate concentration and the area ratio with a correlation coefficient of

0.99. This calibration curve was used in subsequent determinations of diethyl malonate concentrations in unknown samples collected from the mixing tank.

The specifications of the GC are presented in Table 2-1

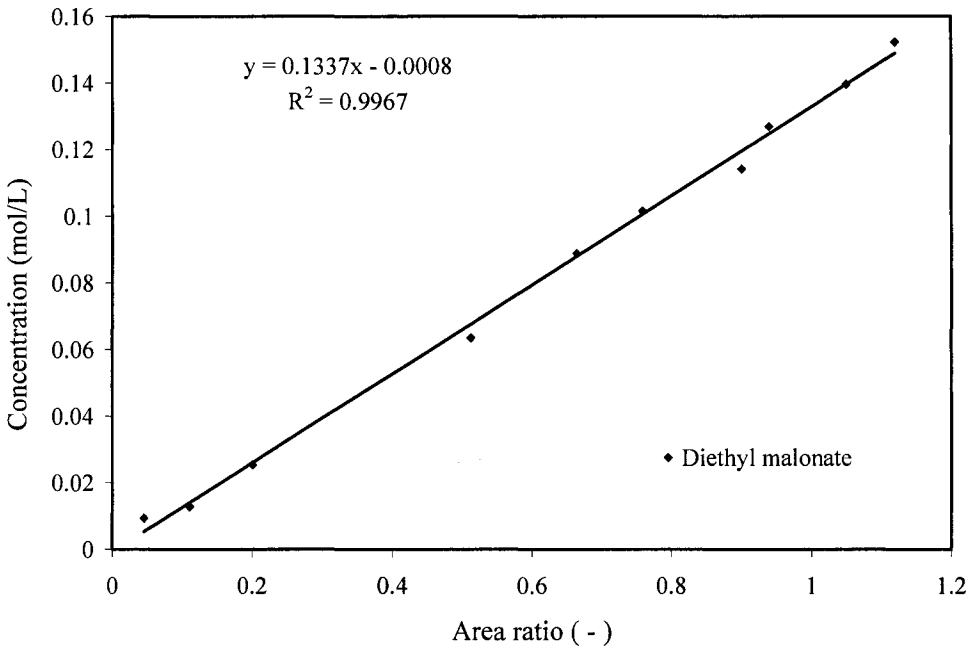

Figure 2-3: GC calibration curve for Diethyl malonate

Table 2-1: GC Equipment specifications

Final Temperature (°C)	*Final Time (min)*	*Stop Time (min)*	*Detector Temperature (°C)*	*Injector Temperature (°C)*
111	0	16	200	150

2.4 Phase Doppler Particle Analyser (PDPA)

The PDPA is an extension of Laser Doppler Velocimetry (LDV) and is used for simultaneous measurement of drop diameter and one of the three components of velocity for small droplets. When the PDPA is used in size and velocity measurements, the instrument is in PDPA mode. However, when it is used for velocity measurements, it is in LDV mode. The PDPA is finding increasing use in the field of fluid dynamics because it is non-intrusive on the flow field and provides very high resolution when used in drop size distribution measurement.

2.4.1 Overview

The PDPA consists of a laser-based optical transmitter and receiver; an electronic signal processor and software for data acquisition and analysis (see Figure 2-4).

The PDPA is based upon the principles of light scattering interferometry. It uses a low power laser that is split into two beams by a beam splitter and a frequency module (Bragg cell). Measurements are made at an optical probe volume defined by the intersection of the two Gaussian laser beams. The intersection of the two beams creates a fringe pattern within the optical probe volume. As a particle passes through the optical probe volume, it scatters light from the beams and receiving lenses located at an off-axis collection angle collect the scattered light beams. All the collected signals have a frequency which is proportional to the particle velocity. The phase shift between a pair of signals at two different collection angles is related to the diameter of the spherical particle.

The PDPA requires no calibration because the particle size and velocity are dependent only on the laser wavelength and optical configuration. PDPA measurements are not based upon the scattered light intensity and, consequently,

are not subject to errors from beam attenuation or deflection, which occur in dense particle and combustion environments.

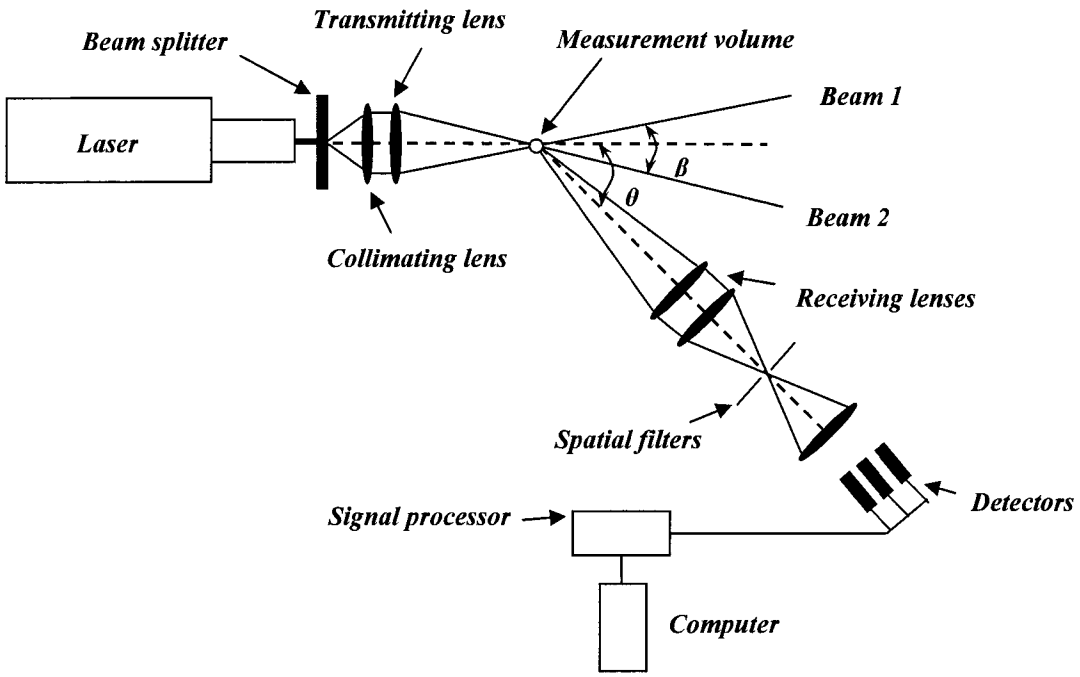

Figure 2-4: Schematic of Phase Doppler Particle Analyzer (PDPA)

2.4.2 Optical Configuration

The PDPA parameter specifications used in this study are summarized in Table 2-2 below. Zhou (1997) verified and optimized the specifications for accurate drop size measurements for this instrument.

Table 2-2: PDPA equipment specification

Voltage (V)	*Track Number (-)*	*Position of Receiver (°)*	*Focal Length (mm)*		*Diameter Measurement range (μm)*	
			Transmitter	Receiver	Minimum	Maximum
721	1	22.5	500	500	1.1	338

2.5 Materials and Methods

2.5.1 System studied

Liquid-liquid systems are a mixture consisting of two parts, the continuous phase and the dispersed phase. The dispersed phase is the liquid which is dispersed in the continuous phase as droplets.

The use of optical equipment for the measurement of drop size distributions puts some constraints on the specification of continuous and dispersed phases. In the case of the PDPA, the liquid system selected has to be transparent for good optical resolution. The ratio of refractive indices between the continuous phase and the dispersed phase is also an important factor affecting the Doppler signal quality. A large ratio reduces the forward scattering signal strength while a low ratio reduces the signal quality. Also, for a uniform dispersion within the stirred tank, the liquids must have comparable densities and be non-sticky.

The continuous phase for this study was Deionized Ultra Filtered (DIUF) water. DIUF water is transparent and is preferred to tap water because it is free of particulate matter that would contaminate the measured drop size distribution. The dispersed organic phase selected for this study is diethyl malonate. The physical properties of diethyl malonate are presented in Table 2-3.

Table 2-3: Physical properties of Diethyl malonate

Organic phase	*Solubility in water (g/100ml) at 20°C*	*Density (g/cm^3)*	*Surface Tension (dyne/cm)*	*Viscosity (cP)*	*Refractive Index*	*Appearance*
Diethyl malonate	2.7	1.055	31.83	2.15	1.41	Colorless

2.5.2 Procedure

The experimental setup is shown in Figure 2-5. It consists of the following sections: weighing, pumping, mixing tank, PDPA and GC. A sample of diethyl malonate is weighed and pumped into the tank. The impeller rotational speed is fixed for each experimental run.

The experimental procedure is described below:

- All pieces of equipment (mixing tanks, impellers, syringes) were washed with warm water and dried.
- 2 liters of Deionized Ultra-Filtered (DIUF) water was measured and poured into the mixing tank containing the baffles. The mixing tank with the DIUF water and baffles was placed inside an outer square tank, which contains tap water to a level above the liquid height in the mixing tank to minimize refraction effects.
- A constant impeller speed required to achieve turbulence in the mixing tank was specified. For the experimental runs considered, 550 rpm, 650 rpm and 750 rpm were used.
- About 60ml of diethyl malonate was poured into a beaker and placed on the weighing balance and an initial weight of diethyl malonate was taken. Nose mask and hand gloves are required when handling diethyl malonate.

- 25ml of diethyl malonate was pumped into the mixing tank containing the DIUF water and the final weight of diethyl malonate in the beaker was measured. The mass of diethyl malonate added into the mixing tank was computed by difference. The feed time for 25 ml diethyl malonate was 20 seconds.
- At intervals of 20 seconds, simultaneous drop size and concentration measurements were taken. The PDPA was used for continuous drop size measurements. Samples were taken for GC analysis from the mixing tank using a 2mm pipette. The pipette was placed 2-3 cm above the impeller blade in a vertically erect position and care was taken to avoid any external agitation using the pipette.
- The collected samples were discharged into small sampling bottles inclined at 45° to the horizontal axis on a rack and allowed to settle for about 10 mins. This angle of tilt ensures faster settling times and separation of the drops from the continuous phase.
- Using a micropipette, 1.2 ml of the continuous (water) phase was collected into a clean sampling bottle.
- 0.02 ml of 2-butanone (internal standard) was added to the sample and vigorously mixed for about 30 seconds. 2-butanone is hygroscopic and must not be exposed to air for prolonged periods. The same safety precautions should be used in handling 2-butanone as with diethyl malonate.
- The syringe was flushed at least 10 times with samples from the mixture to ensure there were no bubbles in the syringe. 0.6 ml of the mixture was then injected into the septum of the GC.
- The GC integrator was stopped after 16 mins – longer than the retention time of diethyl malonate in the GC.
- The experimental set up, along with the syringes and beakers, was cleaned and dried in preparation for another experimental run.

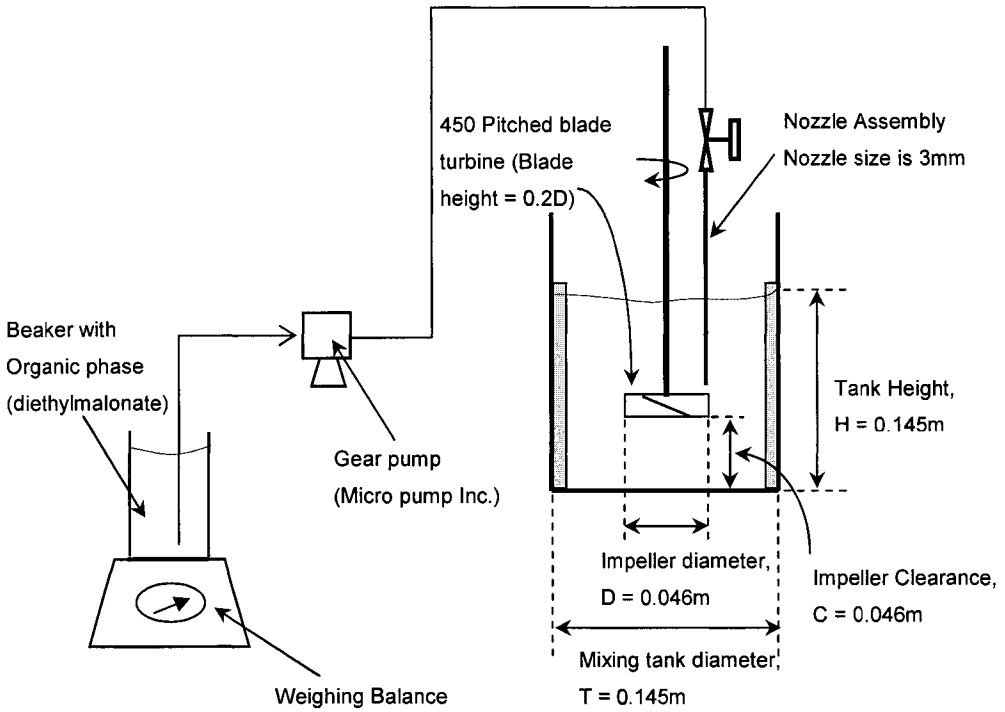

Figure 2-5: Experimental Set-up

2.6 Bibliography

Drain L.E., 1986, The Laser Doppler Technique, John Wiley & Sons, Chichester Great Britain.

Grehan G., Gouesbet G., Naqwi A., and Durst F., 1993, *Particle Trajectory Effects in Phase Doppler Systems: Computations and Experiments,* Part. Part. Syst. Charact., **10**, 332 - 338.

Naqwi A. A., 1994, *Innovative Phase Doppler Systems and their Applications*, Part. Part. Syst. Charact., **11**, 7 - 21.

Zhou G., 1997, *Characteristics of Turbulence Energy Dissipation and Liquid-Liquid Dispersions in An Agitated Tank*, Ph.D. Dissertation, Department of Chemical & Materials Engineering, University of Alberta, Canada.

Zhou G., and Kresta S.M., 1998, *Evolution of Drop Size Distribution in Liquid-Liquid Dispersions for various Impellers*, Chem. Eng. Sci., **53** (11), 2101 - 2105.

Chapter 3

Model Development

3.1 Model Overview

The model developed to predict the dissolution kinetics and drop size distribution properties of liquid-liquid systems operated in the turbulent regime under isothermal conditions will be discussed in this chapter. Due to the complexities of the flow and the inhomogeneity of turbulence in different regions of the stirred tank, the use of models that assume homogeneous properties throughout the mixing tank would clearly be oversimplified. Also, a comprehensive and detailed discretization of the mixing tank into the tiny cells (grids) required for CFD would require a lot of computational time and resources with a precision that far exceeds the accuracy of the breakup and dissolution equations. However, a compromise can be achieved by reducing the number of discretized regions to the extent that the local regions where steep variations have been reported can be well represented. An approach such as this will both save on the computational time and resources and accurately capture the inhomogeneity in the mixing tank.

The modeling approach used here is the zone-model, which uses zones to represent regions where significant variations in local hydrodynamic properties exist within the mixing tank. In each zone, the turbulence and flow properties will be defined, the mechanisms which determine the drop size distribution will be modeled using published correlations; and the resulting transient drop size population balances will be solved numerically.

The codes are written in FORTRAN 90 and implemented on the Compaq Visual Fortran platform. The model program is structured in modules and subroutines to facilitate easier program maintenance and debugging to accommodate the inclusion and/or removal of individual components of the program and to improve the general esthetics and presentation of the program.

Figure 3-1 gives the structure of the model in its basic form showing the ***mixing (Eulerian) field***, the ***drop tracking (Lagrangian)*** approach used in solving the differential equations for each drop class size, the ***mechanistic models*** for drop size evolution and the ***numerical solution strategy*** used in implementing the numerical solution scheme. The development of each basic component will be described in future sections and the logic flow diagram showing the integration of all these components is presented in Figure 3-23.

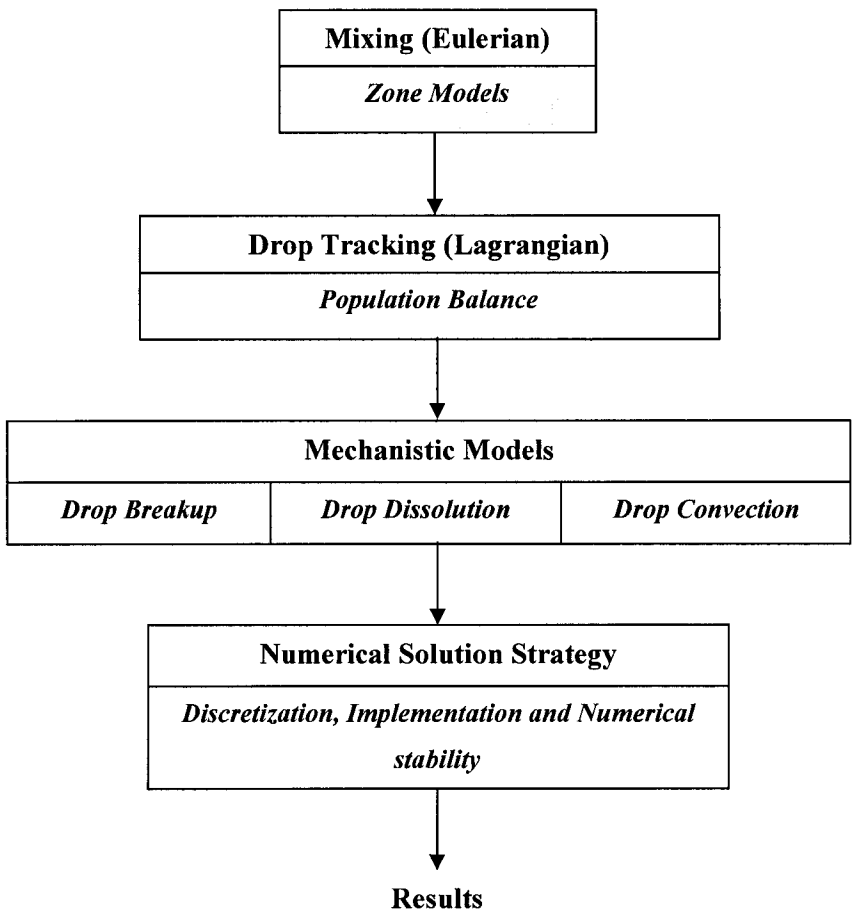

Figure 3-1: Design architecture for the numerical model

3.2 Flow Field

The mean velocity and turbulence characteristics of the flow field produced by an impeller in a stirred tank are complicated by time varying circulation patterns in the mean velocity field, large inhomogeneities in the turbulence field and the influence of both tank and impeller geometry on the flow. The distribution of the shear rate and energy dissipation rate depend on the flow pattern (Hemrajani and Tatterson, 2004) and the flow pattern obtained is determined by both the impeller type used and its position relative to the tank walls. Accurate modeling of the stirred tank thus requires specification of the tank and impeller geometries, and the impeller rotational speed which in turn determines the level of turbulence in the tank. The mixing field model described here is for a down-pumping, 4 bladed, 45° pitched blade turbine (PBT).

3.2.1 Stirred tank geometry

The tank configuration and the tank and impeller variables are presented in Figure 3-2 and Table 3-1 respectively. The tank diameter (T) and the liquid height in the tank are equal, i.e. H = T. The tank is equipped with four baffles (width, w = T/10), equally spaced around the periphery of the tank. The clearance condition, C/D =1.0, where C is the off bottom clearance of the impeller measured to the lower edge of the blade and D is the diameter of the PBT.

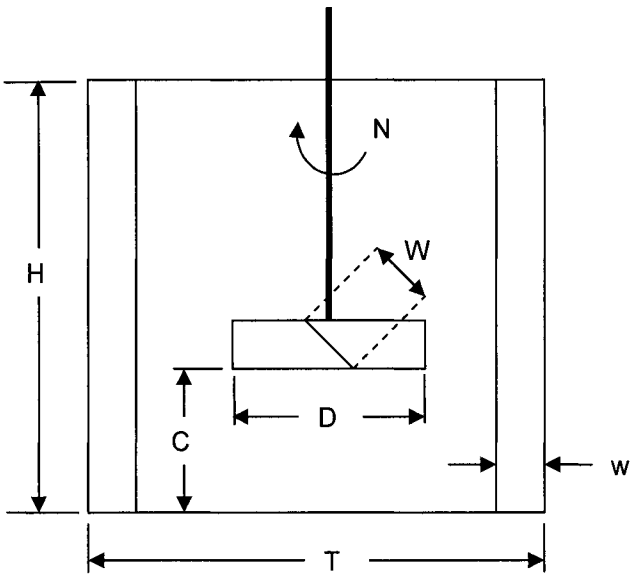

Figure 3-2: Geometry of the stirred tank

Table 3-1: Tank and Impeller variables

Tank variables		***Impeller variables***	
Number of baffles	4	Impeller	PBT
Width of baffles	w = T/10	Number of blades	4
Liquid height	H = T	Diameter	D = T/3
Diameter	T = 145mm	Width of blades	W = D/5
		Blade thickness	t = D/100
		Off-bottom clearance	C = T/3
		Pitch angle	45°
		Rotational speed	N = 550, 650, 750 rpm

3.2.2 Circulation Pattern

The PBT impeller is an axial flow impeller and can be operated in either an upward or downward pumping configuration depending on the direction of rotation of the impeller shaft. When the impeller operates in down pumping mode, the discharge flow from the impeller impinges on the bottom of the tank and spreads out in all directions toward the wall. The flow rises along the walls up the liquid surface and is pulled back to the impeller at the impeller suction. Zhou and Kresta (1996) showed that the equipment geometry and configuration can have profound effects on the turbulent conditions in the stirred tank. Depending on the impeller clearance condition or the impeller diameter, the flow circulation pattern can become radial or have secondary circulation loops which differ from the conventional circulation pattern of a single strong primary circulation loop. The configuration of D = T/3 and C/D = 1.0 has been reported to produce a circulation pattern that resembles the conventional view (Figure 3-3), with a strong primary circulation loop (Kresta and Wood, 1993).

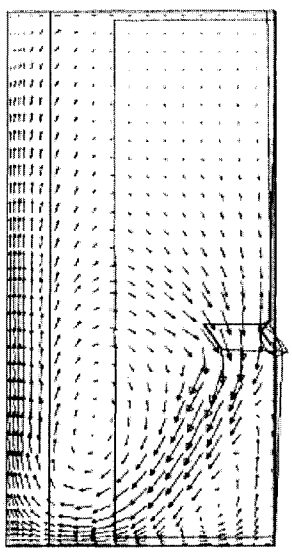

Figure 3-3: Mean average velocity vectors in half plane for a down-pumping PBT Impeller; C/D = 1.0, D = T/3 (Bhattacharya and Kresta, 2002)

3.2.3 Mixing (Eulerian) Model

The turbulence in a stirred tank is often characterized by the average power input (injected through the impeller) per unit mass. In turbulent flow, perfect isotropic turbulence does not exist in the tank, and local variations of the turbulent kinetic energy are difficult to estimate. Park and Blair (1975) reported that it was common to assume that the turbulent flow field is homogenous and therefore, homogenous interaction models were applied, but this approach is now overly restrictive and inaccurate. Maggioris et al. (2000), observed that significant variations exist in the turbulence experienced at different positions in the tank, especially between the impeller region and the rest of the tank. Kresta (1998) reported that the turbulence energy dissipation in agitated tanks, especially in the impeller region (the volume swept out by the impeller blades) and the impeller discharge region is needed to advance our fundamental understanding of mixing phenomena, such as the formation of dispersions. From the foregoing, the impeller swept volume; the impeller discharge region; and the rest (bulk) of the tank have been identified as the regions within the stirred tank exhibiting distinct variations in turbulent characteristics. The turbulent properties in these three regions will be discussed in the sections that follow.

The distribution of the energy dissipation over each of the regions identified above depends on the location of the control volumes or zones which make up the mixing field. Relevant investigations carried out to determine the distribution of turbulent energy dissipation rate within the stirred tank show significant discrepancies in the data reported. However, these discrepancies can be reconciled since the measurements were done using different methods and different specifications for the control volumes. Jaworski and Fort (1991) measured the axial velocity and pressure profiles using a three-hole Pitot tube and reported that the power was distributed as follows: 32% in the impeller region; 54% in the region below the impeller; and 14% in the remaining volume of the tank. Similarly, macro scale energy balance calculations done by Zhou (1997)

using LDA measurements at specified control volumes show that the distribution of the power is: 52% in the impeller region; 75.1% in the combined impeller and impeller discharge region, resulting in 23.1% in the impeller discharge region; and 24.9% in the remaining volume of the tank. In the model described here, the dimensions of the zones are quite different; therefore, the percent power input into each zone is adjusted to reflect reasonable energy dissipation rates while preserving an overall energy balance in the tank.

Figure 3-4 shows the half plane of the stirred tank with the mixing zones identified above.Table 3-2 and Table 3-3 give the formulated equations and values respectively.

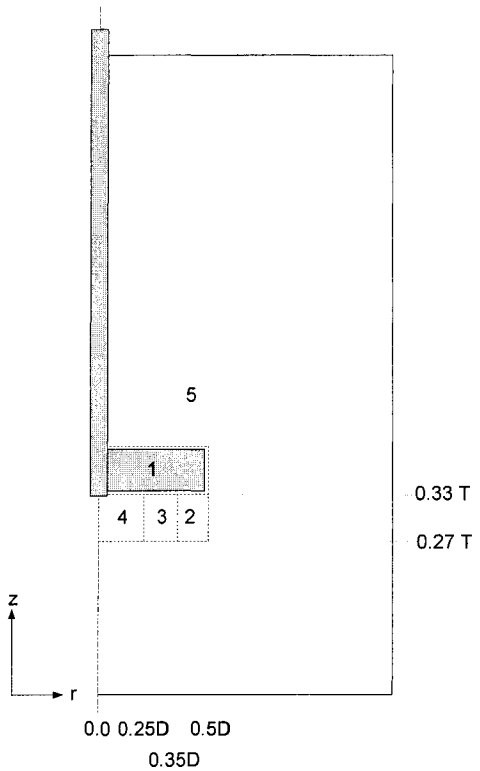

Figure 3-4: Half-plane showing the dimensions of the mixing zones

Zone 1: Impeller Swept Volume

We assume that 22% of the power dissipated by the impeller is expended in this region (the impeller swept volume). The volume swept by the impeller defines the volume of the region and is given by;

$$\frac{D_{swept}}{D} = \left[1 - \left(\frac{W\cos(45^0)}{D} + \frac{t\sin(45^0)}{D}\right)^2\right]^{-0.5} \qquad (3.1)$$

$$V_{swept} = \frac{\pi D_{swept}{}^2\left(W\cos(45^0) + t\sin(45^0)\right)}{4} \qquad (3.2)$$

where W is the blade width and t is the blade thickness. The volumetric flow rate in this zone is well defined by $Q = N_q N D^3$ and the turbulent kinetic energy dissipation rate (ε) is calculated as 22% of the shaft power (P) injected divided by the mass of fluid in the swept volume (ρV_{swept}). The residence time (t_i) for the fluid in this region is the ratio of the impeller swept volume and the volumetric flow rate.

Impeller discharge region

Velocity studies carried out near the impeller blade for axial impellers show very distinct profiles for all three velocity components. Figure 3-5 to Figure 3-7 show the dimensionless axial, radial and tangential velocity components respectively for varying traverses just below the impeller blade along the radial direction of the blade from the hub of the impeller. From the figures, it is evident that axial impellers exhibit weak radial flow but show strong tangential and axial flow. The velocity profiles for both the axial and tangential components reveal a maximum close to the tip of the blade, which has been associated with the trailing vortices.

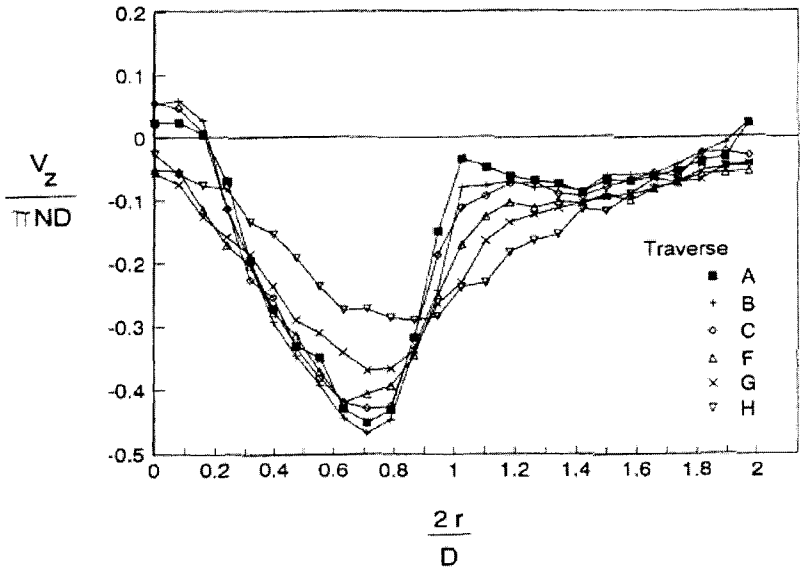

Figure 3-5: Decay of axial velocity component of a PBT (D = T/3, C = T/3) at positions 2z/W: A (-0.1), B (-0.5), C (-1.0), F (-2.5), G (-4.0), H (-6.0) below the impeller (Kresta and Wood, 1993)

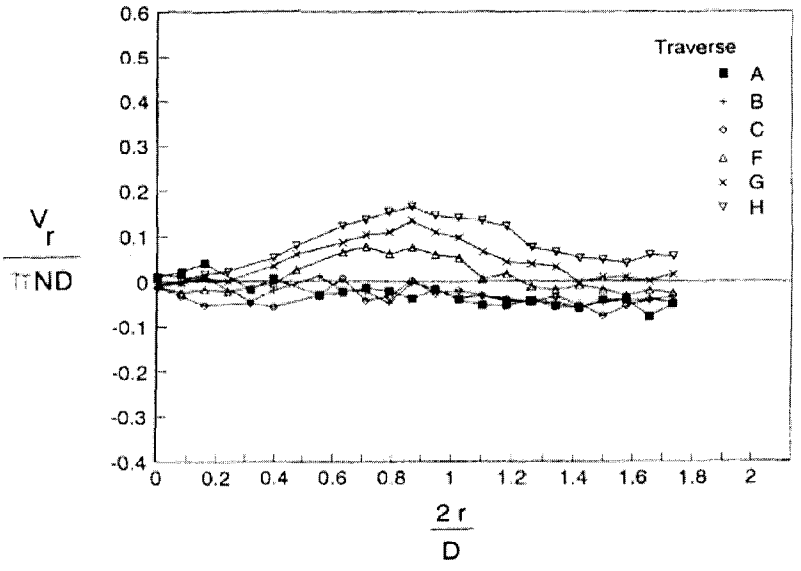

Figure 3-6: Decay of radial velocity component of a PBT (D = T/3, C = T/3) at positions 2z/W: A (-0.1), B (-0.5), C (-1.0), F (-2.5), G (-4.0), H (-6.0) below the impeller (Kresta and Wood, 1993)

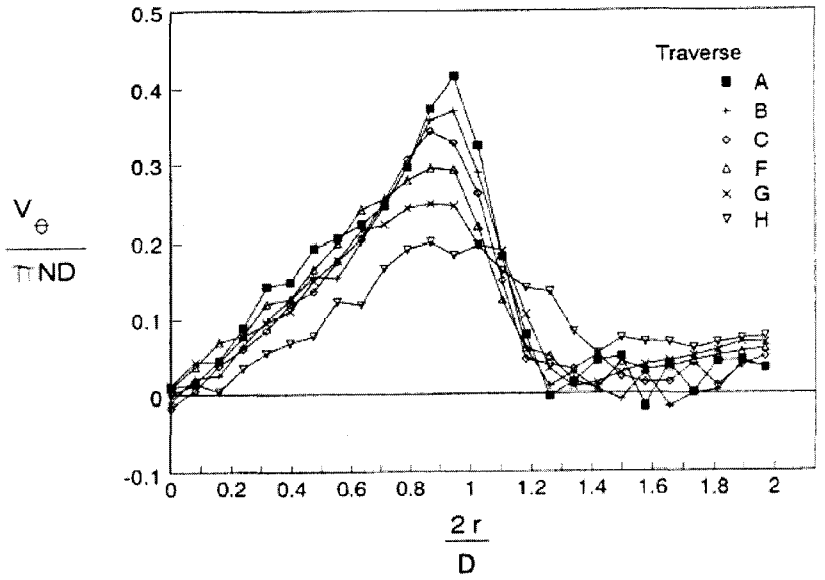

Figure 3-7: Decay of tangential velocity component of a PBT (D = T/3, C = T/3) at positions 2z/W: A (-0.1), B (-0.5), C (-1.0), F (-2.5), G (-4.0), H (-6.0) below the impeller (Kresta and Wood, 1993)

The trailing vortices are considered an important mechanism for dispersion, as well as for drop breakup in liquid-liquid mixing because of the high level of turbulence dissipated in them. The formation of trailing vortices behind the impeller blades has been reported by several investigators: Hockey and Nouri (1996) and Jaworski et al. (1996); all suggest that the trailing vortices should be treated separately, at least in the impeller discharge stream. Kresta and Wood (1993) reported that the trailing vortex extends over approximately 20% of the blade and is formed at the lower tip of the blade, with a smaller one at the top corner of the blade. Zhou and Kresta (1996) and Yianneskis et al. (1987) report that the characteristic diameter of the trailing vortices is $W/2$ or $D/10$. A good visual representation of the trailing vortex behind a 45° PBT impeller blade is presented in Figure 3-8 showing the spiral shape formed by the interaction of the flow along the blade edge.

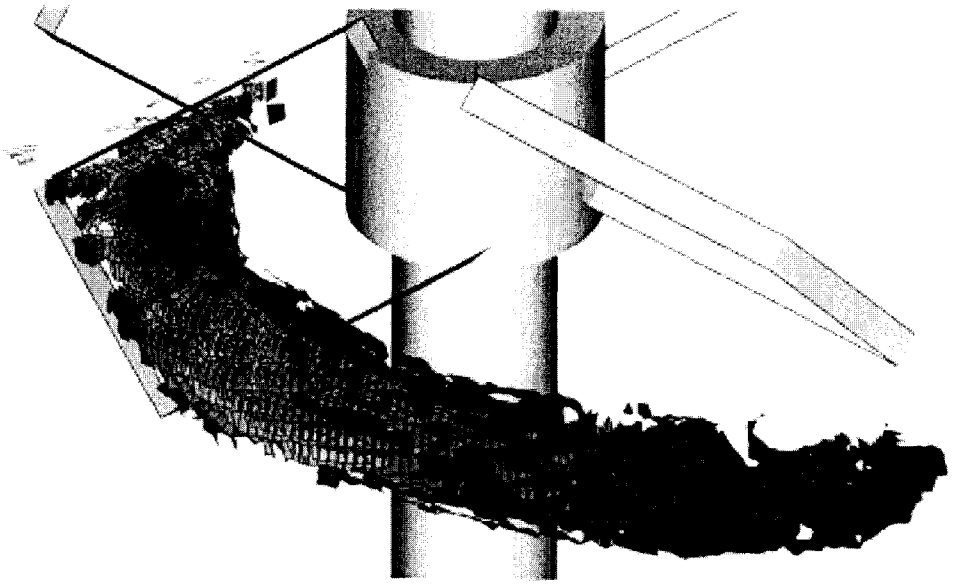

Figure 3-8: Isosurface of vorticity at the edge of the trailing vortex for a down-pumping PBT impeller (Schafer et al., 1998)

Figure 3-9 shows a scaled plot of the turbulent kinetic dissipation energy for various impeller rotational speeds in the turbulent regime. This is further justification for the need to model the impeller discharge with separate consideration for the trailing vortices. From the figure below, the turbulent kinetic energy dissipation decays after the peak at the trailing vortex to almost zero magnitude at the hub of the impeller. Therefore, our model will require three zones to fully define the impeller discharge region.

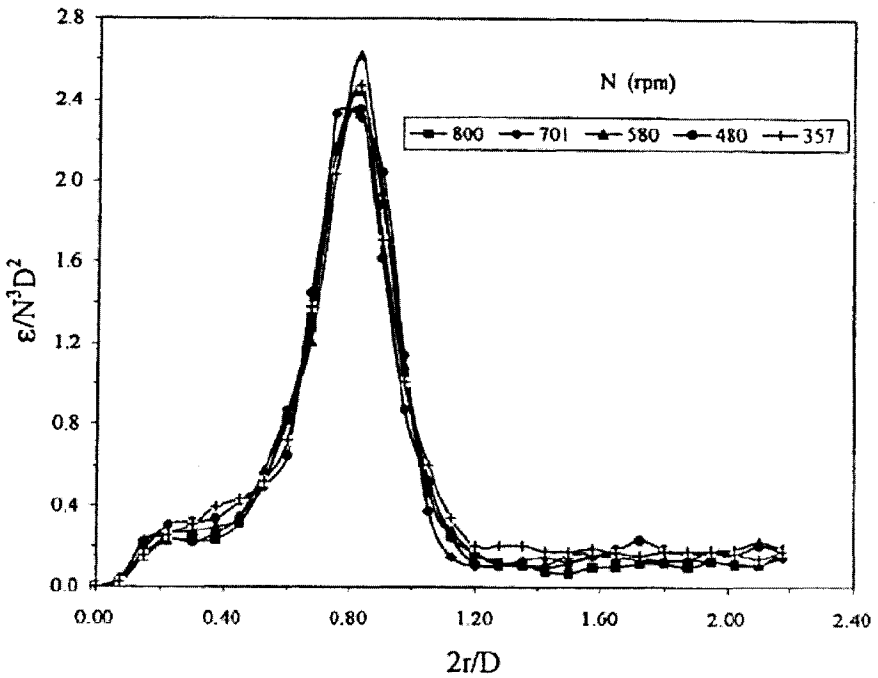

Figure 3-9: Dissipation energy (ε) scaled with different impeller rotational speed (N) for a PBT (D/T = 1/3, 2z/W = 1.35); from Zhou and Kresta (1997)

The volume in each zone is approximated as annular and calculated using equation (3.3)

$$V_i = \pi\left(z_{2,i} - z_{1,i}\right)\left(r_{2,i}^{\ 2} - r_{1,i}^{\ 2}\right) \qquad (3.3)$$

where r_1 and r_2 define the radial distances and $\left(z_2 - z_1\right)$ is the change in the elevation of the zone and the subscript i represents the zone considered. The volumetric flow rate for each zone can be obtained by integrating the axial velocity (Figure 3-5) along the radial distances of each zone i.e.

$$Q_i = 2\pi \int_{r_1}^{r_2} Urdr \qquad (3.4)$$

Zone 2: Impeller discharge volume – trailing vortex

The height of all the zones in the impeller discharge is specified as $D/5$, while the radial width of the trailing vortex is chosen as 0.15D from the tip of the impeller blade. This ensures that the position where the maximum dissipation occurs in the trailing vortex, 0.4D from blade symmetry, is included in this zone. It is assumed that 38% of the power dissipated will be dissipated in this zone.

Zone 3 & 4

Zones 3 and 4 are chosen to describe the decay in turbulent intensities below the impeller blade as the profile moves radially towards the hub of the impeller. Zone 3 overlaps the edge of the trailing vortices; hence more power will be dissipated in it. The power dissipated in these regions is set at 10% and 2% for zones 3 and 4 respectively, giving a total of 50% in the impeller discharge and 22% in the impeller swept volume.

Zone 5: Bulk

The volume of the bulk is obtained by subtracting the volumes of zones 1, 2, 3 and 4 from the total tank volume. The volumetric flow rate in the bulk is obtained from continuity and is the same as the volumetric flow rate into and out of the impeller swept region (zone 1), since all the fluid from the impeller discharge region is unfolded into the bulk and re-entrained into the suction. The power dissipated in the bulk is assumed to be 28% of the total power input; therefore, the average turbulence dissipation rate in the bulk is obtained from a ratio of the power and the volume of the bulk region.

Table 3-2: Representative equations for the mixing fields

Zone	Dimension	Volume (m^3)	Volumetric flow rate (m^3/s)	Rate of turbulence energy dissipation (W/kg)	Residence time, t (s)
1. Impeller swept volume	$z_1 = D$ $z_2 = D + (Wp\cos45° + tp\sin45°)$ $r_1 = 0.0$ $r_2 = 0.5D$	V_1	N_qND^3	$0.22N_pN^3D^5/V_1$	$V_1/(N_qND^3)$
2. Trailing vortex	$z_1 = 0.8D$ $z_2 = D$ $r_1 = 0.35D$ $r_2 = 0.5D$	V_2	Q_2	$0.38N_pN^3D^5/V_2$	V_2/Q_2
3.	$z_1 = 0.8D$ $z_2 = D$ $r_1 = 0.25D$ $r_2 = 0.35D$	V_3	Q_3	$0.1N_pN^3D^5/V_3$	V_3/Q_3
4.	$z_1 = 0.8D$ $z_2 = D$ $r_1 = 0.0$ $r_2 = 0.25D$	V_4	Q_4	$0.02N_pN^3D^5/V_4$	V_4/Q_4
5. Bulk	Everywhere else	V_{bulk}	N_qND^3	$0.28NpN^3D^5/V_{bulk}$	$V_{bulk}/(NqND^3)$

Table 3-3: Parameter values for each zone in the mixing fields

Zone	Dimension (m)	Volume (m^3) $V_i = \pi(z_2 - z_1)(r_2^2 - r_1^2)$	Volumetric flow rate (m^3/s)	Rate of turbulence energy dissipation (W/kg)	Residence time, t (s)
1. Impeller swept volume	$z_1 = D$ $z_2 = 1.15D$ $r_1 = 0.0$ $r_2 = 0.5D$	$0.118D^3$	$0.79ND^3$	$2.368N^3D^2$	0.15/N
2. Trailing vortex	$z_1 = 0.8D$ $z_2 = D$ $r_1 = 0.35D$ $r_2 = 0.5D$	$0.080D^3$	$0.17ND^3$	$6.033N^3D^2$	0.47/N
3.	$z_1 = 0.8D$ $z_2 = D$ $r_1 = 0.25D$ $r_2 = 0.35D$	$0.038D^3$	$0.41ND^3$	$3.342N^3D^2$	0.093/N
4.	$z_1 = 0.8D$ $z_2 = D$ $r_1 = 0.0$ $r_2 = 0.25D$	$0.039D^3$	$0.21ND^3$	$0.651N^3D^2$	0.186/N
5. Bulk	Everywhere else	$20.931D^3$	$0.79ND^3$	$0.017N^3D^2$	26.49/N

3.3 Drop Tracking (Lagrangian)

The dynamic change in the drop size distribution of the dispersed phase can be modeled using the population balance approach. The population balance is a statement of continuity for particulate systems (Hounslow, 1990). In simple terms, the population balance equation describes the rate of change of the number of drops of a specific drop size by accounting for the processes that increase or reduce its number density. This approach has been used extensively for studying dispersion systems and can be adapted for numerical discretization schemes.

3.3.1 Population Balance

The population balance equation is a Boltzmann-type equation used in describing the spatial and temporal change in the distribution of one species in another, which in our case will be the distribution of the dispersed drops in the continuous liquid phase. If a statistical function p is used in describing the number of drops with sizes in a particular size class, the population balance equation will be written as

$$\frac{\partial p}{\partial t}+\nabla_z\cdot(Up)+\nabla_z\cdot(Fp)=-\frac{\partial}{\partial L}(Gp)+Q'_b+Q'_c+\Omega \qquad (3.5)$$

where Q'_b is the change due to breakup, Q'_c is the change due to coalescence, Ω is change due to collisions which do not result in coalescence, G is the change due to dissolution, evaporation or condensation, F is the force per unit area acting on the drop and U is the local velocity of each drop particle. Integrating over the whole velocity space in each mixing zone will eliminate the velocity dependence of each drop size, and one obtains (Williams, 1985)

$$\frac{\partial N}{\partial t}+\nabla_z\cdot(\overline{U}N)+\nabla_z\cdot(FN)=-\frac{\partial}{\partial L}(GN)+\int Q'_b+\int Q'_c+\Gamma \qquad (3.6)$$

where $N(L,t) = \int p \cdot N_T(L,t)dL$ denotes the probable number of drop particles of size in the range dL about L at time t, $\overline{U}$ is the mean velocity of all drop particles of size L in a specified mixing zone at time t. In the absence of forces external to the dispersed system and for low dispersed phase volume, the frequency of collision becomes negligible and the collision/coalescence terms vanish resulting in

$$\frac{\partial N}{\partial t} + \nabla_z \cdot \left(\overline{U}N\right) = -\frac{\partial}{\partial L}(GN) + \int Q'_b \, dU \qquad (3.7)$$

$$\frac{\partial N}{\partial t} + \nabla_z \cdot \left(\overline{U}N\right) = -\frac{\partial}{\partial L}(GN) + Q_b \qquad (3.8)$$

with $Q_b = \int Q'_b \, dU$. The change due to dissolution and breakup can be represented by equations (3.9) and (3.10) respectively thereby giving a simplified equation (3.11) representing the drop interactions in the modeled system.

$$\frac{\partial N_m}{\partial t} = -\frac{\partial}{\partial L}(GN) \qquad (3.9)$$

$$\frac{\partial N_b}{\partial t} = Q_b \qquad (3.10)$$

$$\frac{\partial N}{\partial t} = \frac{\partial N_m}{\partial t} + \frac{\partial N_b}{\partial t} - \nabla_z \cdot \left(\overline{U}N\right) \qquad (3.11)$$

Although the contribution of the convective term $\nabla_z \cdot \left(\overline{U}N\right)$ vanishes when integration is done over the batch stirred vessel, it is retained in each mixing zone because it affects the redistribution of the drops – each mixing zone is

likened to a continuously stirred zone. To close the modeling problem, reliable models for drop breakup and drop dissolution processes will be required.

3.4 Mechanistic Models

As discussed in the previous sections, only drop breakup and dissolution processes play a significant role in dilute systems. Mechanistic models that describe these processes are many and varied (see Section 1.2). In the following sections, specific models for drop breakup and dissolution will be selected for use in this modeling effort and some rationale for their choice will also be provided.

3.4.1 Drop Breakup Model

The general expression used in tracking changes due to particle breakup events is given by

$$\frac{\partial N_b}{\partial t} = \int_L^\infty m(L_0) f(L, L_0) g(L_0) N(L_0, t) dL_0 - g(L) N(L, t) \qquad (3.12)$$

where $g(L)$ is the breakup frequency, $m(L_0)$ the number of fragments resulting from the breakup of a particle of diameter L, $f(L, L_0)$ the size probability density function of the fragments and $\frac{\partial N_b}{\partial t}$ gives the net change in the drop population that has occurred for a particular event. The breakup process for any drop will be defined by these three functions.

Number of daughter drops $m(L_0)$

Binary breakup of drops at every breakup event is a very common approach used in modeling of liquid-liquid dispersions using population balances. This assumption will be retained in this modeling effort, that is:

$$m(L_0) = 2 \qquad (3.13)$$

Drop breakup frequency $g(L)$

The first term on the right hand side of the breakup equation accounts for the rate of formation of drops of size L from the breakup of drops of sizes larger than L while the second term accounts for the rate of breakup of drops of diameter size L.

From the gamut of models predicting drop breakup frequencies, the kinetic-theory model proposed by Luo and Svendsen (1996) was selected because there are no experimentally determined or fitted parameters. The drop breakup model is based on the following key assumptions:

i. the turbulence is local and isotropic;
ii. only binary breakage of fluid particles occurs in the turbulent dispersion;
iii. the breakage volume fraction can be treated as a stochastic variable;
iv. the occurrence of breakup was determined by the energy level of the arriving eddy; and
v. only eddies of length scale smaller than or equal to the particle diameter can induce particle oscillations.

Following from the above assumptions, the rate model for fluid particle breakage in a turbulent field is given by

$$g(L) = \theta_{Le} F(L) \qquad (3.14)$$

The breakup rate $g(L)$ is expressed as a product of the collision frequency between eddies and particles, θ_{Le}, and the collision efficiencies, $F(L)$, resulting in particle breakup. The collision frequency of eddies of sizes comparable to the drop diameter can be expressed as a function of some hydrodynamic variables as

$$\theta_{Le}(\xi) = \beta_1(1-\varphi)(\varepsilon L)^{1/3}\frac{(1+\xi)^2}{L^2\xi^{11/3}} \qquad (3.15)$$

where φ is the volume fraction of the dispersed phase, ε is the local dissipation, β_1 is a constant and ξ is the ratio of the eddy size to the particle size. The breakup efficiency is expressed based on mean kinetic energy of the eddies and the surface energy of the drops

$$F(L) = \exp\left(-\frac{12C_f\sigma}{\beta_1\rho_C\varepsilon^{2/3}L^{5/3}\xi^{11/3}}\right) \qquad (3.16)$$

C_f is the increase coefficient of surface area.

The resulting combination of equations is the breakup frequency of a particle of volume L_j^3 that breaks into particles of volume L_i^3 and $L_j^3 - L_i^3$ is

$$g(L_i, L_j) = \beta_1(1-\varphi)\left(\frac{\varepsilon}{L_i^2}\right)^{1/3}\int_{\xi_{\min}}^{1}\frac{(1+\xi)^2}{\xi^{11/3}}\exp\left(-\frac{12C_f\sigma}{\beta_1\rho_C\varepsilon^{2/3}L_i^{5/3}\xi^{11/3}}\right)d\xi \qquad (3.17)$$

$$\xi_{\min} = \frac{L_{\min,e}}{L}\ ; \qquad \frac{L_{\min,e}}{\eta} \approx 11.4 - 31.4 \text{ (Tennekes and Lumley, 1972)}$$

Although Luo and Svendsen argued that their model is void of any fitting parameter, the model does depend on the lower and upper integral limits (Lasheras et al., 2002). The selection of 1.0 as the upper limit of integration can be understood as integrating from the viscous scale to a length scale equal to that of the drop but the lower limit varies over a range. For this model, a mid value of $L_{\min,e}/\eta = 21.4$ is taken as the lower limit.

Daughter drop distribution function $f(L,L_0)$

$f(L,L_0)$ is the probability of forming a drop of size L from the breakup of a mother drop of size L_0. The daughter drops resulting from any breakup event can not be larger than $\frac{L_{max}}{2^{1/3}}$ (Lasheras et al., 2002). L_{max} is the maximum stable drop size (Kolmogorov, 1949; Hinze, 1955).

The correlations available in the literature for the prediction of daughter size distribution resulting from a single breakup event have been discussed in Section 1.2.1. The beta-distribution model proposed by Lee et al. (1987) is a two parameter (α,β) model and has been shown to fit a wider range of data compared to other one parameter models (Lasheras et al., 2002). The beta distribution is of the form

$$f(L,L_0)=\frac{\Gamma(\alpha+\beta)}{\Gamma(\alpha)\Gamma(\beta)L_0}\left(\frac{L}{L_0}\right)^{\alpha-1}\left(1-\frac{L}{L_0}\right)^{\beta-1} \qquad (3.18)$$

Konno et al (1980) proposed a statistical model based on the distribution of kinetic energy among turbulent eddies of different scales. The probability of forming a daughter drop size was expressed as a function of the kinetic energy contained in eddies of that length scale. Their model was shown to be well approximated by a beta-distribution where the parameters α,β are determined as 9 and 3 respectively:

$$f(L,L_0)=\frac{\Gamma(12)}{\Gamma(9)\Gamma(3)L_0}\left(\frac{L}{L_0}\right)^{8}\left(1-\frac{L}{L_0}\right)^{2} \qquad (3.19)$$

Equation (3.19) is used for this modeling effort because it requires no fitted parameters. It will be shown that it gives good agreement with experimental data.

3.4.2 Dissolution Model

The rate of change of mass of a drop by dissolution, $\frac{dm}{dt}$, can be described by a form of Fick's law

$$\frac{dm}{dt} = k_L A(C_S - C_{bulk}) \qquad (3.20)$$

where k_L is the mass transfer coefficient, C_S the saturation concentration of the dispersed phase at the prevailing temperature, C_{bulk} is the uniform concentration of the solute in the well stirred bulk, and A is the interfacial area of the spherical drop. The mass m and the interfacial area A of the drop can be expressed as a function of its diameter L:

$$m = \frac{\rho_C \pi L^3}{6} \quad ; \quad A = \pi L^2$$

Equation (3.20) becomes

$$\frac{dL}{dt} = \frac{2k_L}{\rho_C}(C_S - C_{bulk}) = G \qquad (3.21)$$

Equation (3.21) defines the rate at which the drop size shrinks due to mass transfer into the continuous phase. $\frac{dL}{dt}$ will sometimes be referred to as the dissolution rate G (see equation 3.5). To completely define the dissolution model, a correlation for the mass transfer coefficient k_L is required.

Brian et al. (1969) postulate that mass transport in stirred tank resulting from locally isotropic eddies can be described by a function of the form:

$$Sh = f\left[\frac{\varepsilon L^4}{\nu^3}, Sc, \frac{gL^3(\Delta\rho)}{\rho_C \nu^2}, \frac{\rho_d}{\rho_C}\right] \qquad (3.22)$$

Equation (3.22) can be seen to have some similarities to equation (1.12). The dimensionless group $\frac{\varepsilon L^4}{\nu^3}$ is understood to be the drop Reynolds number, Re, based on the local energy dissipation rate, ε, the Sherwood number $Sh = \frac{k_L L}{D_{AB}}$, and Schmidt number, $Sc = \frac{\nu}{D_{AB}}$.

Comprehensive reviews of mass transfer correlations can be found in Perry's Handbook (Tables 5-21 to 5-28); Pangarkar et al (2002); Kumar and Hartland (1999). These correlations are derived for specific vessel geometry, fluid systems, fluid properties and the level of turbulence in the agitated tank. Thus, selecting an appropriate mass transfer correlation for our model required a comparison of different correlations identified for liquid-liquid systems with experimentally determined results.

Some of the mass transfer correlations applicable to liquid-liquid systems are: Glen (1965); Boyadzhiev and Elenkov (1966); Calderbank (1967); Lamont and Scott (1970); and Levins and Glastonbury (1972). The predicted cumulative drop size distribution curves obtained from these models were compared with experimental data obtained using diethyl malonate as the dispersed phase in Deionized Ultra Filtered (DIUF) water (0.01 dispersed phase fraction and impeller speed of 650 rpm) (Figure 3-10 to Figure 3-14).

From these figures it is evident that the mass transfer coefficient correlation proposed by Glen (1965) gives the best fit.

$$k_L = \frac{D_{AB}}{D}\left(\frac{\Delta\rho}{\rho_d}\right)^{1/2}\left(\frac{L}{D}\right)^{1/3} \mathrm{Re}\, Sc^{1/3} \qquad (3.23)$$

The dissolution model accounting for the mass transfer of the dispersed phase into the continuous phase is coupled with the dispersed phase material balance in the continuous phase.

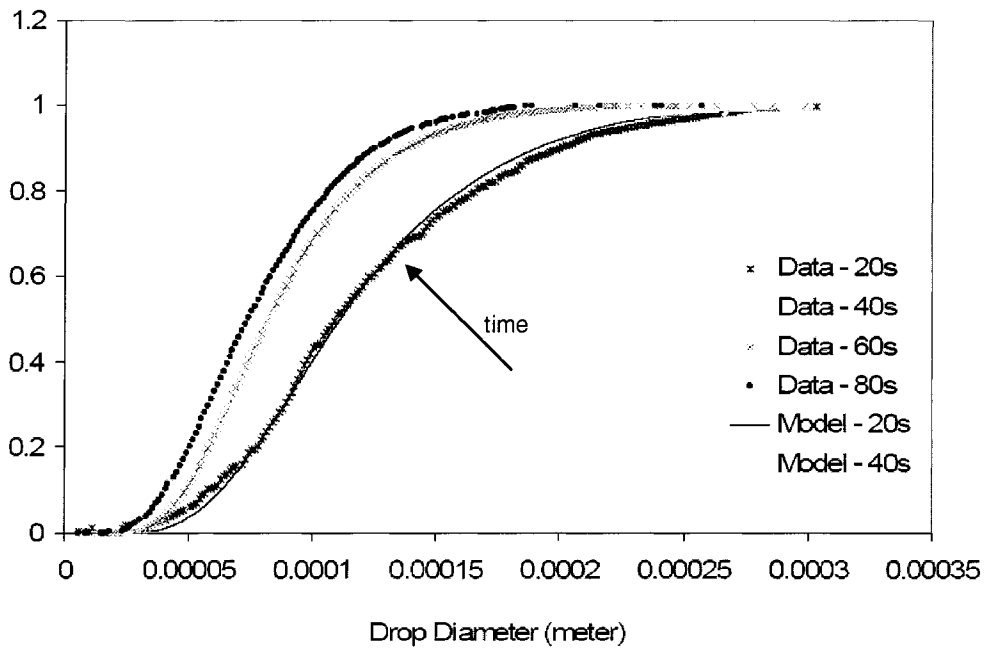

Figure 3-10: Cumulative number density plot obtained using correlation by Lamont and Scott (1970)

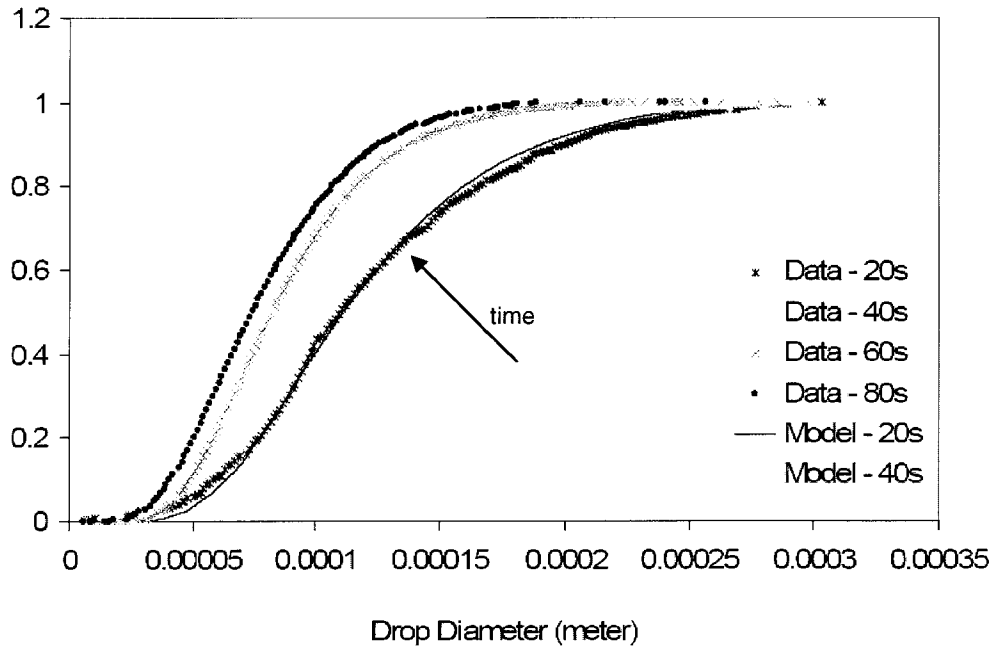

Figure 3-11: Cumulative number density plot obtained using correlation by Boyadzhiev and Elenkov (1966)

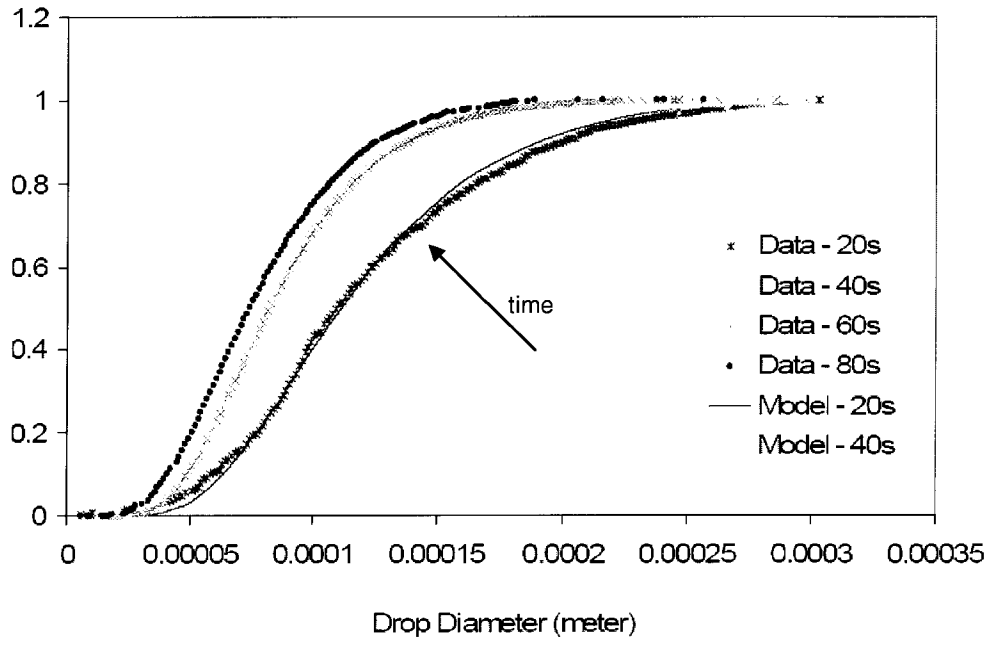

Figure 3-12: Cumulative number density plot obtained using correlation by Levins and Glastonbury (1972)

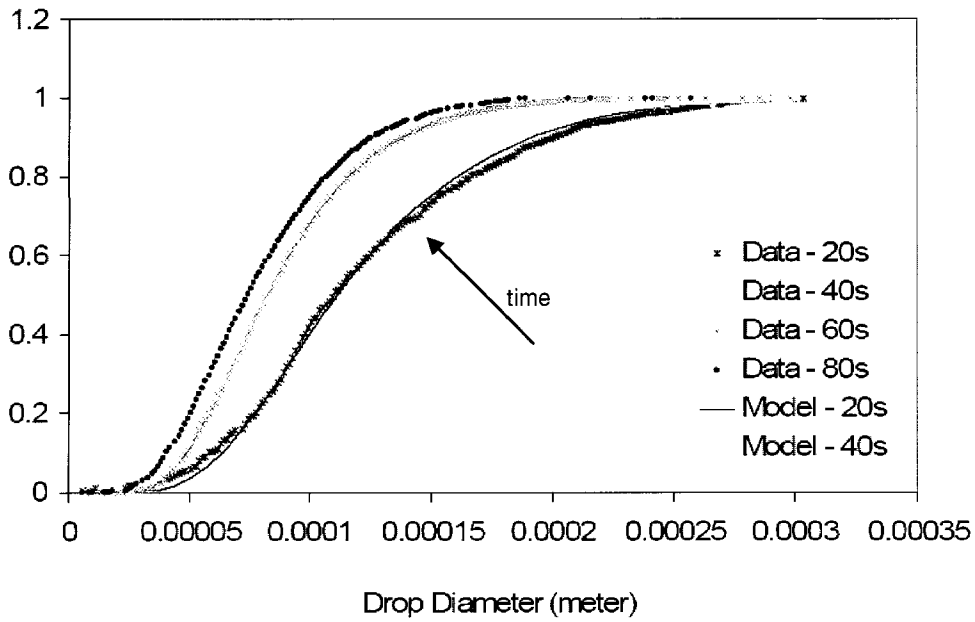

Figure 3-13: Cumulative number density plot obtained using correlation by Calderbank (1967)

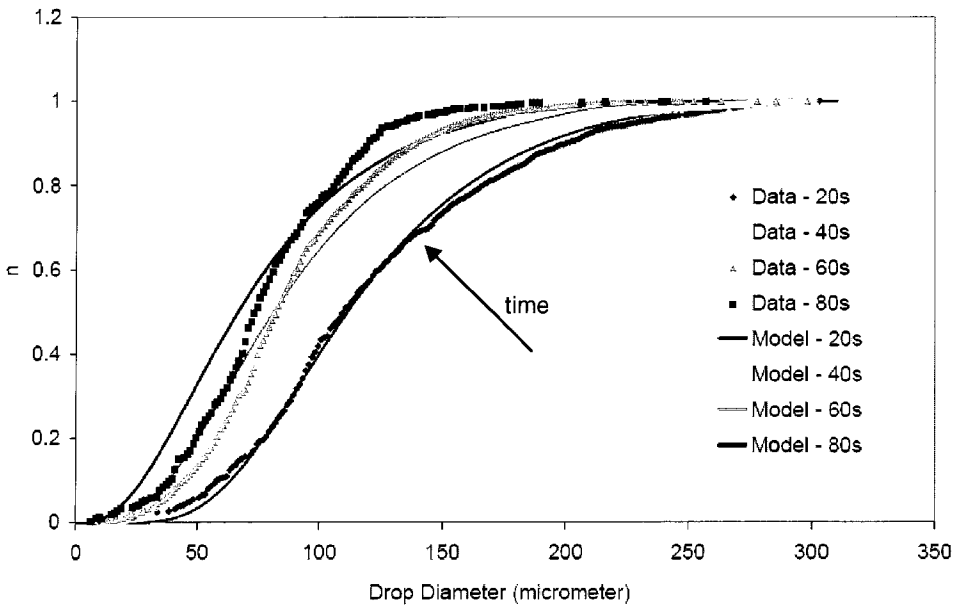

Figure 3-14: Cumulative number density plot obtained using correlation by Glen (1965)

3.5 Material Balances

Mass conservation of the dispersed phase concentration in the stirred tank is ensured by material balances in both the continuous and dispersed phases. When drops shrink and disappear from the dispersed phase into the continuous phase, the solute concentration in the continuous phase increases. This increase can be accounted for by continuity.

The stirred tank is assumed to be well mixed after every hydrodynamic event; therefore, the solute concentration in the tank (bulk concentration) can be obtained by difference according to the equation below:

$$C_{bulk} = \frac{M_{d,0} - \frac{\rho_d \pi \sum_{i=1}^{P} N_i L_i^3}{6}}{V_T - \frac{\pi \sum_{i=1}^{P} N_i L_i^3}{6}} \qquad (3.24)$$

where C_{bulk} is the solute concentration in the bulk at any time, $M_{d,0}$ is the initial mass of dispersed phase added, V_T is the total fluid volume of the stirred tank (dispersed phase volume inclusive) and N_i, L_i and P remain drop absolute number, drop characteristic class size (diameter) and total number of drop size classes respectively.

3.6 Numerical Solution Strategy

The integro-differential population balance equation expressing the time evolution of the dispersed drop population in the stirred tank does not have an explicit analytic solution. However, the population balance equation can be expressed numerically using discrete formulations of the number density of the dispersed drops in a finite dimensional space.

Length scale

Numerical solutions of the population balances require the discretization of the length domain. Choice of a suitable discretization method depends on the processes that determine the transient drop size distribution. For processes that lead to larger drop sizes (growth or coalescence processes), linear discretization scales will give better resolution of the length domain while the geometric discretization scales will be better suited for processes resulting in smaller drop sizes (breakup and dissolution processes). For multi-mechanistic processes that simultaneously increase and reduce the drop size distribution (such as breakup/coalescence, growth/dissolution processes), the symmetric geometrical length scale (Kresta et al., 2005) method has been reported to give very good results. The liquid-liquid system that is being modeled here is a multi-mechanistic processes leading to the simultaneous breakup and dissolution of the dispersed drops. Both processes lead to reduction in the drop sizes so the geometric discretization method will be employed.

Figure 3-15 shows the standard geometric discretization scale. An inherent weakness of the geometric discretization scale is that it asymptotically approaches the zero value. The geometric length scale requires three parameters to fully describe the discretization. The parameters are the minimum drop size, ℓ_0, maximum drop size, ℓ_p, and the number of drop size classes, P. The minimum and maximum drop sizes are selected to cover the spectrum of the measured drop sizes obtained using the PDPA. To minimize both the error due to discretization scales and number of discretized equations viz-a-viz the computational load, the number of drop size classes (p) was reduced progressively starting from 400 until an appreciable error was observed in the number density, then the previous value was selected. The values specified for the minimum drop size, maximum drop size and number of drop size classes are $5\text{x}10^{-6}$m, $4.5\text{x}10^{-4}$m and 80 respectively.

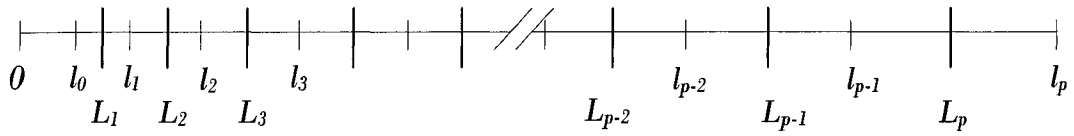

Figure 3-15: Schematic showing the geometric discretized length scale

$$r = \left(\frac{\ell_p}{\ell_0}\right)^{1/p} \tag{3.25}$$

$$\ell_i = r\ell_{i-1} \tag{3.26}$$

$$L_i = \frac{l_i + l_{i-1}}{2} = \left(\frac{r+1}{2r}\right)\ell_i \tag{3.27}$$

$$\Delta L_i = l_i - l_{i-1} = \left(\frac{r-1}{r}\right)\ell_i \tag{3.28}$$

where P is the total number of drop size classes, r is the geometric factor, ℓ_0 is the minimum drop size, ΔL_i is the geometric spacing for the *ith* class size, ℓ_p is the maximum drop size, ℓ_i is the upper limit and L_i is the characteristic length of the *ith* class.

Time scale

The population balance equation is in a partial differential form with respect to drop size and time. In conjunction with the spatial discretization, already described in the previous sections, a time stepping scheme is required to fully define the numerical discretization scheme. The equation obtained from the spatial discretization is in the form:

$$\frac{\partial N}{\partial t} = F(N) \tag{3.29}$$

Using a Taylor's series expansion truncated after the first term on equation (3.29) gives:

$$\frac{\partial N}{\partial t} = \frac{N^{n+1} - N^n}{\Delta t} + \mathrm{O}(\Delta t) \tag{3.30}$$

$$N^{n+1} = N^n + \Delta t F(N^n) \tag{3.31}$$

This formulation corresponds to the "explicit forward Euler scheme" and is only first order accurate. New values are computed iteratively by integrating equation (3.29) given previous time-step values. Although this is the simplest time discretization scheme, it will be used in preference to other more complex time discretization schemes (Runge-Kutta etc.) so long as small scale numerical noise is damped and scheme is stable. Discretization schemes such as the Runge-Kutta techniques achieve good quadratic convergence properties but require sub-step time integrations which increase the computational load.

The condition for stability of a time discretized scheme is defined using the Courant number, C:

$$C = \frac{c\Delta t}{\Delta x} \tag{3.32}$$

where c is the phase speed or the advection velocity, Δt is the step size and Δx is the bin size. CFL (Courant-Friedrich-Levy) condition implies that

$$C < 1.0 \tag{3.33}$$

A Courant number, C, larger than 1.0 indicates an integration time scale too large to adequately capture the transfer of material within the bin size, resulting in uncontrolled oscillation in the numerically computed dispersed drop distribution. The time scale Δt_s based on the Courant condition is given by

$$\Delta t_s = \frac{C\Delta L_1}{G} \qquad (3.34)$$

where G (m/s) and ΔL_1 (m) denote the dissolution rate and the interval spacing in the smallest drop size class, and C is fixed at 0.5 to ensure numerical stability.

The integration time calculated from equation is compared with the residence times in each zone and the smallest time step is selected for the integration.

3.6.1 Discrete Formulation

The drop size distribution and index notation used in this model effort are presented in Figure 3-16.

The representative diameter for each discretized drop size class is computed as

$$L_i = \frac{l_{i-1} + l_i}{2} \qquad (3.35)$$

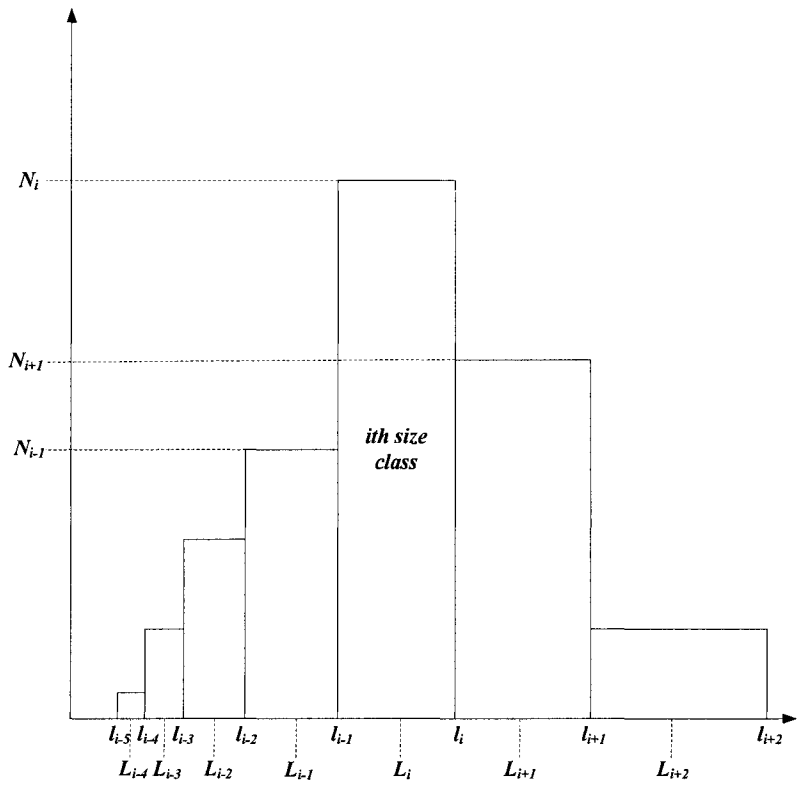

Figure 3-16: Discretized drop size distribution with drop diameter as internal coordinate

An initial approximation of the drop size distribution is obtained by curve fitting the experimental drop size distribution data acquired after an initial time (say 20 seconds). There are numerous standard empirical distributions that are used for drop size distribution but the log-normal distribution has been shown to adequately represent the profile observed for processes involving size reduction. The log-normal distribution is given by

$$p(L,\mu,\delta) = \frac{1}{\sqrt{2\pi}\delta}\exp\left[-\frac{(\log(L/\mu)^2}{2\delta^2}\right] \qquad (3.36)$$

$$\int_0^\infty p(L,\mu,\delta)dL = 1.0 \qquad (3.37)$$

$p(L,\mu,\delta)$ is the drop probability number density function, and μ and δ are the two adjustable parameters of the log-normal distribution. These parameters determine the scale (shape) and location (modal class) of the log-normal distribution and are chosen in such a way that the errors in representing the normalized and cumulative distributions are minimized simultaneously. As an example, Figure 3-17 and Figure 3-18 show the normalized probability number density function and cumulative number density distribution for one experimental run. The results were best fitted using a log-normal distribution with $\mu = 90.56$ and $\delta = 0.5$; with a least squared error of 0.017.

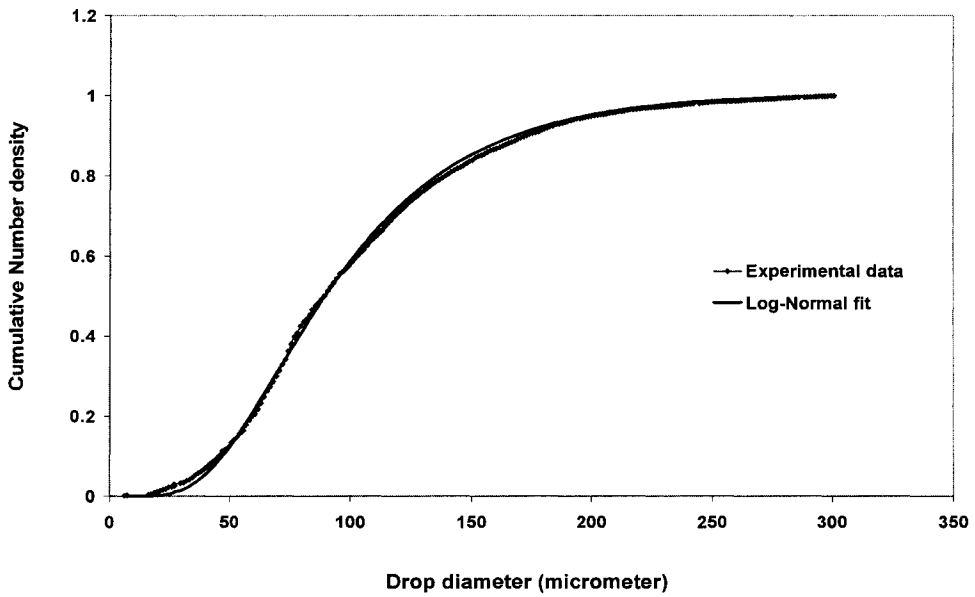

Figure 3-17: Cumulative number density plot

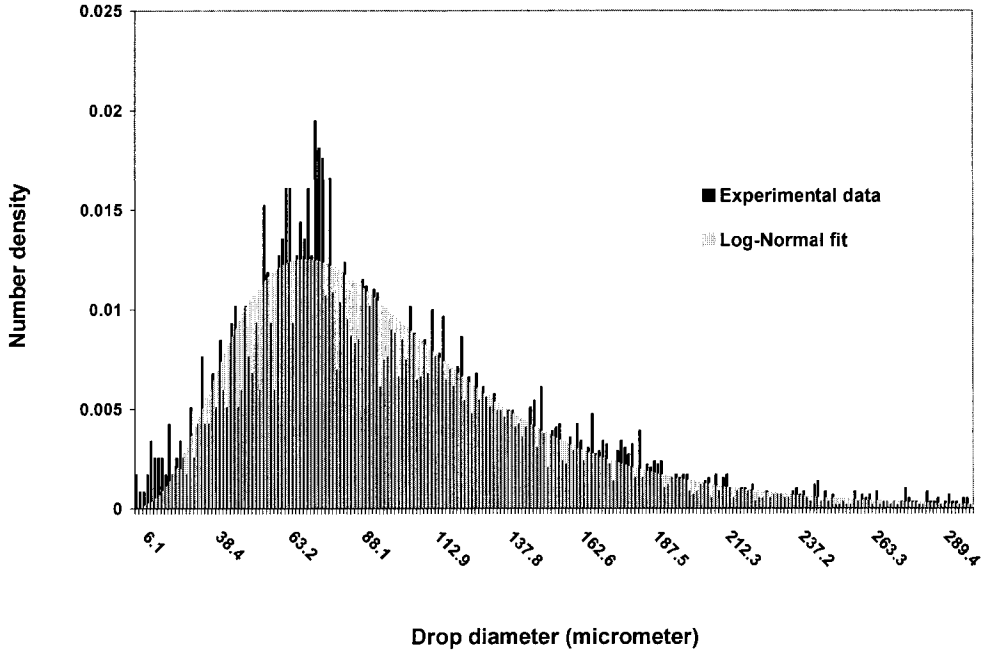

Figure 3-18: Absolute number density plot

The number density distribution for each drop class size is obtained by constructing a volume balance over the entire discretized drop distribution. This is given by the formula below;

$$N_i(L,t_0) = \frac{p(L)\cdot V_T}{\int_{l_i}^{l_{i+1}} \frac{p(L)\cdot \pi L^3}{6} dL} \qquad (3.38)$$

V_T is the total volume of the undissolved dispersed phase in the stirred tank at the initial measurement period while l_i and l_{i+1} represent the class interval for the ith drop class size.

Breakup Discretization

The breakup rate of a drop size L_j to two drops, one of size L_i and another of corresponding size $\left(L_j^{\,3} - L_i^{\,3}\right)^{1/3}$, assuming binary breakup of drops, is given by (Luo and Svendsen, 1996):

$$g(L_i, L_j) = \beta(1-\varphi)\left(\frac{\varepsilon}{L_j^{\,2}}\right)^{1/3} \int_{\xi_{\min}}^{1} \frac{(1+\xi)^2}{\xi^{11/3}} \exp\left(-\frac{12 C_f \sigma}{\beta \rho_C \varepsilon^{2/3} L_j^{\,5/3} \xi^{11/3}}\right) d\xi \qquad (3.39)$$

where the parameters in the equation are either physical properties of the system or hydrodynamic functions defined as

$$C_f = \left(\frac{L_i}{L_j}\right)^2 + \left(1 - \frac{L_i^{\,3}}{L_j^{\,3}}\right)^{2/3} - 1 \qquad (3.40)$$

$$\beta = \left(\frac{8\Gamma(1/3)}{5\pi}\right)\alpha \qquad (3.41)$$

$$\psi = \left(\frac{15\pi^{1/3}}{8 \cdot 2^{2/3}\Gamma(1/3)}\right)\beta^{1/2} \qquad (3.42)$$

C_f is the increase coefficient of surface area and varies between 0 and 0.26 depending on the breakage volume. β and ψ are hydrodynamic constants while α is a constant (Batchelor, 1982) based on turbulence theory. Energy spectrum studies for the inertial subrange (Tennekes and Lumley, 1972) can be described by:

$$E(k) = \alpha \varepsilon^{2/3} k^{-5/3} \qquad (3.43)$$

where α is specified as 1.5. Therefore, β and ψ are calculated as 2.0466 and 0.9238 respectively (Alopaeus et al., 1996).

Alopaeus et al. (1996) showed an alternative expression for equation (3.39) using the incomplete gamma functions

$$g(L_i,L_j)=\frac{-3\psi(1-\varphi)}{11b^{8/11}}\left(\frac{\varepsilon}{L_j^{\,2}}\right)^{1/3}\begin{Bmatrix}\Gamma(8/11,t_m)-\Gamma(8/11,b)+2b^{3/11}(\Gamma(5/11,t_m)\\-\Gamma(5/11,b))+b^{6/11}(\Gamma(2/11,t_m)-\Gamma(2/11,b)\end{Bmatrix} \quad (3.44)$$

$$b=\frac{12C_f\sigma}{\beta\rho_C\varepsilon^{2/3}L_j^{\,5/3}} \quad (3.45)$$

$$t_m=b\left(\frac{\eta}{L_j}\right)^{-11/3} \quad (3.46)$$

η is the Kolmogorov microscale defined as $\eta=\left(\frac{\mu}{\rho^3\varepsilon}\right)^{1/4}$ (Tsouris & Tavlarides, 1994). The local dissipation (ε) in each zone is used to calculate the corresponding Kolmogorov microscale drop size.

The total breakage of any drop is obtained by integrating equation (3.6) over the entire size space (Luo and Svendsen, 1996)

$$g(L_i)=\frac{1}{2}\int_0^1 g(L_i,L_j)dl_j \quad (3.47)$$

Equation (3.47) can be rewritten in a finite length space as

$$g(L_i) = \sum_{i=1}^{j} \frac{g(L_i, L_j)}{2} dl_j \qquad i, j = 1,2,3....p \qquad (3.48)$$

the factor ½ accounts for the symmetrical breakage range for the integrand.

The daughter drop distribution function (probability distribution of daughter drops) used in the discretized model proposed by Konno et al. (1980) which can be well approximated by the gamma function relation (Lasheras et al., 2001)

$$f(L_i, L_j) = \frac{\Gamma(12)}{\Gamma(9)\Gamma(3)L_j}\left(\frac{L_i}{L_j}\right)^8\left(1-\frac{L_i}{L_j}\right)^2 \qquad (3.49)$$

$$\int_0^{l_p} f(L_i, L_j) dl_j = 1.0 \qquad (3.50)$$

The change in drop size distribution due to breakup for a specific drop size class L_i can now be obtained by

$$\frac{\partial N_b(L_i)}{\partial t} = \sum_{j=i+1}^{p} m(L_j) f(L_i, L_j) g(L_j) N(L_j) - g(L_i) N(L_i, t) \qquad (3.51)$$

$$D_B = g(L_i) N(L_i, t) \qquad (3.52)$$

$$B_B = \sum_{j=i+1}^{p} m(L_j) f(L_i, L_j) g(L_j) N(L_j) \qquad i, j = 1,2,3....p \qquad (3.53)$$

$$\frac{\partial N_b}{\partial t} = B_B - D_B \qquad (3.54)$$

where B_B and D_B denote the rate of formation and destruction of drops of size L_i respectively.

Dissolution Discretization

If the drop size distribution is taken to be well represented by Figure 3-16, with the drop diameter as the internal coordinate, then the number of drops, dN_{in}, that will shrink into the *(i-1)th* class size from the *ith* class size in time *dt* will be given by;

$$dN_{Out} = G_i n(L_i)dt \qquad (3.55)$$

$$dN_{Out} = \frac{N_i}{l_{i+1} - l_i} G_i dt \qquad (3.56)$$

where G is the dissolution rate function (m/s) or $\frac{dL}{dt}$.

Similarly, a number of drops will shrink into the *ith* class size from the *(i+1)th* class size according to:

$$dN_{in} = G_{i+1} n(L_{i+1})dt \qquad (3.57)$$

$$dN_{in} = \frac{N_{i+1}}{l_{i+2} - l_{i+1}} G_{i+1} dt \qquad (3.58)$$

The overall change in the *ith* size class due to dissolution will be obtained by difference as

$$\frac{dN_i}{dt} = \left(G_{i+1} \frac{N_{i+1}}{l_{i+2} - l_{i+1}} - G_i \frac{N_i}{l_{i+1} - l_i} \right) \qquad (3.59)$$

Equation (3.59) can be written in a more general form as

$$\frac{\partial N_i}{\partial t} = G \frac{\partial N_i}{\partial l} \qquad (3.60)$$

This is the net effect of dissolution on drops in the *ith* size class

The accuracy of any discretized scheme is validated based on its prediction of the rate of change of the moments. The *jth* moment equation of any distribution is given by

$$m_j = \int_0^\infty L^j n(L) dL \qquad (3.61)$$

and the discretized form of the moment equation is

$$m_j = \sum_j \int_{L_i}^{L_{i+1}} L^j n dL \qquad (3.62)$$

consequently, the rate of change of the moment equation is now obtained as

$$\frac{\partial m_j}{\partial t} = \sum_i \overline{L_i^j} \frac{dN_i}{dt} \qquad (3.63)$$

The first four moments are of particular interest; the total number, length, area and volume of drops per unit volume are described by

$$m_0 = N_T = \sum \int_{L_i}^{L_{i+1}} ndL \qquad (3.64)$$

$$m_1 = k_L L_T = \sum \int_{L_i}^{L_{i+1}} L\, ndL \qquad (3.65)$$

$$m_2 = k_A A_T = \sum \int_{L_i}^{L_{i+1}} L^2 ndL \qquad (3.66)$$

$$m_3 = k_V V_T = \sum \int_{L_i}^{L_{i+1}} L^3 ndL \qquad (3.67)$$

The discretized method proposed by Hounslow et al. (1988) has been shown to give very good results with only an error of 1.8% in the prediction of the third moment. Some other methods in literature are those proposed by David et al. (1991), Marchal et al. (1988) and the conventional means (equation) but all these earlier methods fail to accurately predict all the moments accurately (Kresta et al., 2005). Although these discretized models are proposed for growth processes, they can also be utilized for dissolution processes by simply putting a minus sign (-) in front of the growth rate function.

However, when the method proposed by Hounslow et al. is used, the drop size distribution reveals uncontrolled oscillations, starting from the first drop size class and propagating through the entire discretized length. To illustrate this problem, an initial distribution using a normal distribution function with mean drop size a = 1.17×10^{-7}m and standard deviation b = 2.10×10^{-8}m is used for a pure dissolution case with size-independent dissolution rate G = -4.0×10^{-10}m/s. The transient analytical solution for this problem using the method of characteristics (Randolph and Larson, 1971) is given by

$$n(t,L)=\frac{N_T}{b\sqrt{2\pi}}\exp\left[-\left(\frac{-G\left(t+\frac{L}{G}\right)+a}{b\sqrt{2}}\right)^2\right] \qquad (3.68)$$

where L is drop size, t is the simulation time and N_T is the total number of drops. The comparison between model prediction using Hounslows' discretized model and the analytical solution (3.68) for a simulation time of 100s is presented in Figure 3-19.

This weakness in the model by Hounslow et al. is due to the fact that the discretized model was designed based on central differencing method and processes that shrink to the smallest drop class will always result in this uncontrolled oscillation.

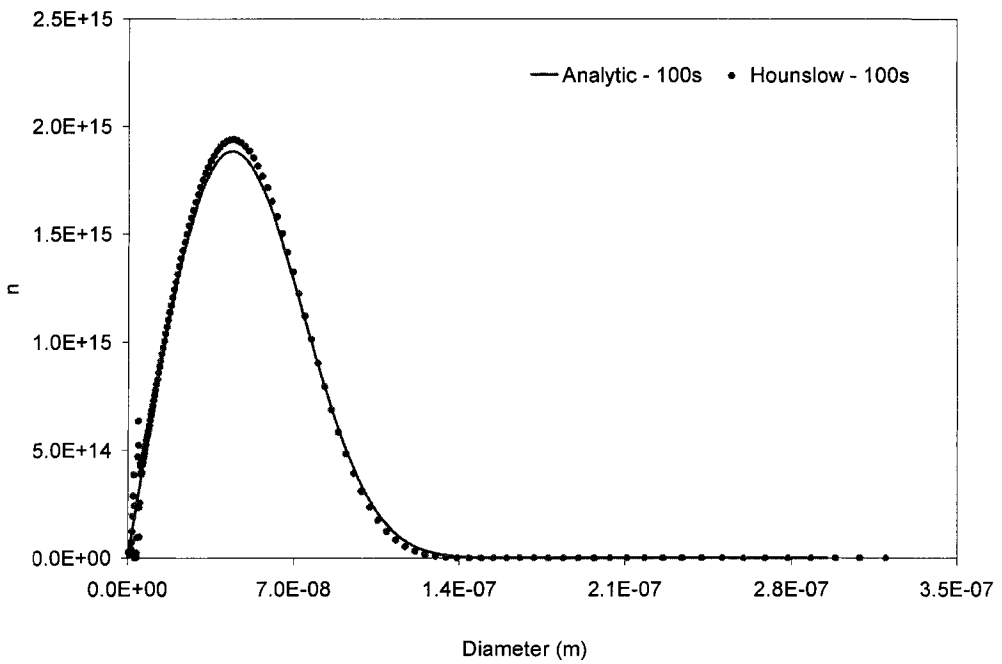

Figure 3-19: Drop size distribution showing the uncontrolled oscillation beginning in the first drop size class using method by Hounslow et al. (1998)

A corrective approach that will eliminate the uncontrolled oscillation with no significant error is one that involves a proper choice of differencing method for different processes. Processes that lead to a reduction in particle size will be more accurately predicted by using the forward differencing methods conversely, processes that lead to an increase in drop size will be better modeled using the backward differencing approach. This is the motivation for the new discretized method proposed below.

A modified Hounslow discretized dissolution scheme is now proposed using the forward differencing scheme. This scheme is capable of predicting the first four moments of the distribution without any error and also eliminates the uncontrolled oscillation in the distribution which occurs when using either the backward or central differencing scheme.

The expression for the modified scheme is given by

$$\frac{\partial N_i}{\partial t} = \frac{G}{L_i}(aN_i + bN_{i+1} + cN_{i+2} + dN_{i+3}) \qquad (3.69)$$

where a, b, c and d are constant, which are determined based on the criteria required to satisfy as many moments as possible (which in this case are the first four moments). Applying equation (3.63) to equation (3.69) we get;

$$\frac{\partial m_j}{\partial t} = \sum_i \bar{L}_i{}^j \frac{dN_i}{dt} = jGm_{j-1} \qquad (3.70)$$

$\bar{L}_i$ is the characteristic drop size for the *ith* class and is defined as, for a geometric length scale,

$$\bar{L}_i = \left(\frac{1+r}{2r} L_i\right) \qquad (3.71)$$

Thus equation (3.70) becomes

$$\frac{\partial m_j}{\partial t} = G\sum_i \left(\frac{1+r}{2r}\right)^j L_i^{j-1}(aN_i + bN_{i+1} + cN_{i+2} + dN_{i+3}) \qquad (3.72)$$

$$\frac{\partial mj}{\partial t} = G\sum_i \left(\frac{1+r}{2r}\right)^j L_i^{j-1} N_i(a + br^{1-j} + cr^{2-2j} + dr^{3-3j}) \qquad (3.73)$$

Comparing equation (3.70) with equation (3.73) shows that the rate of change of the jth moment will be predicted correctly if:

$$\left(\frac{1+r}{2r}\right)(a + br^{1-j} + cr^{2-2j} + dr^{3-3j}) = j \qquad (3.74)$$

Setting j to 0, 1, 2 and 3 in equation will generate four systems of linear equations that can be solved to give:

$$a = \frac{r(3r^3 + 4r^2 + 3r + 1)}{(r^2 - 1)(r^2 + r + 1)} \qquad (3.75)$$

$$b = \frac{(r^4 + 2r^3 + 3r^2 + 2r + 1)}{(1 - r)(r^2 + r + 1)} \qquad (3.76)$$

$$c = \frac{r(r^2 + r + 1)}{(r^2 - 1)} \qquad (3.77)$$

$$d = \frac{r^3}{(1 - r)(r^2 + r + 1)} \qquad (3.78)$$

The discretized equation for the dissolution process becomes

$$\frac{\partial N_i}{\partial t} = \frac{G}{L_i}\left(\begin{array}{l} \dfrac{r(3r^3+4r^2+3r+1)}{(r^2-1)(r^2+r+1)}N_i + \dfrac{(r^4+2r^3+3r^2+2r+1)}{(1-r)(r^2+r+1)}N_{i+1} \\ + \dfrac{r(r^2+r+1)}{(r^2-1)}N_{i+2} + \dfrac{r^3}{(1-r)(r^2+r+1)}N_{i+3} \end{array}\right) \qquad (3.79)$$

This discretized form will now be used to predict the change in number density of the drops in each mixing field. The drop size distribution prediction obtained using this new method is now compared with that proposed by Hounslow et al (when used for dissolution processes) in Figure 3-20 and Figure 3-21. The zeroth, first, second and third moments were accurately predicted, as expected.

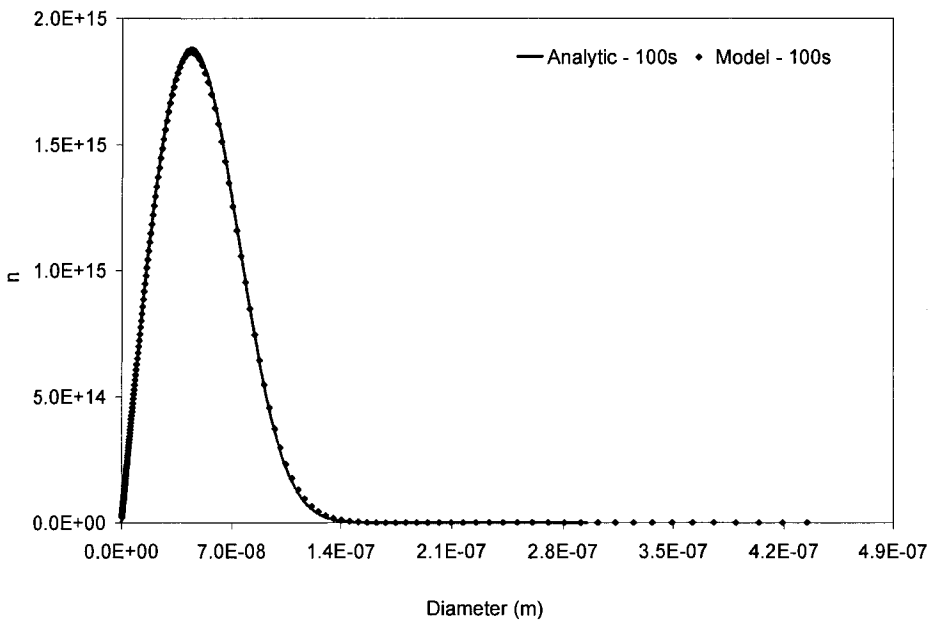

Figure 3-20: Drop size distribution using the new discretized method showing very good agreement with analytical solution

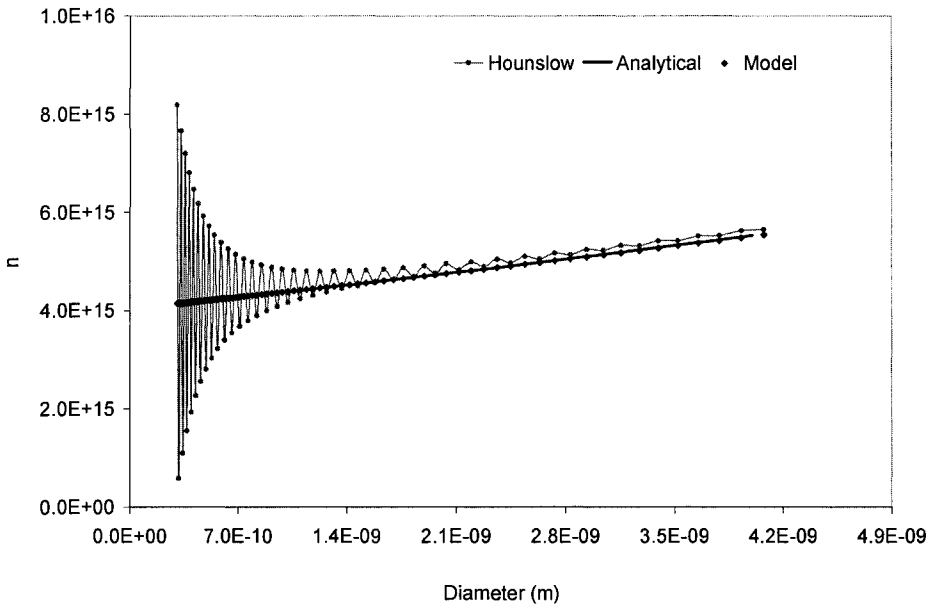

Figure 3-21: Comparison between the prediction of the new discretized method and the method by Hounslow et al. (1988)

Convective Flow Discretization

Figure 3-22 is a schematic representation of the convective flow circulation pattern for the redistribution of the dispersed drop distribution. The flow originates from the impeller swept volume (zone 1), where it is discharged into the impeller discharge regions (zones 1, 2 & 3) and eventually unfolded into the bulk of the tank. The stirred tank is operated in the batch mode but each mixing zone is a continuous stirred cell. The spatial boundaries and flow properties of each mixing zone have been defined (see Table 3-2 and Table 3-3). We assume that the flow circulation is only in the axial direction and there is no flow through the prescribed boundaries in the tangential and radial directions. We further assume that each mixing zone is well mixed after each hydrodynamic event for the specified integration time.

The convective terms in the discretized population equation can be calculated as

$$N_{i,j,in} = \sum_{k=1}^{5} \frac{Q_{kj} N_{i,k}}{V_j} \qquad (3.80)$$

$$N_{i,j,out} = \sum_{k=1}^{5} \frac{Q_{jk} N_{i,j}}{V_j} \qquad (3.81)$$

where the double indexed $N_{i,j}$ is the number distribution of drop of size i in mixing zone j, and *in* or *out* denote the direction of flow in the mixing zone. k is a dummy variable that represents the mixing zones that contribute to the convective flow for a specified mixing zone j.

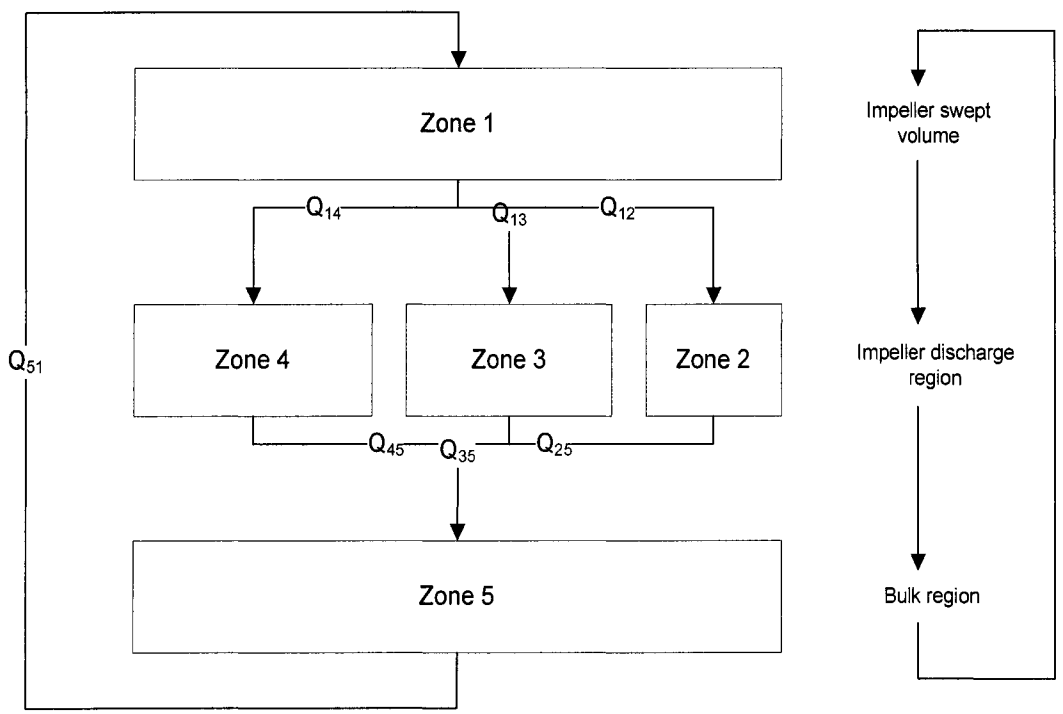

Figure 3-22: Block diagram of the flow circulation between zones

3.6.2 Population Balance Implementation

The solution sequence for the discretized population balance is given in the flow sheet below (Figure 3-23). The input requirements for the simulation include equipment geometry, vessel diameter, fluid height, impeller speed and diameter; transport and physical properties of the liquid-liquid systems (density, viscosity, interfacial tension, diffusivity, molecular mass); flow parameters such as the power number, and the pumping capacity (flow number) for that tank-impeller configuration; and two statistical descriptors describing the initial drop size distribution of the dispersion (taken as the drop size distribution obtained experimentally 20 seconds after complete injection of the dispersed phase into the continuous phase).

The flow field within the mixing tank is assumed to be fully turbulent since Re > 20000, and isotropic turbulence is applied in each mixing zone. The volume, volumetric flow rates, kinetic energy dissipation rates and residence in each prescribed zone can be calculated according to Table 3-2 and Table 3-3. Having defined the mixing model and the flow parameters, the length domain discretization and an initial drop size distribution are calculated (equation (3.36)). The time step required for the iterative scheme is calculated (equation (3.34)) and compared with the residence time in each zone; the smallest value is selected as the integration time step. For each iterative step, the hydrodynamic events (drop breakup, drop dissolution and convective transport of drops) affecting the drop size distribution are computed for each drop size class and redispersed in each mixing zone according to the convection model (Figure 3-22). The dispersion is assumed to be well mixed after each time integration cycle, so a material balance of the dispersed phase is computed (equation (3.24)) for the entire stirred tank to update the change in concentration in the continuous phase due to the dissolution process. This iterative scheme is continued until the simulation time is reached.

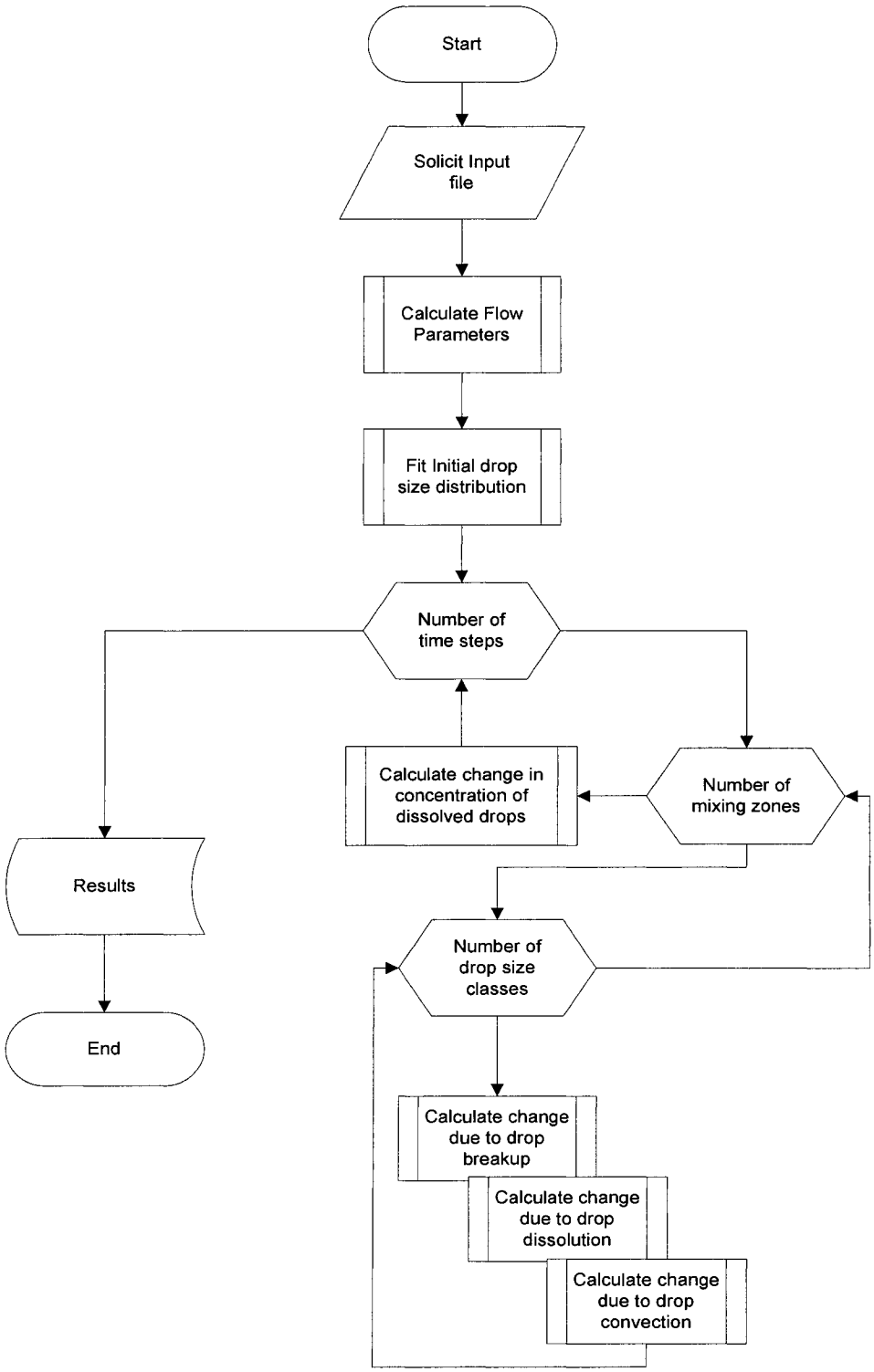

Figure 3-23: Flow sheet of the model implementation scheme

3.7 Conclusions

A framework for the numerical model and the discrete formulations of the population balance has been developed. The turbulence inhomogeneity in the stirred tank has been modeled using five (5) mixing zones which capture the regions where significant variations exist in the fluid properties. Changes in the drop size distribution and dispersed phase concentration for a low dispersed phase volume fraction are modeled using population balances and material balances respectively.

In the next chapter, the model results will be compared with the experimentally determined values of the system variables (drop size distribution, mean drop diameter, and the bulk concentration of the dispersed phase in the continuous medium).

3.8 References

Alopaeus V., Koskinen J., and Keskinen K. I., 1999, *Simulation of the Population Balances for Liquid-Liquid Systems in a Non-ideal Stirred Tank. Part 1: Description and Quantitative validation of the Model,* Chem. Eng. Sci., **54** (24), 5887 - 5899.

Batchelor G. K., 1982, *The Theory of Homogenous Turbulence,* Cambridge University Press, Cambridge, England.

Bhattacharya S., Kresta M. S., 2002, *CFD Simulations of Three-dimensional Wall Jets in a Stirred Tank,* Can. J. Chem. Eng., **80**, 1 - 15.

Boyadzhiev L., and Elenkov D., 1966, *On the Mechanism of Liquid-Liquid Mass Transfer in a Turbulent Flow Field,*, Chem. Eng. Sci., **21** (11), 955 - 959.

Brian P. L. T., Hales H. B., and Sherwood T. K., 1969, *Transport of Heat and Mass Between Liquids and Spherical Particles in An Agitated Tank,* AIChE J., **15** (5), 727 - 731.

Calderbank P. H., 1967, Mass Transfer: In Mixing Theory and Practice; Uhl V. W., Gray J. B., Eds.; Academic Press: New York, **2**.

David R., Villermaux J., Marchal P., and Klein J. P., 1991, *Crystallization and Precipitation Engineering IV: Kinetic Model of Adipic Acid Crystallization,* Chem. Eng. Sci., **46** (4), 1129 – 1136

Glen J. B., 1965, *Mass Transfer in Dispersed Systems*, cited from: Skelland A. H. P., and Kanel, J. S., "*Simulation of Mass Transfer in a Batch Agitated Liquid-Liquid Dispersion*", Ind. Eng. Chem. Res., **31** (3), 910-913.

Hemrajani R. R., and Tatterson G. B., 2004, *Mechanical Stirred Vessels,* cited from: Handbook of Industrial Mixing: Science and Practice; Paul E. L., Atiemo-Obeng V. A., and Kresta S. M., Eds.; John Wiley & Sons, Inc: Hoboken, New Jersey; 345 - 390.

Hinze J. O., 1955, *Fundamentals of the Hydrodynamics Mechanisms of Splitting in Dispersion Process*, AIChE J., **1** (3), 289 - 295.

Hockey R. M., and Nouri J. M., 1996, *Turbulent Flow in a Baffled Vessel Stirred by a 60° Pitched Blade Impeller*, Chem. Eng. Sci., **51** (19), 4405 - 4421.

Hounslow M. J., 1990, *A Discretized Population Balance for Continuous Systems at Steady State*, AIChE J., **36** (1), 106 - 116.

Hounslow M. J., Ryall R. L., and Marshall V. R., 1988, *A Discretized Population Balance for Nucleation, Growth and Aggregation*, AIChE J., **34** (11), 1821 - 1832.

Jaworski Z., and Fort I, 1991, *Studies on Mixing .79: Energy Dissipation Rate in a Baffled Vessel with Pitched Blade Turbine Impeller*, Collection of Czechoslovak Chem. Comm., **56** (9), 1856 - 1867.

Jaworski Z., Nienow A. W., and Dyster K. N., 1996, *An LDA Study of the Turbulent Flow Field in a Baffled Vessel Agitated by An Axial, Down-pumping Hydrofoil Impeller*, Can. J. Chem. Eng. **74** (1), 3 - 15.

Kolmogorov A. N., 1949, *On the Breakage of Drops in a Turbulent Flow*, Dokl. Akad. Navk. SSSR **66** (5), 825 - 828.

Konno M., Matsunaga Y., Arai K., and Saito S., 1980, *Simulation Model for Breakup Process in An Agitated Tanks,* J. Chem. Eng. Jpn.., **13** (1), 67 – 73.

Kresta S. M., 1998, *Turbulence in Stirred Tanks: Anisotropic, Approximate, and Applied*, Can. J. Chem. Eng. **76** (3), 563 - 576.

Kresta S. M., and Wood P. E., 1993, *The Mean Flow Field Produced by a 45° Pitched Blade Turbine – Change in the Circulation Pattern due to Off-Bottom Clearance*, Can. J. Chem. Eng. **71** (1), 42 - 53.

Kresta S., Anthieren G., and Parsiegla K., 2005, *Model reduction for Prediction of Silver Halide Precipitation*, Chem. Eng. Sci., **60** (8/9), 2135 - 2153.

Kumar A., and Hartland S., 1999, *Correlations for Prediction of Mass Transfer Coefficients in Single Drop Systems and Liquid-Liquid Extraction Columns*, Chem. Eng. Res. & Des., **77** (A5), 372 - 384.

Lamont J. C., and Scott D. S., 1970, *An Eddy Cell Model of Mass Transfer into the Surface of a Turbulent Liquid*, AIChE J., **16** (4), 513 - 519.

Lasheras, J.C., Eastwood, C., Martinez-Bazan, C., Montanes, J.L., 2002, *A Review of Statistical Models for the Break-up of an Immiscible Fluid Immersed into a Fully Developed Turbulent Flow,* International Journal of Multiphase Flow, **28**, 247-278

Lee C. H., Erickson L. E., and Glasgow L. A., 1987, *Dynamics of Bubble Size Distribution in Turbulent Gas-Liquid Dispersions,* Chem. Eng. Comm., **61** (1/6), 181 – 195.

Levins D. M., and Glastonbury J. R., 1972, *Particle-Liquid Hydrodynamics and Mass Transfer in a Stirred Vessel II: Mass Transfer*, Trans. Inst. Chem. Eng., **50** (2), 132.

Luo H., and Svendsen F., 1996, *Theoretical Model for Drop and Bubble Breakup in Turbulent Dispersions*, AIChE J., **42** (5), 1225 - 1233.

Maggioris D., Goulas A., Alexopoulos A. H., Chatzi E. G., and Kiparissides C., 2000, *Prediction of Particle Size Distribution in Suspension Polymerization Reactors: Effect of Turbulence Nonhomogeneity,* Chem. Eng. Sci., **55** (20), 4611 - 4627.

Marchal P., David R., Klein J. P., Villermaux J., 1988, *Crystallization and Precipitation Engineering 1: An Efficient Method for Solving Population Balance in Crystallization with Agglomeration*, Chem. Eng. Sci., **43** (1), 59 – 67.

Pangarkar V. G., Yawalkar A. A., Sharma M. M., and A. A. C. M. Beenackers, 2002, *Particle-Liquid Mass Transfer Coefficient in Two-/Three-Phase Stirred tank Reactors*, Ind. Eng. Chem. Res., **41** (17), 4141 - 4167.

Park, J. Y., and Blair, L.M., 1975, *The Effect of Coalescence on Drop Size Distribution in an Agitated Liquid-Liquid Dispersion*, Chem. Eng. Sci., **30** (9), 1057 - 1064.

Perry's Chemical Engineers' Handbook, 1997, 7th Ed., Perry R. H., and Green D. W., eds., McGraw-Hill.

Randolph A. D. and M. A. Larson, 1971, *The Theory of Particulate Processes*, Academic Press, New York.

Schafer, M., Yianneskis, M., Wachter, P., and Durst, F., 1998, *Trailing Vortices around a* 45^0, Fluid Mechanics and Transport Phenomena, AIChE J., p1233-1246

Tennekes H., and Lumley J. L., 1972, *A First Course in Turbulence*, MIT Press, Cambridge, MA, USA.

Tsouris C., and Tavlarides L. L., 1994, *Breakage and Coalescence Models for Drops in Turbulent Dispersions*, AIChE J., **40** (3), 395 - 406.

Williams F. A., 1985, Combustion Theory, 2nd ed., Benjamin/Cummings, Menlo Park, CA, USA.

Yianneskis M., Popiolek Z., and Whitelaw J. H., 1987, *An Experimental Study of the steady and Unsteady Flow Characteristics of Stirred Reactors*, Journal of Fluid Mechanics., **175**, 537 - 555.

Zhou G. W., and Kresta S., M., 1996, *Impact of Tank Geometry on the Maximum Turbulence Energy Dissipation Rate for Impellers*, AIChE J., **42** (9), 2476 - 2490.

Zhou G., 1997, *Characteristics of Turbulence Energy Dissipation and Liquid-Liquid Dispersions in An Agitated Tank*, Ph.D. Dissertation, Department of Chemical & Materials Engineering, University of Alberta, Canada.

Chapter 4

Results: Experiments & Simulations

The model described in Chapter 3 can be used as a tool for predicting the transient drop size distribution in liquid-liquid dispersions; the dissolved solute concentration; and also the dissolution time. However, the usefulness of the model is dependent on its ability to accurately predict these properties in real liquid-liquid dispersion systems. Thus, this chapter will focus on the experimental validation of the numerical model; its use in further understanding the controlling mechanism(s) affecting drop dissolution; the influence of some of the system variables on the dissolution time; and to test if any consistent correlation between the dissolution time and the blend time exists.

4.1 Experimental Runs

The equipment and experimental procedure have been discussed in Chapter 2. The system properties studied experimentally are the dispersed phase concentration in the continuous phase, which was measured using gas chromatograph; and the transient drop size distributions, measured using the PDPA. Three separate runs were done using a dispersed phase volume fraction of 0.01 and impeller rotational speeds of 550 rpm, 650 rpm and 750 rpm according to the procedure given in Section 2.5.2. These experimental runs will be used to validate the model prediction.

4.2 Experimental Validation

The input parameters for the model are only those which define the experimental condition. There are no fitting parameters as such, although the mass transfer coefficient correlation was selected according to the best fit, as given in Section 3.4.2.

The dissipation rates predicted by the model are compared to experimental measurements done by Zhou and Kresta (1996). Table 4-1 shows the dissipation in all the zones and the average dissipation in the tank (assuming homogeneity in

the tank). The model sets the maximum dissipation in the tank (recorded in zone 2) equal to 45 times the average dissipation while the dissipation in the bulk is 0.1 times the average in the tank. Zhou and Kresta (1996) reported that the maximum dissipation in the tank is 37 times the average dissipation and dissipation in the bulk is 0.7 times the average dissipation. These values are of the same order of magnitude as the reported values Zhou and Kresta (1996), but will tend to slightly increase the breakup at the impeller. The value at the tip is intended to reflect the very high energy contained in the trailing vortex, very close to the impeller blade.

Table 4-1: Local energy dissipation rate for different impeller rotational speeds

N (rpm)	N (rps)	Average Dissipation (m^2/s^3)	Local Dissipation in zones (m^2/s^3)					$\varepsilon_{max}/\varepsilon_{avg}$	$\varepsilon_{bulk}/\varepsilon_{avg}$
			1	2	3	4	5		
550	9.17	0.32	3.86	14.61	3.55	1.11	0.03	45.26	0.10
650	10.83	0.53	6.36	24.07	5.85	1.82	0.05	45.17	0.10
750	12.50	0.82	9.78	37.00	8.99	2.80	0.08	45.21	0.10

Concentration Profile

Figure 4-1 to Figure 4-3 show the concentration of the dissolved diethyl malonate plotted against the dissolution time. The initial measured concentration corresponding to the initial drop size distribution 20 seconds after injection of diethyl malonate in the tank is about 10.5 kg/m^3. This dissolved concentration represents about 85% of the injected diethyl malonate indicating very fast dissolution rates in the early seconds of the process.

The data obtained from the GC is calibrated based on the calibration curve (Figure 2-3). The error in the measured concentration is very small (the calibration curve has a coefficient of determination of 0.99), hence, it will be a good validation criteria for the numerical model.

Figure 4-1 shows the bulk concentration profile for an impeller rotational speed of 550 rpm. The model over predicts the dissolved bulk concentration and gives poor agreement with the experimentally observed values. This over prediction is either due to an over estimation of the mass transfer rate in the model; or the presence of drop coalescence in the tank, resulting in a reduction of the specific interfacial area for mass transfer, hence, mass transfer is reduced. When the impeller rotational speed is increased to 650 rpm, the model prediction shows good agreement with the experimental results (Figure 4-2). For an impeller rotational speed of 750 rpm, the model prediction also gives good agreement with experimental results (Figure 4-3). An increase in impeller rotational speed implies an increase in the turbulent conditions in the stirred tank and increased drop breakup and mass transfer. These observations show that when the impeller rotational speed increases, the effects due to coalescence are overwhelmed by the drop breakup processes.

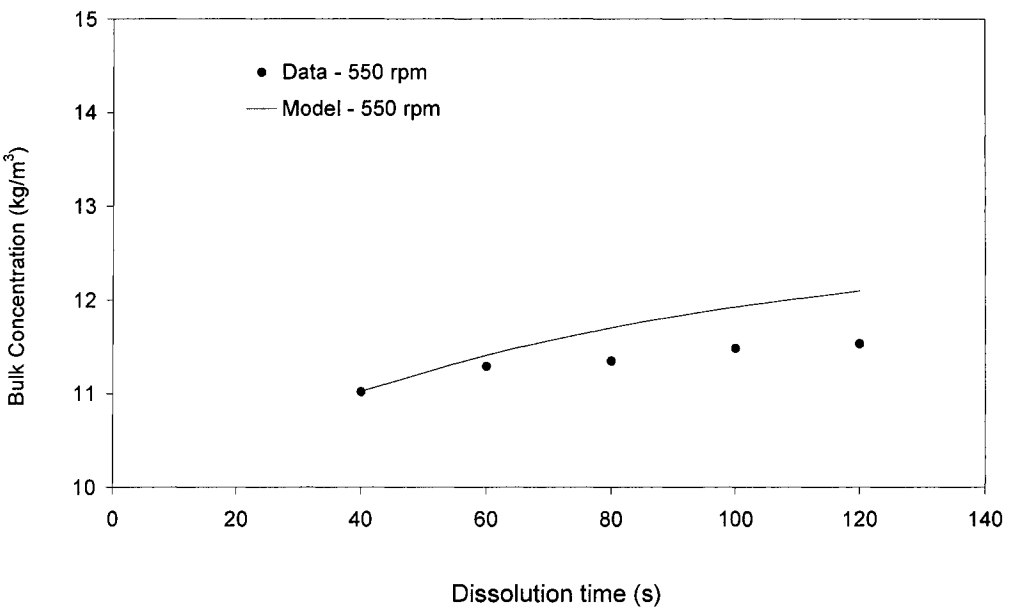

Figure 4-1: Dissolved dispersed phase concentration profile for N = 550 rpm

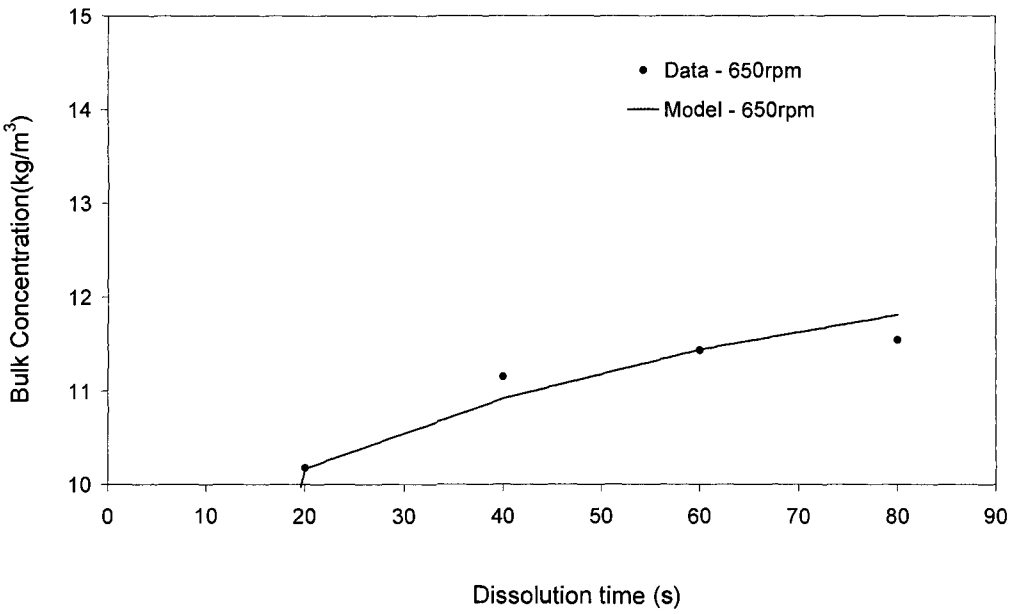

Figure 4-2: Dissolved dispersed phase concentration profile for N = 650 rpm

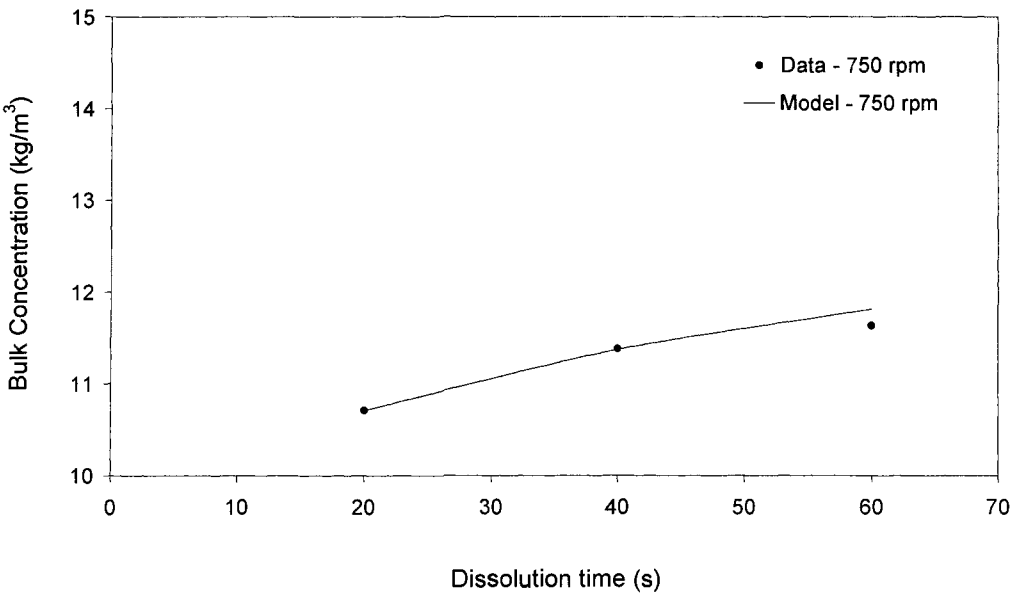

Figure 4-3: Dissolved dispersed phase concentration profile for N = 750 rpm

Sauter mean diameter

The Sauter mean diameter of a dispersed drop size distribution is very important in calculating the mass transfer rate. For this reason, the model prediction of the Sauter mean diameter will be compared with the experimentally determined value for the drop size distribution.

Figure 4-4 to Figure 4-6 show the comparison between the model prediction and the experimental result for 550, 650 and 750 rpm. All three profiles show very good agreement between the model prediction and the experimental result. As the impeller rotational speed increases, fewer data points are measured due to reduced dissolution time.

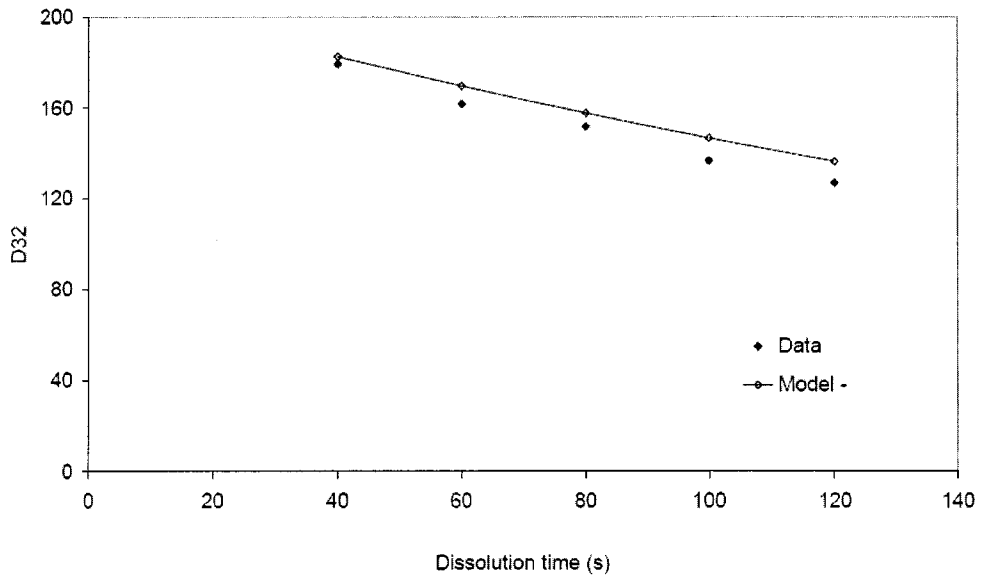

Figure 4-4: Sauter mean diameter profile for N = 550 rpm

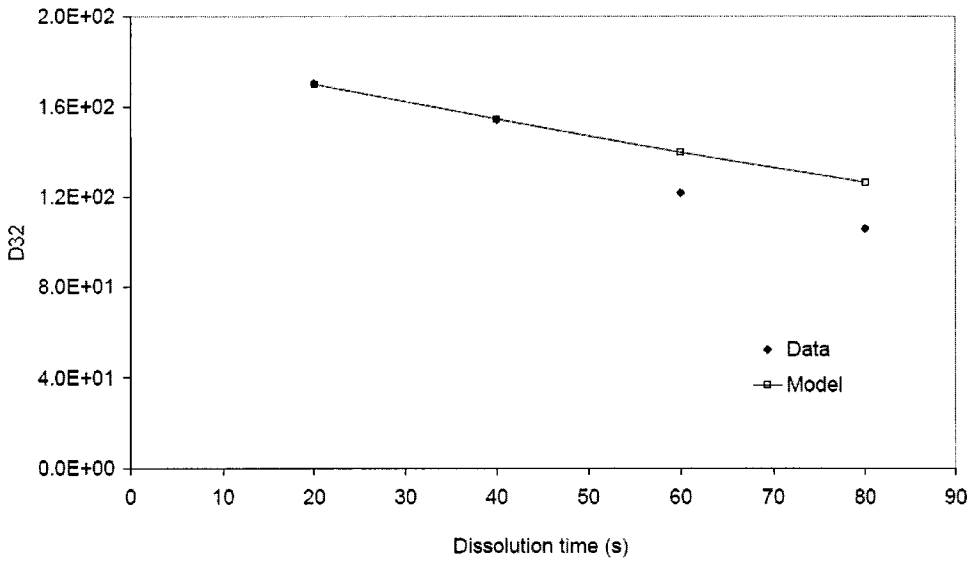

Figure 4-5: Sauter mean diameter profile for N = 650 rpm

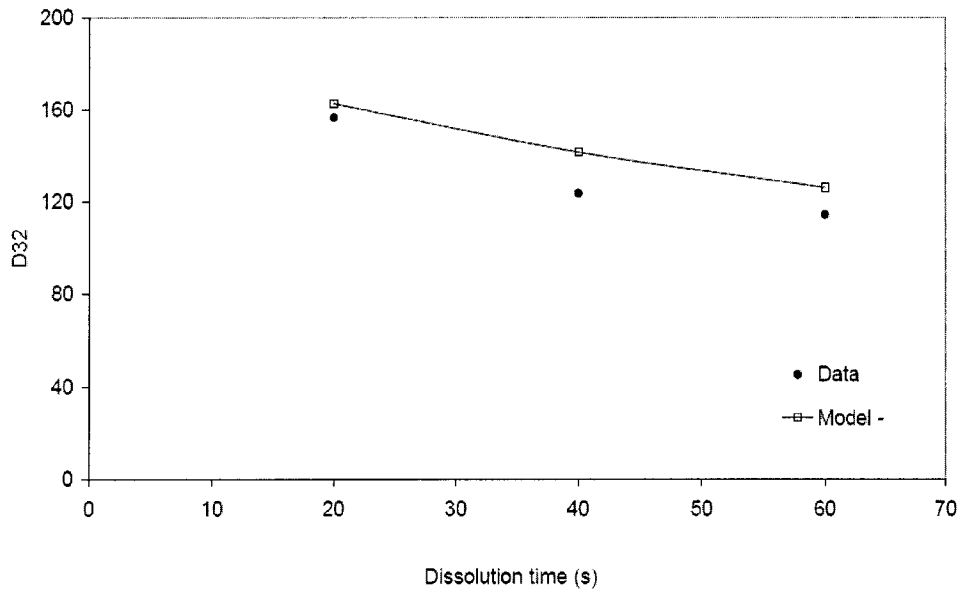

Figure 4-6: Sauter mean diameter profile for N = 750 rpm

Drop Size Distribution

The initial drop size distribution for the model is a 2-parameter log normal fit to the experimental distribution collected by the PDPA 20 seconds after the injection of the dispersed phase into the stirred tank. The parameters determine the shape (scale parameter) and modal class (location parameter) of the initial discrete experimental distribution. Because real life distributions are non-smooth, the parameters selected are those offering the minimum least squared error for the distribution (Section 3.6.1).

The drop size distributions obtained from PDPA are for drops of size range 6 μm to 303 μm with a bin spacing of 1.24 μm. The curve obtained using this distribution is non smooth, exhibiting a significant measure of scatter. Using a smooth function such as the 2 parameter log normal distribution function to represent this distribution introduces a mathematical artifact since the ends of the smooth distribution always taper down to zero but experimental observations show that the smallest bin size contains a discrete number of drops. Because of this artifact, the raw experimental drop size distribution profile will be presented along with the model prediction.

The initial data from PDPA is collected as a series of drop diameter measured as time progresses. Central averaging is used to obtain the drop size distribution for a specific time interval. That is, for 20 seconds, the data collected between 10 and 30 seconds was used. Similarly, for 40 seconds, data between 30 and 50 seconds was used and so on. Although the error inherent in this approach can not be ascertained, it may be significant.

The drop size distributions shown in Figure 4-7 to Figure 4-9 represent the normalized distribution (y-axis) plotted against the drop diameter (x-axis). The normalized number density is given by the expression below;

$$\text{Normalized distribution} = \frac{N}{N_T \Delta L} \qquad (4.1)$$

where N is the absolute number of drops in a size class, N_T is the total number of drops in the distribution and ΔL is the size class interval.

Figure 4-7 gives the transient drop size distribution for an impeller rotational speed of 550 rpm. The experimental drop size distribution data shows that the peak of the distribution after 40 seconds is at about 80 μm; about 90 μm after 60 seconds; and about 95 μm after 80 seconds. The numerical model predicts the peak distribution class to be 80 μm, 60 μm and 50 μm for 40 seconds, 60 seconds and 80 seconds respectively. Since both drop breakup and mass transfer result in drop size reduction and an overall shift to the left for the drop distribution profile, this contradiction in the drop distribution profile shift to the right is indicative of either the presence of coalescence between the drops or faster dissolution rates for smaller drops. When the impeller rotational speed is increased to 650 rpm, the experimental drop distribution profile shows a stationary distribution peak for drop size 70 μm for dissolution times 40, 60 and 80 seconds while the model predicts the distribution peak at drop sizes 70 μm , 60 μm and 50 μm for 40, 60 and 80 seconds respectively (Figure 4-8). For 750 rpm, the model prediction is in good agreement with the experimental result. The experimental result shows a gradual shift of the peak distribution to the left i.e. 70 μm after 20 seconds; 60 μm after 40 seconds; and 50 μm after 60 seconds and similarly, the model predicts 70 μm after 20 seconds; 60 μm after 40 seconds; and 50 μm after 60 seconds (Figure 4-9).

Cumulative Number Distribution

Figure 4-10 to Figure 4-12 show the cumulative drop number distribution. Similar to the drop size distribution profiles, the performance of the model prediction improves with an increase in impeller rotational speed.

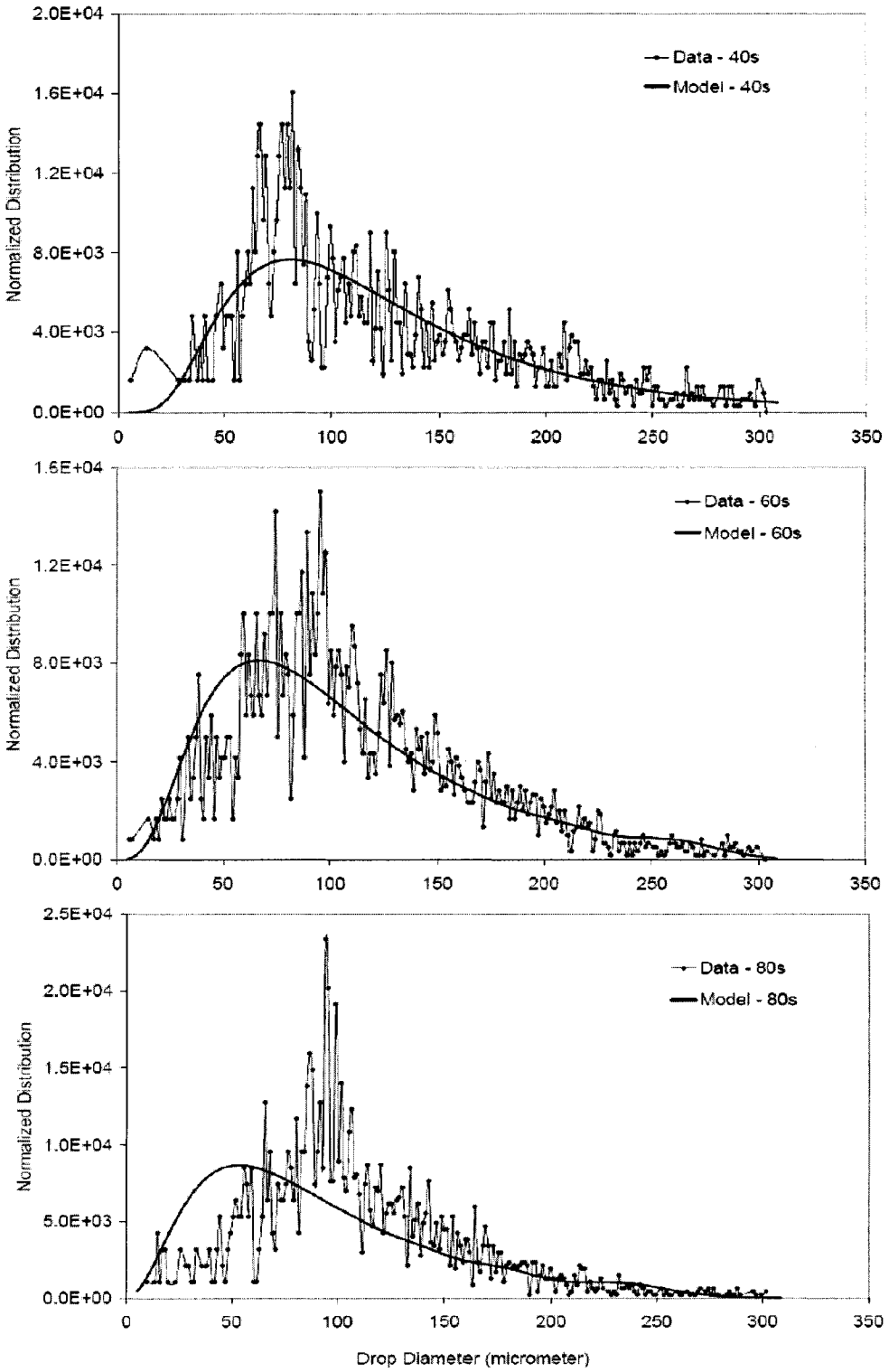

Figure 4-7: Drop size distribution profile for $\varphi = 0.01$ and N = 550 rpm

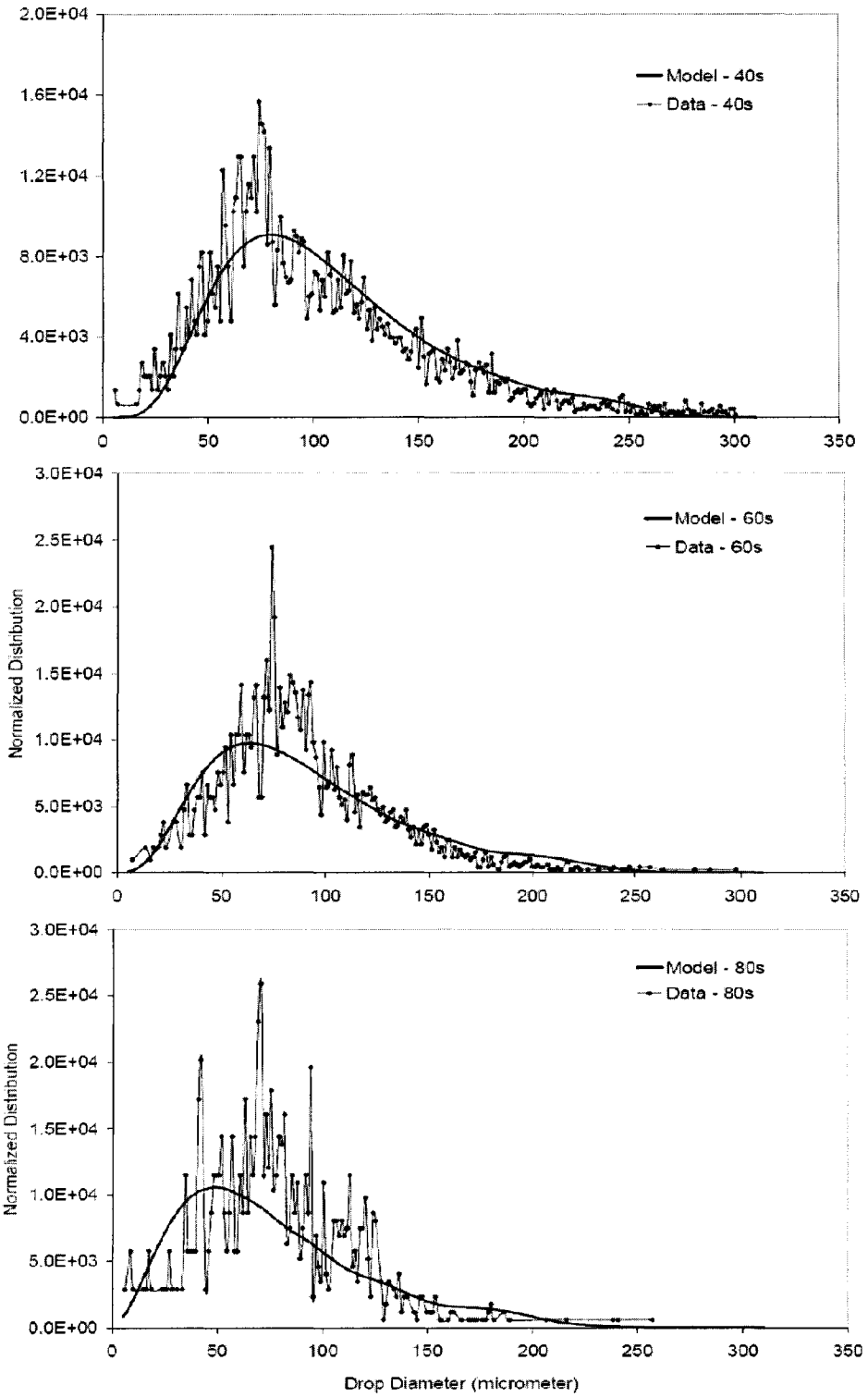

Figure 4-8: Drop size distribution profile for $\varphi = 0.01$ and N = 650 rpm

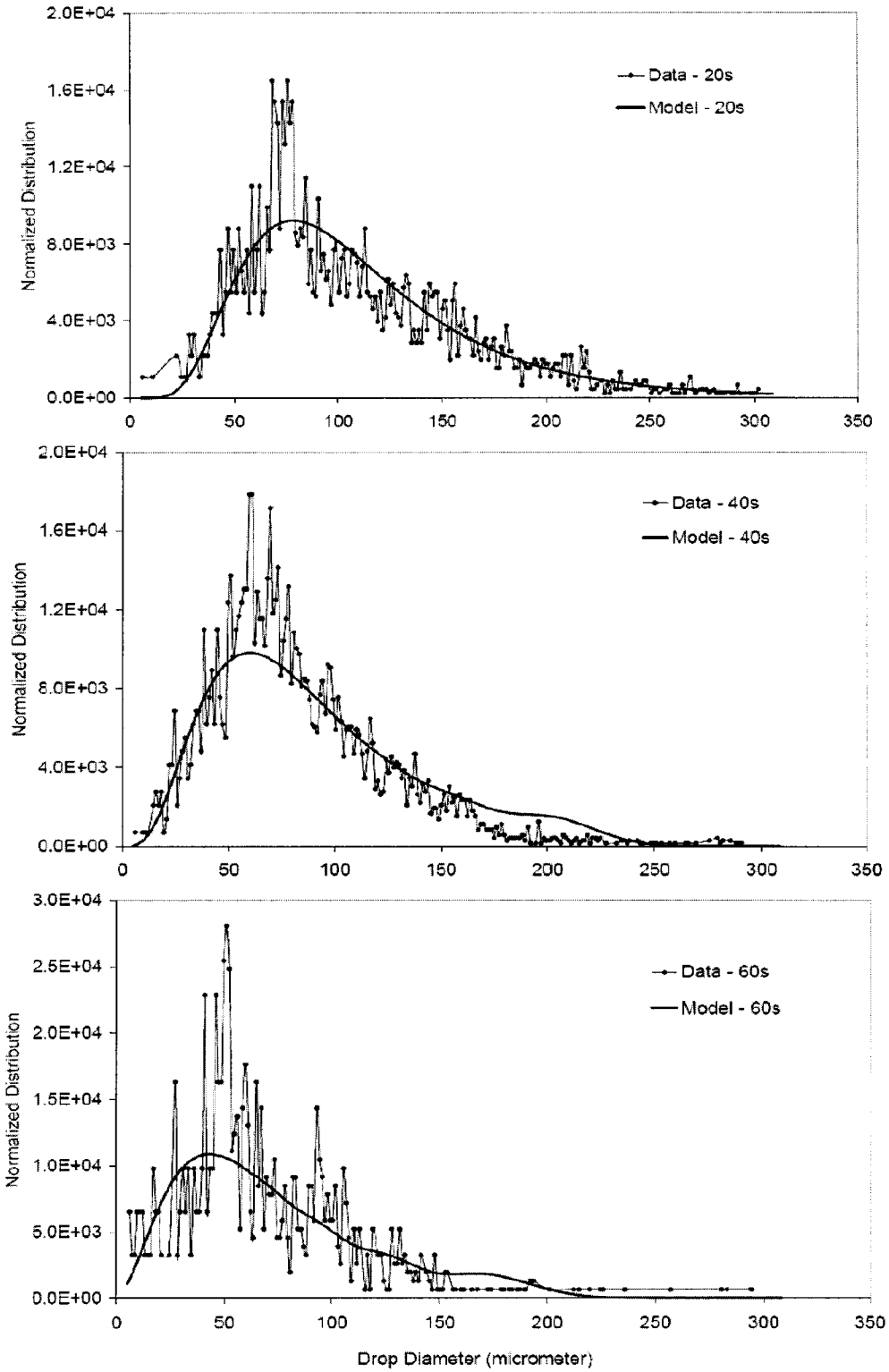

Figure 4-9: Drop size distribution profile for $\varphi = 0.01$ and N = 750 rpm

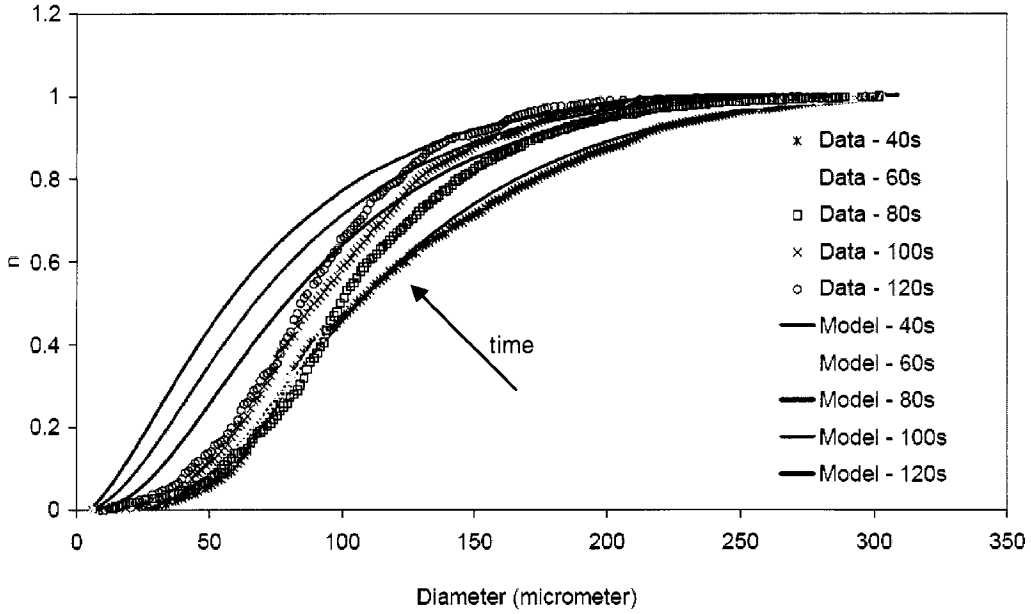

Figure 4-10: Cumulative drop size distribution profile for N = 550 rpm

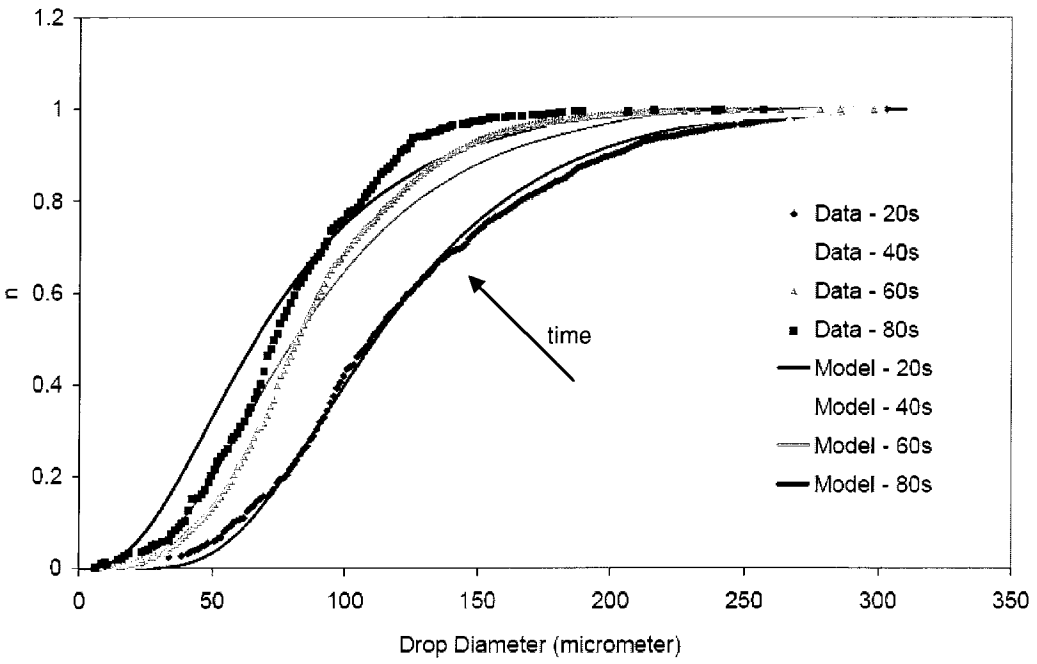

Figure 4-11: Cumulative drop size distribution profile for N = 650 rpm

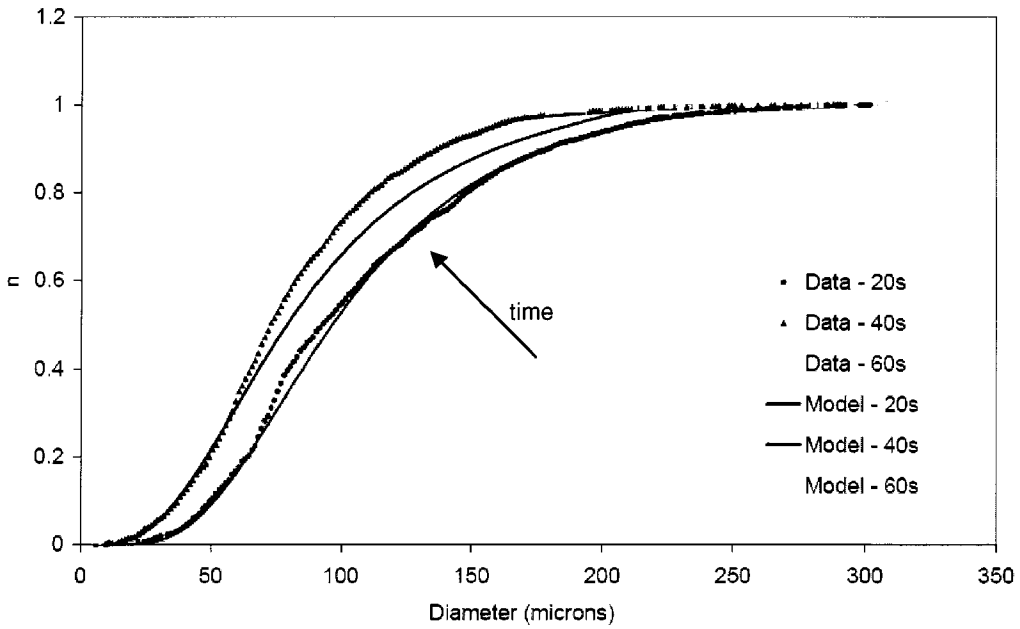

Figure 4-12: Cumulative drop size distribution profile for N = 750 rpm

4.3 Breakup Rates

In an attempt to understand the model over prediction of drop dissolution rate observed for an impeller rotational speed 550 rpm, the drop breakup rates in all five zones in the model are now analyzed for impeller rotational speeds 550, 650 and 750 rpm.

Figure 4-13 shows that the breakup rate is negligible in all five zones, for 550 rpm. This suggests that the drop size evolution is due to the mass transfer process alone. Since mass transfer results in drop size reduction and an overall shift to the left for the drop distribution profile, the drop distribution profile shift to the right suggests coalescence between the drops.

When the impeller rotational speed is increased to 650 rpm, only drops greater than 280 μm experience breakup in zone 2 (Figure 4-14). The breakup rates in zones 1, 3, 4 and 5 remain negligible (similar to Figure 4-13). However,

very few drops are exposed to the high turbulence in zone 2 due to its small volume, resulting in very few drop breakup processes. In this case, the effects of drop coalescence in the stirred tank are reduced due to drop breakup, hence the observed stationary peak distribution at 70 μm.

For 750 rpm, only drops greater than 240 μm breakup to form smaller drops in zone 2 (Figure 4-15). Compared to 650 rpm, the breakup rates are higher and more drops breakup forming smaller drops. Thus the transient drop size distribution shifts to the left indicating that drop breakup and mass transfer overwhelm drop coalescence at high rpm.

The profiles discussed above (Figure 4-13 to Figure 4-15) show that only drops passing through zone 2 will experience significant breakup. The impeller rotational speed will have to be increased much higher for there to be significant breakup in the other zones e.g. when N is 1000 rpm, the breakup rates in zones 1, 2 and 3 become significant (Figure 4-16 to Figure 4-18).

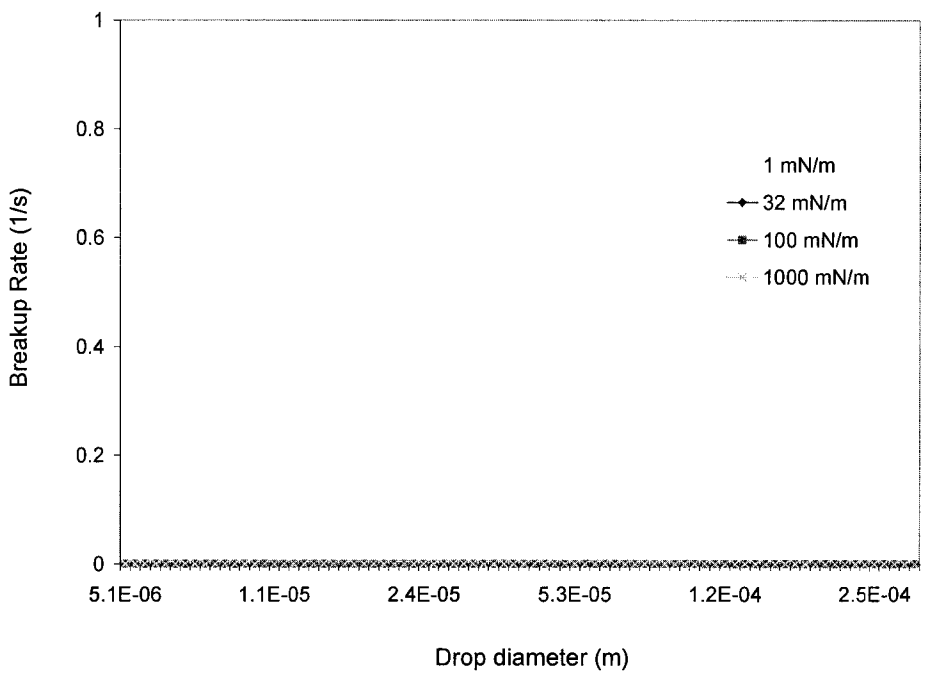

Figure 4-13: Breakup frequencies for zones 1, 2, 3, 4 and 5 (N = 550 rpm)

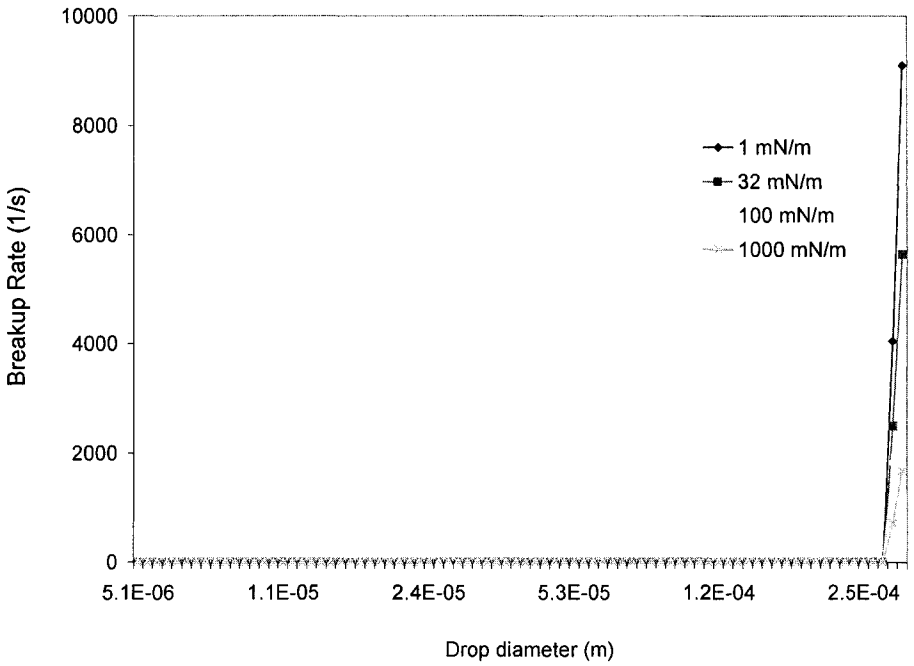

Figure 4-14: Breakup frequency for zone 2 (N = 650 rpm)

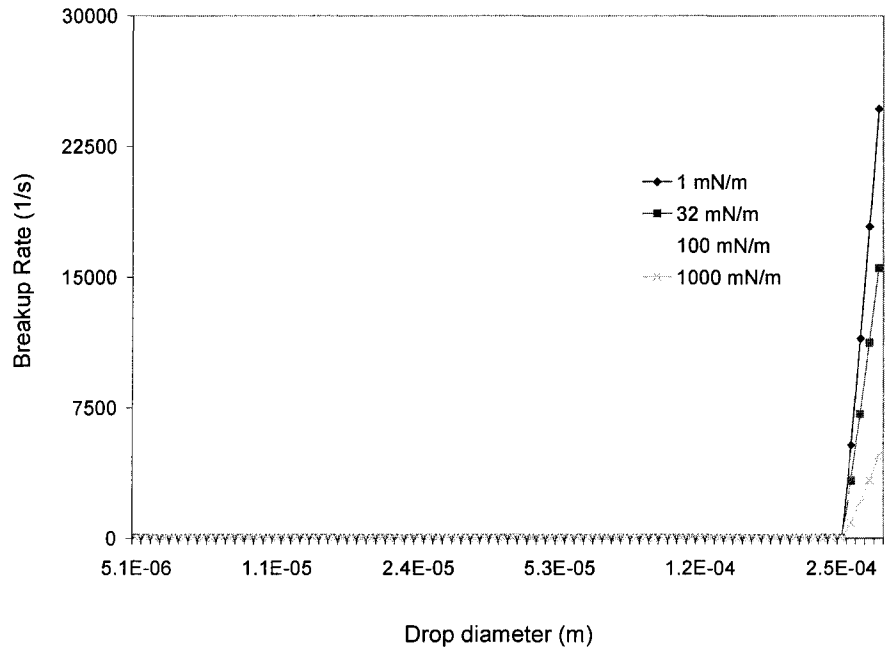

Figure 4-15: Breakup frequency for zone 2 (N = 750 rpm)

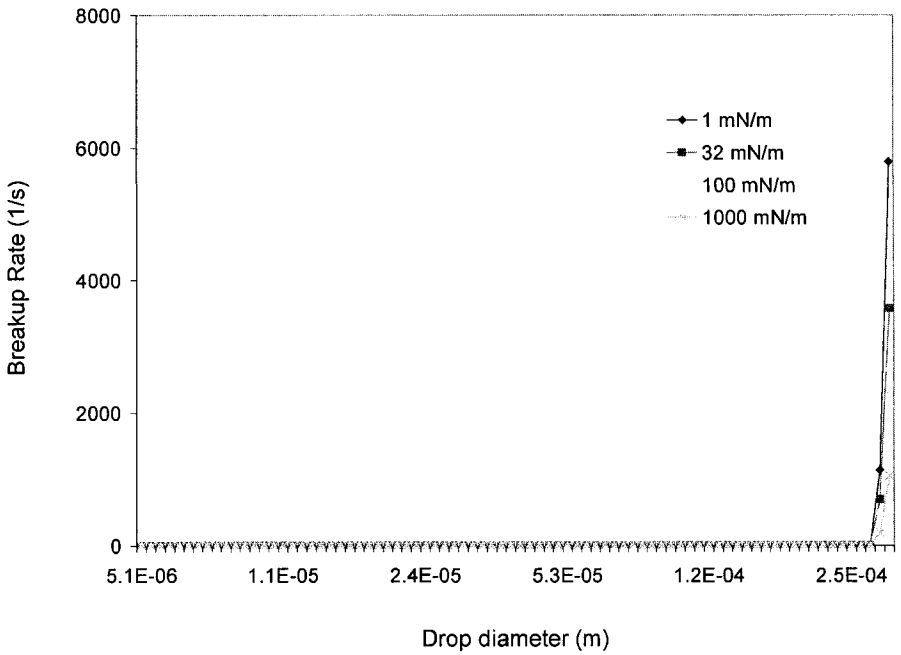

Figure 4-16: Breakup frequency for zone 1 (N = 1000 rpm)

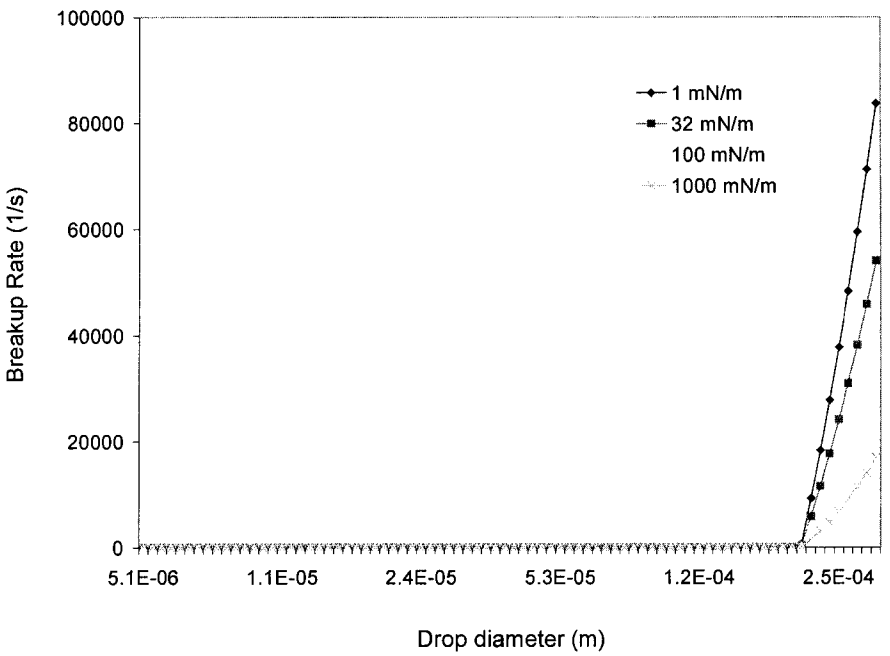

Figure 4-17: Breakup frequency for zone 2 (N = 1000 rpm)

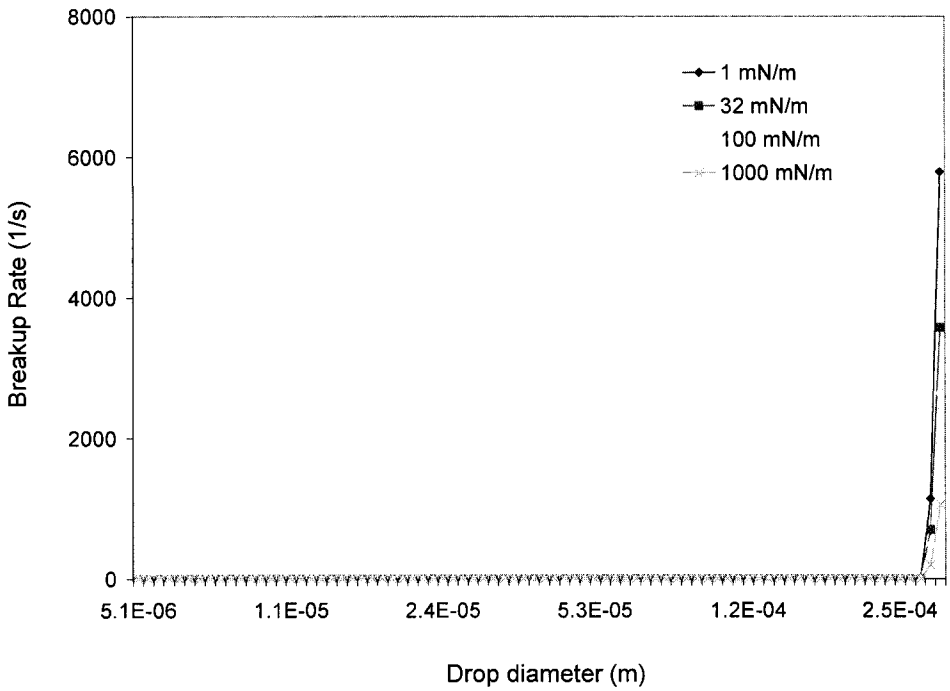

Figure 4-18: Breakup frequency for zone 3 (N = 1000 rpm)

4.4 Sensitivity Analysis

In order to understand the mechanism for drop dissolution and the effect of some variables in liquid-liquid dispersion systems, a sensitivity analysis was done.

Some of the variables in a liquid-liquid dispersion system operated in a stirred tank are: impeller geometry and location, dispersed phase volume fraction (φ), impeller rotational speed (N), continuous phase viscosity (μ) and interfacial tension (σ). However, some assumptions made during the design of the numerical model restrict the variation of certain variables. The circulation pattern and the turbulence condition within the stirred tank are dependent on the impeller geometry and location; and the dispersed phase volume fraction is constrained to ensure that coalescence within the stirred tank is negligible. Thus, within the scope of this model design, the impeller geometry and location and the dispersed

phase volume fraction will remain constant. Therefore, the variables considered for analysis are: impeller rotational speed, continuous phase viscosity and the interfacial tension between the liquid-liquid dispersions.

The dissolution-blend time ratio is a means of comparison between completely miscible liquid-liquid systems and partially miscible liquid-liquid systems given the same hydrodynamic conditions. The blend time for miscible systems is calculated using the correlation reported by Grenville (1992).

$$\theta_{95} = 5.2\frac{T^{1.5}H^{0.5}}{N_p^{1/3}ND^2} \qquad (4.2)$$

θ_{95} is the time taken to achieve 95% homogeneity within the stirred tank.

In order to investigate the main effects of the variables identified above, only the variable under investigation will be varied for any given scenario. The saturation concentration of diethyl malonate is 27.63 kg/m^3 and the actual solute concentration injected is about 50% of the saturation concentration.

4.4.1 Influence of impeller rotational speed

From the experimental validation of the model, the drop breakup rates become significant for impeller rotational speed 650 rpm and higher. For this analysis, 750 rpm and 1500 rpm are used to ensure that effect of drop breakup can be studied.

From Table 4-2, increasing N by a factor of 2, from 750 rpm to 1500 rpm while keeping σ = 0.032 N/m and μ = 0.000894 Pa.s, the dissolution time reduces by more than a factor of 2 (from 337 seconds to 130 seconds). However, the dissolution-blend ratio only reduces by about 20%. (from 91.27 to 70.23). This indicates that N has a profound influence on the mass transfer rate.

Increasing the impeller rotational speed leads to an increase in the continuous phase Reynolds number of the fluid in the tank, hence, a higher turbulent condition is prevalent in the tank. Drop breakup rates within the tank increase creating a larger interfacial area for mass transfer. Also, the mass transfer coefficient increases with an increase in the Reynolds number, thereby resulting in an increased mass transfer rate over the available surface area.

4.4.2 Influence of interfacial tension

The interfacial tension between most liquid-liquid dispersion systems lies in the range 1 to 100 mN/m. The use of surface active agents (surfactants) to reduce interfacial tension in two-phase systems is a common practice. There is no general correlation between interfacial tension and the solubility limit for liquid-liquid dispersion systems, although some researchers have reported that it exists for some liquid-liquid groups. The effect of interfacial tension will first be treated in isolation without any considerations as to its influence on the solubility limit.

Table 4-2 shows that reducing σ from 32 mN/m to 1 mN/m while keeping N = 1500 rpm and μ = 0.000894 Pa.s, the dissolution time remains the same. This suggests that the interfacial tension does not affect the mass transfer rate.

This finding may appear counter intuitive since a lower interfacial tension should lead to an increase in drop breakup rates and an increase in the interfacial area available for mass transfer. However, a probable explanation for this observation is that the increase in mass transfer rate due to an increase in interfacial area is offset by a reduction in the concentration gradient. This is discussed further in Section 4.4

The dissolution-blend time ratio and continuous phase Reynolds number for this scenario remain unchanged since the dissolution time did not change.

4.4.3 Influence of continuous phase viscosity

The viscosity of a liquid is an intrinsic property of the liquid. By varying the viscosity, it is implied that a different liquid is used as the continuous phase although the viscosity of a liquid can also be altered by temperature variation. Table 4-2 shows that increasing μ from 0.000894 Pa.s to 0.002 Pa.s while keeping N = 1500 rpm and σ = 1 mN/m, the dissolution time increases by more than 4 folds (from 130 seconds to 544 seconds). The dissolution-blend time ratio increases by the same factor (from 70.3 to 295). This observation is not surprising because an increase in continuous phase viscosity results in a reduction in the Reynolds number for the system (about 50%). Therefore, the turbulent condition in the tank is reduced, fewer drop breakup events will occur and the mass transfer rate is also reduced in two ways; lower Reynolds number and higher Schmidt number.

Using the turbulent conditions in the tank as a criterion for comparison, for the same conditions discussed above (σ = 1 mN/m and μ = 0.002 Pa.s), to obtain Re ~ 59000, the N required is 3350 rpm! The drop breakup rate will be greatly increased and the mass transfer rate increased due to the formation of larger interfacial area. The dissolution time for this scenario is 27 seconds, and the dissolution-blend time ratio is 32.84.

The dissolution-blend time ratios for some liquids used in the chemical industry are given below in Table 4-3. The liquids studied in Table 4-3 have lower saturation concentrations compared to diethyl malonate and it is intended to investigate the dissolution-blend time ratios for such liquids. The actual solute concentration injected is about 50% of the saturation concentration. The dissolution-blend time ratios show a direct dependence on the concentration gradient in the stirred tank, and for all three liquids studied, the dissolution-blend time ratio falls below 200. However, for liquids with even lower saturation concentration values, the dissolution-blend time ratios may exceed 200. This is because the lower the saturation concentration value, the more immiscible the

liquid is. Hence the dissolution time becomes infinite for immiscible liquids (see the upper limit of Figure 1-1).

Table 4-2: Dissolution/Blend time ratios for varying system parameters

N (rpm)	Re (-)	Interfacial Tension (N/m)	Continuous phase viscosity (Pa.s)	Dissolution Time (s)	Dissolution/Blend time ratio
750.00	29586.13	0.032	0.000894	337.24	91.27
1500.00	59172.26	0.032	0.000894	129.75	70.23
1500.00	59172.26	0.001	0.000894	129.88	70.30
1500.00	26450.00	0.001	0.002000	544.45	294.70
3350.00	59071.67	0.001	0.002000	27.17	32.84

Table 4-3: Dissolution/Blend time ratios for 3 different dispersed phase systems

Dispersed phase	N (rpm)	Re (-)	Saturation concentration (kg/m^3)	Interfacial Tension (N/m)	Continuous phase viscosity (Pa.s)	Dissolution Time (s)	Dissolution/Blend time ratio
Amyl Acetate	750.00	29586.13	1.0	0.02567	0.000894	558.24	151.08
O-Xylene	750.00	29586.13	0.175	0.03031	0.000894	704.03	190.54
Toluene	750.00	29586.13	0.5	0.02850	0.000894	645.92	174.81
Amyl Acetate	3350.00	132151.38	1.0	0.02567	0.000894	100.43	121.41
O-Xylene	3350.00	132151.38	0.175	0.03031	0.000894	155.47	187.94
Toluene	3350.00	132151.38	0.5	0.02850	0.000894	125.47	151.68

4.5 Rate Controlling Mechanism

The mass transfer rate from a spherical drop into the continuous phase is given by Fick's law

$$\overline{N} = k_L A(C_S - C_{bulk}) \qquad (4.3)$$

where A is the interfacial area (m^2), C_{bulk} is the solute concentration in the bulk of the tank (mol/m^3 or kg/m^3), k_L is the mass transfer coefficient (m/s) and, $\overline{N}$ and C_S denote the mass transfer rate (mol/s or kg/s) and the saturation or equilibrium concentration (mol/m^3 or kg/m^3) at the prevailing temperature.

For a discretized drop population, the mass transfer rate from drops in the *ith* class is defined by

$$\overline{N}_i = k_{L,i}(C_S - C_{bulk})A_i N_{T,i} \qquad (4.4)$$

where each variable retains the same definition as above for the *ith* size class and $N_{T,i}$ is the absolute number of drops in the *ith* class interval. At any instant, $N_{T,i}$ is obtained from population balance as

$$N_{T,i} = N_{0,i} + \Delta N_{B,i} + \Delta N_{M,i} + \Delta N_{C,i} \qquad (4.5)$$

$N_{0,i}$ is the initial number of drops, $\Delta N_{B,i}$ is the change due to drop breakup, $\Delta N_{M,i}$ is the change due to dissolution, and $\Delta N_{C,i}$ is the change due to convection. Equation (4.4) can now be written as

$$\overline{N}_i = k_{L,i}(C_S - C_{bulk})A_i(N_{0,i} + \Delta N_{B,i} + \Delta N_{M,i} + \Delta N_{C,i}) \qquad (4.6)$$

The total mass transfer rate for a polydispersed drop system in one complete circulation will be given by

$$\sum_i^P \overline{N}_i = \sum_i^P k_{L,i}(C_S - C_{bulk})A_i(N_{0,i} + \Delta N_{B,i} + \Delta N_{M,i}) \quad i = 1,2,3....P \qquad (4.7)$$

$\sum_i^P \Delta N_{C,i}$ disappears for a complete circulation.

The initial mass transfer rate at time t = 0, is defined as

$$\sum_i^P \overline{N}_i = \sum_i^P k_{L,i}(C_S - C_{bulk})A_i(N_{0,i}) \qquad (4.8)$$

the mass transfer rate after one time step is also defined as

$$\sum_{i}^{P} \overline{N}_i = \sum_{i}^{P} k_{L,i}\left(C_S - C_{bulk}\right)A_i\left(N_{0,i} + \Delta N_{B,i} + \Delta N_{M,i}\right) \qquad (4.9)$$

Therefore, the change in the mass transfer rate for one time step will be defined by equation (4.9) minus equation (4.8)

$$\begin{aligned} \Delta\overline{N}_i = & \sum_{i}^{P} k_{L,i}\left(C_{bulk,0} - C_{bulk,1}\right)A_i N_{0,i} \\ & + \sum_{i}^{P} k_{L,i}\left(C_S - C_{bulk,1}\right)A_i \Delta N_{B,i} \\ & + \sum_{i}^{P} k_{L,i}\left(C_S - C_{bulk,1}\right)A_i \Delta N_{M,i} \end{aligned} \qquad (4.10)$$

The terms on the right hand side of equation (4.10) represent the rate controlling mechanisms for mass transfer. $\sum_{i}^{P} k_{L,i}\left(C_{bulk,0} - C_{bulk,1}\right)A_i N_{0,i}$ (***Conc.***) is the change due to the concentration gradient; $\sum_{i}^{P} k_{L,i}\left(C_S - C_{bulk,1}\right)A_i \Delta N_{B,i}$ (***Breakup***) represents the change in mass transfer rate during drop breakup; and $\sum_{i}^{P} k_{L,i}\left(C_S - C_{bulk,1}\right)A_i \Delta N_{M,i}$ (***MTF***) represents the change in mass transfer rate due to drop shrinkage by dissolution. Figure 4-19 shows the plot of all three controlling mechanisms simulated using N = 50 rps, σ = 32 mN/m, φ = 0.01, and μ = 0.000894 Pa.s.

From Figure 4-19, the contribution of drop breakup to the total mass transfer rate is insignificant. This conclusion is supported by the work done by Skelland et al. (1992). The mass transfer rate is thus controlled by the

concentration gradient at the interface between the dispersed drop and the continuous phase.

Figure 4-20 shows the rate of change for each term identified in equation (4.10). The drop breakup term lies on the positive scale because it results in an increase in the drop number density while the dissolution terms (drop shrinkage and concentration gradient) lead to a reduction in the total drop number density. Drop breakup is shown to occur very fast and lasts for about 6 seconds. The dissolution time is the time at which equilibrium is reached (about 21 seconds).

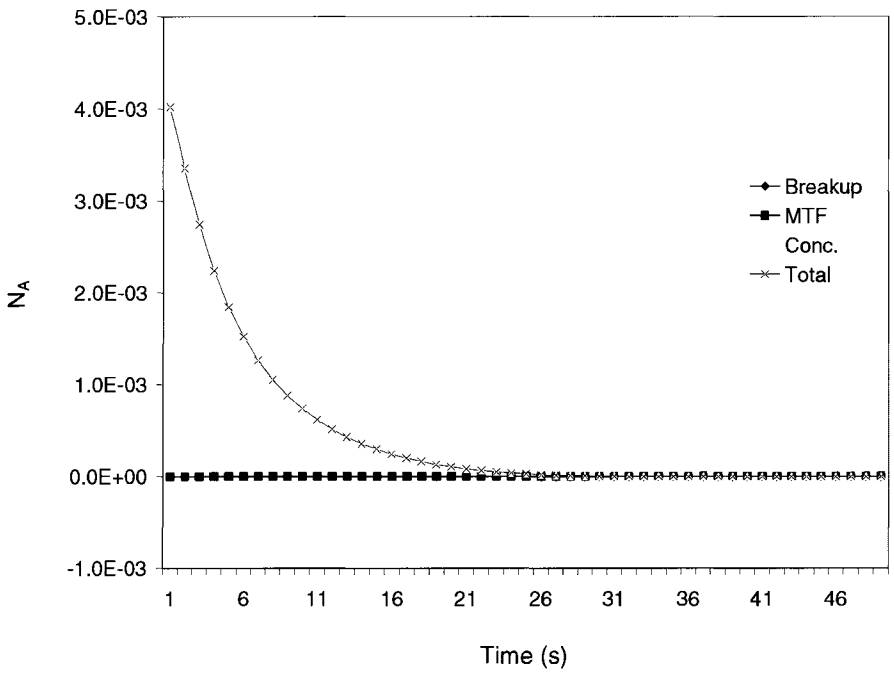

Figure 4-19: Mass transfer rate profile of the controlling mechanisms for N = 50 rps

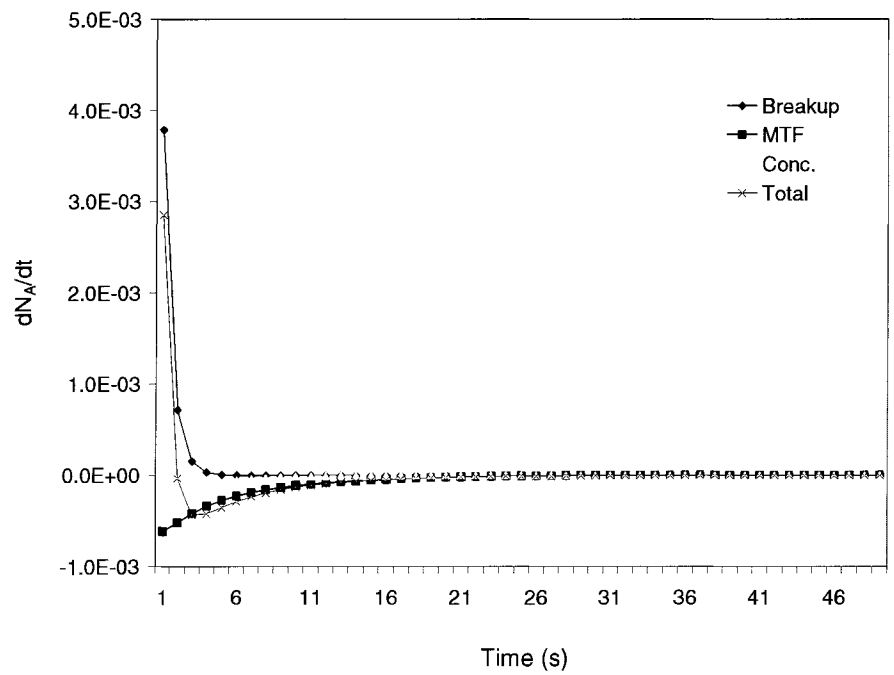

Figure 4-20: Rate of change of mass transfer rate for the drop size distribution controlling mechanisms for N = 50 rps

4.6 Conclusion

From the comparison between the numerical model simulation and the experimental measurements of the drop size distribution and dissolved concentration in the bulk of the continuous phase, the following conclusions can be made:

The model predictions for our study show good agreement with experimental measurements. Therefore, the zone modeling approach is representative of the physical system and can be used in studying liquid-liquid dispersions. The effect of coalescence between drops dispersed in a continuous medium can be significant even in dilute systems. However, at higher turbulence levels, this effect becomes negligible for dissolution processes.

Sensitivity analysis studies show that increasing the impeller rotational speed results in a more turbulent condition in the stirred tank, an increase in the mass transfer rate and the drop breakup rate. Although the relationship between interfacial tension and solubility is not well defined, simulations based on the main effects of interfacial tension show no significant effect on the dissolution rate. The continuous phase viscosity affects both the Reynolds and Schmidt numbers of the dispersion system. A higher continuous phase viscosity reduces the turbulent condition (reduces the Reynolds number) in the stirred tank and also reduces the dissolution rate (increasing the Schmidt number).

Simulation studies on the controlling mechanism for drop dissolution show that the concentration gradient (i.e. the approach to the solubility limit in the stirred tank) dominates the dissolution process. The contribution to overall mass transfer due to the formation of new interfacial area (from drop breakup) is not significant.

No generalizations can be made about the dissolution-blend time ratios. This is because the dissolution time depends on both the physical properties of the

dispersed and the dispersing medium and also the hydrodynamics within the stirred tank while the blend time is not dependent on the physical properties of the liquid-liquid system. However, from the sample liquids studied, a dissolution time of 200 blend times provides an upper limit for design.

4.7 References

Grenville R. K., 1992, *Blending of viscous Newtonian and Pseudo-plastic Fluids,* Ph.D. Dissertation, Cranfield Institute of Technology, Cranfield Bedfordshire, England.

Skelland A. H. P., and Kanel J. S., 1992, *Simulation of Mass Transfer in a Batch Agitated Liquid-Liquid Dispersion,* Ind. Eng. Chem. Res., **31** (3), 908 - 920.

Zhou G., and Kresta S.M., 1998, *Impact of Geometry on the Maximum Turbulence Dissipation Rate for various Impellers*, AIChE J., **42** (9), 2476 - 2490.